LIGHT ACTIVATED GAS NANOSENSORS

Oriol González León

UNIVERSITAT
ROVIRA i VIRGILI

Light activated gas nanosensors

Oriol González León

DOCTORAL THESIS

2018

UNIVERSITAT ROVIRA I VIRGILI
LIGHT ACTIVATED GAS NANOSENSORS
Oriol González León

UNIVERSITAT ROVIRA I VIRGILI
LIGHT ACTIVATED GAS NANOSENSORS
Oriol González León

UNIVERSITAT ROVIRA I VIRGILI
LIGHT ACTIVATED GAS NANOSENSORS
Oriol González León

Oriol González León

Light activated gas nanosensors

Ph. D. Thesis

Supervised by

Dr. Xavier Vilanova Salas

&

Dr. Eduard Llobet Valero

Department of Electronic, Electrical and Automatic Control Engineering

Microsystems and Nanotechnologies for Chemical Analysis (MinoS)

UNIVERSITAT ROVIRA I VIRGILI

Tarragona

2018

UNIVERSITAT ROVIRA I VIRGILI
LIGHT ACTIVATED GAS NANOSENSORS
Oriol González León

UNIVERSITAT ROVIRA i VIRGILI

FEM CONSTAR que aquest treball, titulat "**Light activated gas nanosensors**", que presenta **Oriol Gonzalez Leon** per a l'obtenció del títol de Doctor, ha estat realitzat sota la nostra direcció al Departament d'Enginyeria Electrònica, Elèctrica i Automàtica d'aquesta universitat.

HACEMOS CONSTAR que el presente trabajo, titulado "**Light activated gas nanosensors**", que presenta **Oriol Gonzalez Leon** para la obtención del título de Doctor, ha sido realizado bajo nuestra dirección en el Departamento de Ingeniería Electrónica, Eléctrica y Automática de esta universidad.

WE STATE that the present study, entitled "**Light activated gas nanosensors**", presented by **Oriol Gonzalez Leon** for the award of the degree of Doctor, has been carried out under our supervision at the Department of Electronic, Electrical and Automatic Control Engineering of this university.

Tarragona, 1 de Juliol de 2018

El/s director/s de la tesi doctoral

El/los director/es de la tesis doctoral

Doctoral Thesis Supervisor/s

Xavier Vilanova

Eduard Llobet

UNIVERSITAT ROVIRA I VIRGILI
LIGHT ACTIVATED GAS NANOSENSORS
Oriol González León

UNIVERSITAT ROVIRA I VIRGILI

Departament d'Enginyeria Electrònica, Elèctrica i Automàtica

Escola Tècnica Superior D'Enginyeria
Campus Sescelades
Avinguda dels Països Catalans, 26
43007 Tarragona
Espanya
Tel.: + 34 977 559 610 / 559 728
Fax: + 34 977 559 605

We, Xavier Vilanova Salas and Eduard Llobet Valero, full professors of the Departament of Electronic, Electrical and Automatic Control Engineering of the Universitat Rovira i Virgili,

CERTIFY:

That the present study, entitled "Light activated gas nanosensors", presented by Oriol González León for the award of the degree of Doctor, has been carried out under our supervision at the Department of Electronic, Electrical and Automatic Control Engineering of this university, and that it fulfils all the requirements to be eligible for the International Doctorate Award.

Tarragona, …….2018

Doctoral Thesis Supervisors

Eduard Llobet Valero

Xavier Vilanova Salas

UNIVERSITAT ROVIRA I VIRGILI
LIGHT ACTIVATED GAS NANOSENSORS
Oriol González León

Acknowledgements

UNIVERSITAT ROVIRA I VIRGILI
LIGHT ACTIVATED GAS NANOSENSORS
Oriol González León

Publications derived from the present thesis:

S. Roso; C. Bittencourt; P. Umek; **O. González**; F. Güel; A. Urakawa and E. Llobet **"**Synthesis of single crystalline In2O3 octahedra for the selective detection of NO2 and H2 at trace levels", Journal of Materials Chemistry C, Vol:4, pp 9418 **–** 9427**,** 2016

O. Gonzalez, S. Roso, X. Vilanova, E. Llobet, "Enhanced detection of nitrogen dioxide via combined heating and pulsed UV operation of indium oxide nano-octahedra", Beilstein Journal of Nanotechnology 7(1):1507-1518, October 2016

O. Gonzalez, T. G. Welearegay, X. Vilanova and Eduard Llobet "Using the Transient Response of WO3 Nanoneedles under Pulsed UV Light in the Detection of NH3 and NO2" Sensors 2018, 18(5), 1346

Abstracts of contributions presented at Conferences related to the thesis:

O. Gonzalez, S. Roso, R. Calavia, X. Vilanova, E. Llobet, NO2 Sensing Properties of Thermally or UV Activated In2O3 Nano-octahedra", Procedia Engineering 120:773-776, 2015

O. Gonzalez, T. G. Welearegay, E. Llobet, X. Vilanova, "Pulsed UV Light Activated Gas Sensing in Tungsten Oxide Nanowires" Procedia Engineering 168:351-354, 2016

O. González, S.Roso, E. Llobet, X. Vilanova "Response of indium oxide nano-octahedra activated by switching UV light" oral presentation at the E-MRS 2016 Spring Meeting

O. Gonzalez, C. Jaeschke, T. G. Welearegay, E. Llobet, "Combined pulsed UV and temperature activation of metal oxide nanomaterials in breath analysis applications", ISOCS/IEEE International Symposium on Olfaction and Electronic Nose (ISOEN) Montreal, Canada. 2017

UNIVERSITAT ROVIRA I VIRGILI
LIGHT ACTIVATED GAS NANOSENSORS
Oriol González León

Other Articles and conference contributions:

P. Clément; E. Del Castillo Perez; **O. Gonzalez**; R. Calavia; C. Lucat; E. Llobet; H. Debéda, "Gas discrimination using screen-printed piezoelectric cantilevers coated with carbon nanotubes", Sensors and Actuators B-Chemical, vol: 237, pp:1056-1065, 2016

P. R. Mudimela, M. Scardamaglia, **O. González**, N. Reckinger, R. Snyders, E. Llobet, C. Bittencourt and J. Colomer, "Gas sensing with gold-decorated vertically aligned carbon nanotubes", Beilstein Journal Of Nanotechnology, vol:5, pp 910-918, 2014

K. Assili, **O. Gonzalez**, K. Alouani, K Alouani, X. Vilanova, "Structural, morphological, optical and sensing properties of SnSe and SnSe 2 thin films as a gas sensing material", Arabian Journal of Chemistry, 2017

T. Saidi, T. G. Welearegay, O. Zaim, **O. Gonzalez**, B. Bouchikhi, "Ability of discrimination of breath from smoker and non-smoker volunteers by using an electronic nose based on WO3 nanowires and SnO2 sensors", ISOCS/IEEE International Symposium on Olfaction and Electronic Nose (ISOEN) Montreal, Canada. 2017

O. Gonzalez, R. Calavia, X. Vilanova, E. Llobet, "Green Smart Net: Environmental Data Acquisition, handling and transmission for risk assessment in agriculture and beyond" COST Action TD1105 - New Sensing Technologies for Air-Pollution Control and Environmental Sustainability, Istanbul, 3-5 December 2014

K. Assili, **O. Gonzalez**, K. Alouani, K. Alouani, X. Vilanova, "Sensor performance of nanostructured SnSe thin films grown by means CVD process", May 10-12, 2018 International Conference on Nanomaterials and Applications, Hammamet, Tunisia

UNIVERSITAT ROVIRA I VIRGILI
LIGHT ACTIVATED GAS NANOSENSORS
Oriol González León

Index

UNIVERSITAT ROVIRA I VIRGILI
LIGHT ACTIVATED GAS NANOSENSORS
Oriol González León

1. Introduction

In the last years, the lack of reproducibility, stability and selectivity have been considered as some of the major problems in gas sensing systems based on metal oxide gas sensors. Extracting information from the transient response of metal oxide gas sensors has enabled achieving good results in the improvement of selectivity and also response stability. Response transients can be obtained by producing step-changes in gas concentration [1-3]. For example, focusing on the rise time it was found that this parameter is dependent from the gas and the concentration, using this information nonlinear diffusion-adsorption models were built for the quantification of gas mixtures using pattern recognition techniques [4-6]. Other works studied the transient by modulating or pulsing the sensor operating temperature under constant gas concentration. At first, the effect of oxygen absorption as a function of temperature was studied [7]. Employing the approach of applying short temperature pulses and using different transient analysis techniques, different gas species could be distinguished and quantified [8-10]. Combining different materials as gas sensitive layers in a sensor array, and applying temperature modulating/pulsing, results in the gathering of multivariate data, the analysis of which allows for improving results further [11-12]. Thermal modulation of metal oxide gas sensors has been one of the most used methods for enhancing sensor selectivity and counteracting other shortcomings experienced such as drifts. In that sense, the works of Alexander Vergara modulating the temperature using binary random sequences, multi random sequences and then selecting the optimal frequencies for modulation, by developing feature extraction methods such as Dynamic Moments (DM) or Phase Space (PS) [13-16] have explored extensively this approach, pointing out the advantages of analysing the signal coming from the sensors in temperature modulation mode. Good results were obtained not only in the discrimination rate, but also dramatically reducing the time needed to perform measurements. The main conclusion that can be drawn from his work I, an optimized thermal modulation of the working temperature can significantly increase the selectivity of metal oxide sensors.

Also remarkable is the work done by Andreas Schütze and co-workers at Universität des Saarlandes (Saarbrücken, Germany), where they have specialized in performing tests employing temperature modulated commercially available gas sensors, in order to improve their performance for widening their range of applications [17].

Recently, a different solution has been presented by Manuel Domínguez-Pumar and co-workers at Universitat Politècnica de Catalunya, where the control of surface potential has been proposed to accelerate the response time of MOX gas sensors. Such a technique employs temperature modulation and a feedback loop based on first-order sigma-delta modulators to keep the surface potential constant during gas detection events [18-20].

There are some commercially available digital sensors that probably are using temperature modulation. For example, from June 2018, a new gas sensor platform sensor from IDT [ZMOD 4410] has been marketed, which allows for creating and configuring different temperature sequences to face real application solutions. This means that all research done by temperature modulation is reaching the market. Also, since one year, Sensirion release the Multi-Pixel Gas Sensor (SGP), which consist in 4 different MOx layers, but in that case we do not have access to the temperature modulation applied into the firmware.

Another approximation to improve performance in MOx sensors, is applying light instead of temperature to promote in a different way the occurrence of chemical reactions on their surface. In other words, to use an alternative method than temperature, to promote sensor response and baseline recovery. This technique is harnessed by the chemical industry, in which light is used in many photocatalytic reactions that either allow generating new compounds or increase efficiency in standard processes. Oxide materials play often a key role in such photocatalytic reactions.

Using UV light to activate the reactions taking place on the surface of metal oxide gas sensors has been considered by different research groups. For example, Sbeveglieri and co-workers explored, in the late nineties, the UV activation of both SnO_2 and In_2O_3 sensors operated at room temperature [21-23]. According to their research, excitation by means of UV light can affect, in different ways, charge carrier transport across the grain boundaries appearing in polycrystalline metal oxides. Namely, increasing the density of free carriers by photo generation, decreasing the intergrain barrier height, affecting the intergrain states charge and increasing the probability of tunnelling through intergrain barriers, since the depletion layer width of adjacent grains is decreased. Moreover, light can change the occupancy of defects by both electrons and holes, this affecting the absorption capacity of the metal oxide surface. On the other hand, illumination can also cause structural defects in the oxide lattice. In this case, these defects disappear when UV light is turned off, but with a long recovery period, that is usually temperature dependent. Later, other many

researchers have used UV light to activate gas detection at room temperature employing other metal oxides such as TiO_2 [24-26] or ZnO [27-32]. Trawka and co-workers [33] used a combination of heating and UV radiation to stimulate the interactions between WO_3 and the surrounding gases, analyzing the effect of such interactions on the noise generated.

In other cases, UV light is used exclusively to clean the metal oxide surface, avoiding poisoning [34]. In fact, Trocino and co-workers [35] found that using UV light exclusively during the recovery period of room temperature operated In_2O_3 gas sensors, was more efficient than continuous UV illumination for measuring NO_2. UV promotes desorption of NO_2 and helps regaining the sensor baseline.

For conducting our experiments, a sensor test chamber was designed and constructed in Teflon. Its inner volume was 24 cm^3. The chamber contains sockets to which up to six sensors can be plugged in to be tested. The cover lid houses two UV LEDs so sensors can be operated in 'temperature mode' when a constant current is driven through their heating element while the UV diodes are OFF; in 'UV activation mode' when heaters are not used and the UV LEDs are ON; and in 'mixed mode' when both heating elements and UV LEDs are used simultaneously. The LED to sensing film distance was set to 12 mm, which considering the radiation aperture of the LEDs used (120º), ensured achieving a homogeneous UV irradiation of the sensors. The UV LEDs employed were manufactured by SETI, Sensor Electronic Technology Inc., (model UVTOP320TO39FW) and their maximal emitting optical power was 400 μW at 325 nm. The specifications of the UV-LED indicated that to avoid saturation, the drive current should be kept below 30 mA at an ambient temperature under 55ºC. In our experiments, the drive current was pulsed (diode was on 50% of the time only) and limited to 15 mA. Furthermore, the LED was placed 2 cm away from the heated area of the sensor and kept inserted in a thermally insulating housing. Therefore, the occurrence of saturation effects could be ruled out considering our experimental set-up.

The principal objective of the present thesis was to try combine the use of UV-irradiation and temperature excitation in metal oxides, which we implemented by combining short pulses of UV excitation together with mild heating of the sensing film and analysing the ripple created in film resistance. Both during response and recovery cycles of the sensor towards oxidizing or reducing gases, the UV diode was periodically switched ON and OFF by employing a square driving current signal with a period set to 1 minute, while the sensor was operated at a given constant temperature

(e.g., at room temperature, 50ºC or 100ºC). For example, when the sensor is in the presence of an oxidizing gas such as nitrogen dioxide (detection phase) or in pure dry air (cleaning phase), sensor resistance increases while the UV diode is switched OFF and decreases while the UV diode is switched ON, which results in the overall sensor response presenting a ripple.

This ripple appears because UV light reduces the metal oxide, which tends to re-oxidise when UV light is switched OFF. This ripple, which is caused by the effect of surface cleaning (UV-ON) and oxidation (UV-OFF) processes, is considered a transient signal in sensor response and the rate of resistance change both when the UV is ON or OFF have been found to give useful information for determining gas concentration. Especially the rate of resistance change when the light is OFF has been explored in this thesis, since it can be assumed to be closely dependent on the adsorption and reaction processes taking place on the gas-sensitive surface. Evaluating the rate in the period when the light is ON leads to similar information, but the signal has been found to be noisier, especially for tungsten oxide sensors, as it is shown in Figure 1. This rate is computed as the local derivative of the resistance response curve, that is, the derivative when the UV diode is switched OFF is calculated according to the following expression: $\text{Rate}(n) = (R(n)-R(n-1))/\Delta t$

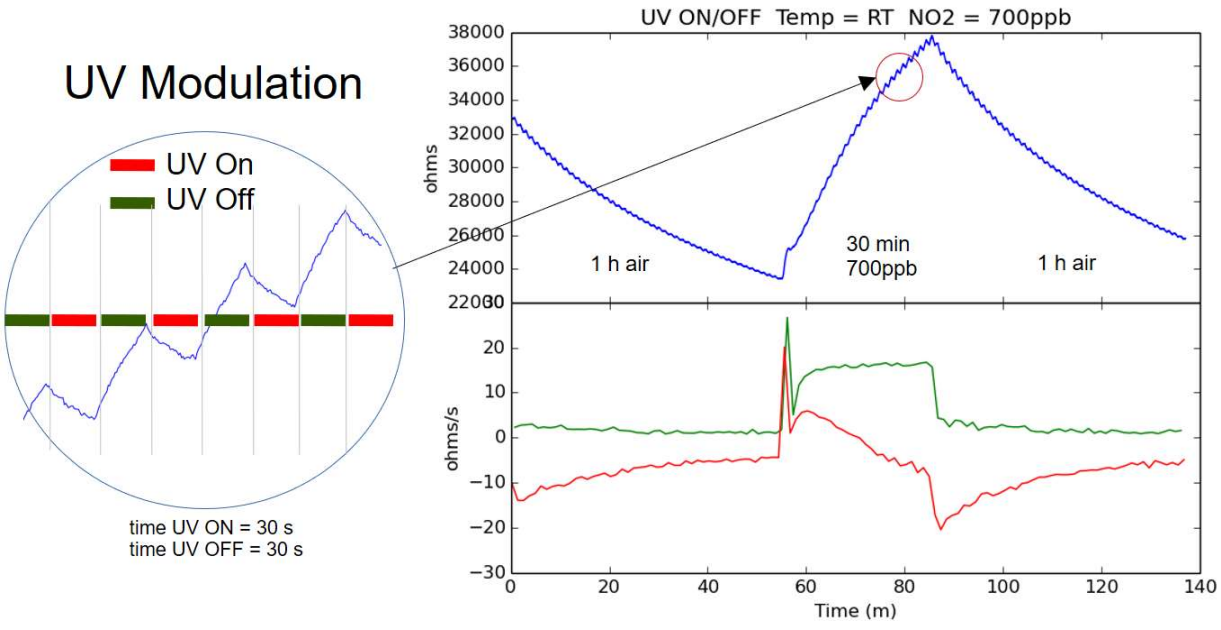

Figure 1: Ripple caused by the pulsed UV on the sensors resistance (blue), and green is the rate when UV is OFF and, red line is the rate when UV is ON.

where R(n) and R(n-1) correspond to the final and initial value of sensor resistance for a period in which UV light remains switched off and Δt is the duration of this period. We have found that the signal transients generated from pulsing UV light are dependent on gas concentration. In particular the rate of resistance change defined above shows a sudden increase when the sensor becomes exposed to the rising edge of a gas pulse, and that a quite stable plateau is attained, the value of which is related to gas concentration (see Figure 2). The time needed for this plateau to be reached is much faster than the response time of the sensor when operated in isothermal conditions and in the absence of UV light (i.e. standard operation). When the gas is removed from the ambient, the resistance rate shows a sharp decrease as well. When the operating temperature is increased from RT to, for example, 100ºC, the value of the rate stabilizes at higher values, indicating that the adsorption-reaction process is faster. In this thesis we show that pulsed-UV activation has great potential for improving the sensitivity and selectivity in MOx sensors for oxidant and reducing gases, while applying only mild heating or even operating sensors at RT.

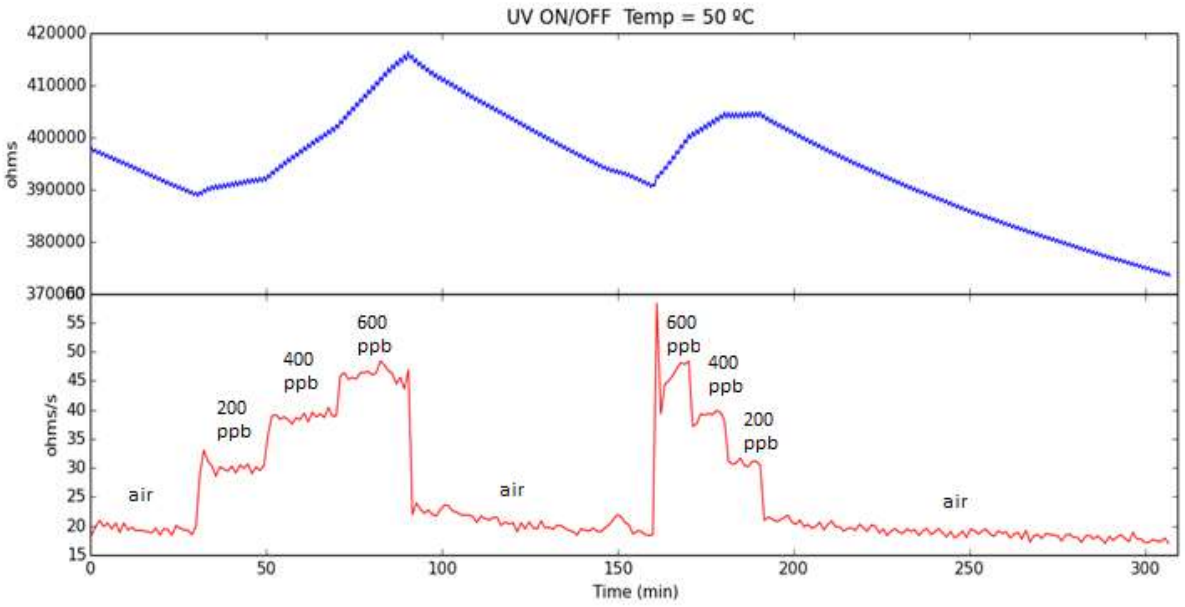

Figure 2: Response of WO3 sensor to 200,400 and 600 ppb of NO2 in increasing and decreasing steps, at 50 °C. Blue line repersents the evolution of the resistance and the red line is computed rate during UV-Off periods.

This alternative sensor operation approach helps decreasing both response time and power consumption. In Figure 3, a comparison between the response times for a sensor operated under different temperature and UV activations while exposed to 10 ppm of NH_3 can be observed. In this figure, we applied a base line correction and then a normalization to the signals, to ease the process of comparing response times. We can observe that for the same sensor we can obtain a faster response for low temperatures using the pulsed-UV technique.

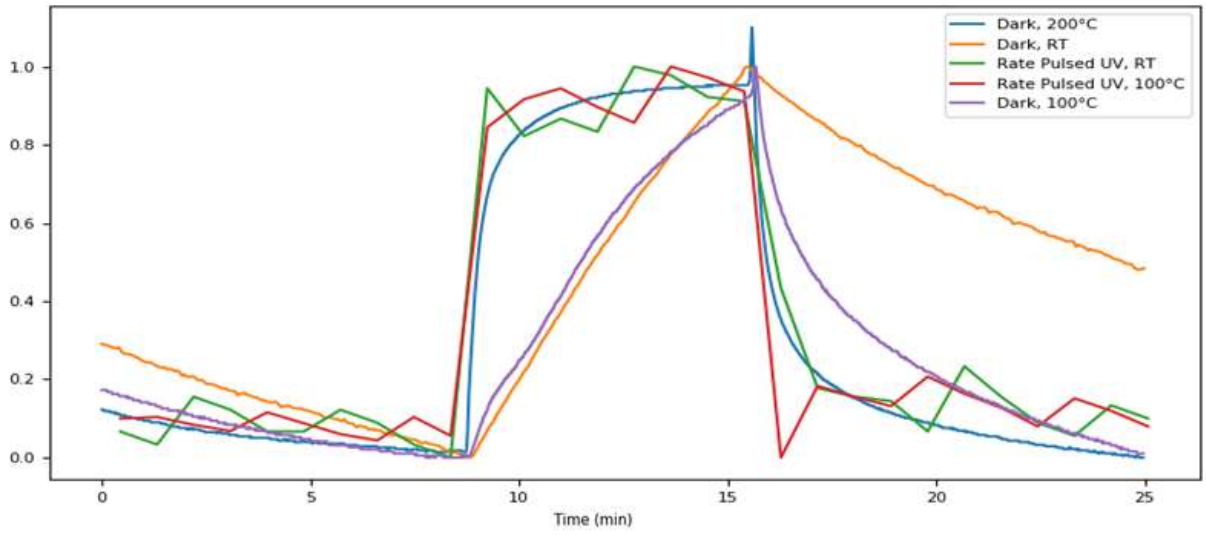

Figure 3: Normalized response for 10 ppm NH3, at different operating temperatures and UV irradiation conditions, in order to compare response times.

During the first year we focused our efforts in the synthesis and characterization of a nanostructured In_2O_3 material in collaboration with Sergio Rosso [36]. We obtained crystalline In_2O_3 nano-octahedra via a vapour phase transport growth method. This material is the first one we used for applying the pulsed-UV methods developed in this thesis. Sensors were produced by employing a screen-printing technique, because given the high synthesis temperature involved in vapour phase transport, indium oxide octahedral could not be grown directly onto the application substrate. Therefore, the as-synthesized nano-octahedra were mechanically removed from the growth substrate employing a razor blade and mixed in a solution of 1,2-propanediol to form a printable ink. This ink was screen-printed on top of commercially-available (Ceram Tech GmBH), alumina transducer elements, which comprised a pair of Pt interdigitate electrodes (front side) and a Pt heating resistor (back side). The first reporting of the results obtained with our approach was in the

2015 edition of the Eurosensors conference [37] and then in a full journal paper [38], were pulsed-UV was compared against standard thermal activation for the detection of NO_2. Also, the work done with UV light and In_2O_3 nano-material was presented at the E-MRS 2016 conference [39]. Later on, we extended our methodology employing WO_3 as gas sensitive layer. WO_3 nanoneedles were grown directly on ceramic alumina application substrates using an aerosol assisted CVD. Tungsten hexacarbonyl ($W(CO)_6$) dissolved in a mixture of acetone and methanol was used as precursor. A piezoelectric ultrasonic atomizer generated an aerosol that was transported to the CVD reactor, where the substrates were located, by means of a nitrogen flow. The CVD reactor temperature was set to 500 ºC, which was significantly lower than the temperature employed in the vapour phase transport synthesis of indium oxide octahedra. The growth process took about 15 minutes to complete. This resulted in the growth of randomly oriented, tungsten oxide nanoneedles of about 19 microns in length and 140 nm in diameter, fully coating the electrode area of the alumina substrate. The pulsed UV light methodology was applied in tungsten oxide sensor by first measuring NO_2 [40], and then NH_3 and NO_2 in the presence of humidity [41]. Finally the discrimination between ethanol and acetone at high humidity levels was also explored [42]. The experiments performed at the end of my Phd are sowed in figure 4, where we can observe both materials working together (in a long experiment, where we were applying the same concentrations of Ethanol and Acetone but changing the excitation source. It is clear that at RT and under dark conditions there are no detecting reactions (no response). In contrast, under UV activation we can detect the presence of acetone but not ethanol, so pulsed UV is a good candidate technique for improving the discrimination between similar compounds. In chapter 5 the corresponding rates and PCA analysis were reported [42].

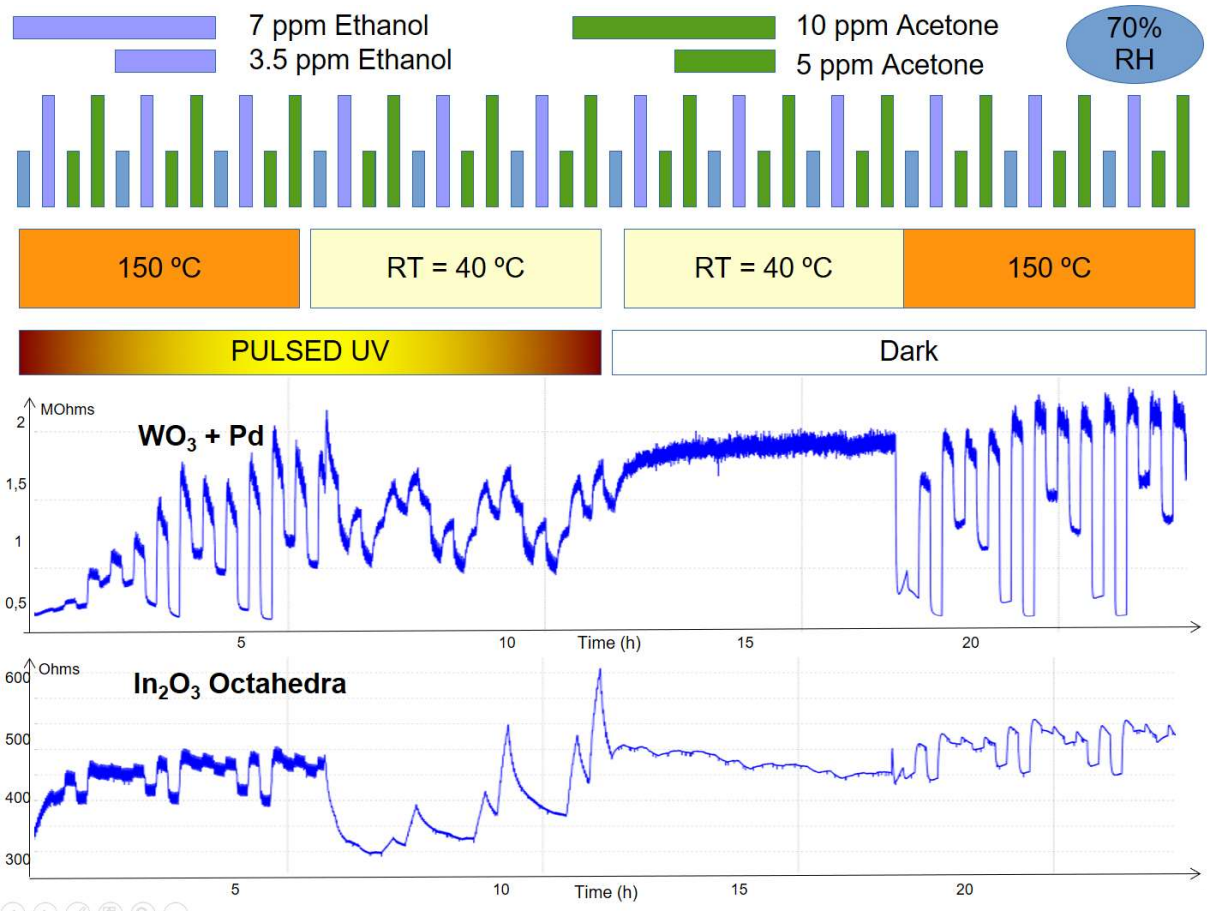

Figure 4: 24 hours experiment under Ethanol and Acetone concentrations comparing temperature and pulsed-UV irradiation responses.

As a general conclusion of the present thesis, this pulsed-UV procedure enables the determination of the gas concentration in a faster way using lower temperatures (even at RT), also under humidity conditions and both for oxidising and reducing gases.

References

[1] E. Llobet, X. Vilanova, J. Brezmes, R. Alcubilla, J. Calderer, J.E. Sueiras, X. Correig, Conductance-transient analysis of thick-flint tin oxide gas sensors under successive gas-injection steps, Measurement Science and Technology 8 (1997) 1133-1138

[2] E. Llobet, J. Brezmes, X. Vilanova, J.E. Sueiras, X. Correig. Qualitative and quantitative analysis of volatile organic compounds using transient and steady-state responses of a thick-film tin oxide gas sensor array, Sensors and Actuators B 41 (1997) 13-21

[3] E. Llobet, X. Vilanova, J. Brezmes, J.E. Sueiras, R. Alcubilla, X. Correig, Steady-state and transient behavior of thick-film tin oxide sensors in the presence of gas mixtures, Journal of the Electrochemical Society 145 (1998) 1772-1779

[4] E. Llobet, X. Vilanova, J. Brezmes, J.E. Sueiras, X. Correig, Transient response of thick-film tin oxide gas-sensors to multicomponent gas mixtures Sensors and Actuators B 47 (1998) 104-112

[5] R. Gutierrez-Osuna, H.T. Nagle, S.S. Schiffman, Transient response analysis of an electronic nose using multi-exponential models, Sensors and Actuators B 61 (1999) 170-182

[6] K. A. Ngo, P. Lauque, K. Aguir, Identification of toxic gases using steady-state and transient responses of gas sensor array, Sensors and Materials 18 (2006) 251-260

[7] P.K. Clifford, D.T. Tuma, Characteristics of semiconductor gas sensors 2. Transient-response to temperature-change Sensors and Actuators 3 (1983) 255-281

[8] Y. Kato, K. Yoshikawa, M. Kitora, Temperature-dependent dynamic response enables the qualification and quantification of gases by a single sensor, Sensors and Actuators B 40 (1997) 33-37

[9] H. Kohler, J. Rober, N. Link, I. Bouzid, New applications of tin oxide gas sensors - I. Molecular identification by cyclic variation of the working temperature and numerical analysis of the signals, Sensors and Actuators B 61 (1999) 163-169

[10] R. Gutierrez-Osuna, A. Gutierrez-Galvez, N. Powar, Transient response analysis for temperature-modulated chemoresistors, Sensors and Actuators B 93 (2003) 57-66

[11] Y. Yamada, M. Ogita, Transient response of resistive-type NO2 sensor on temperature change, Sensors and Actuators B 93 (2003) 546-551

[12] F. Parret, Ph. Menini, A. Martinez, K. Soulantica, A. Maisonnat, B. Chaudret, Improvement of micromachined SnO2 gas sensors selectivity by optimised dynamic temperature operating mode, Sensors and Actuators B 118 (2006) 276-282

[13] A. Vergara, E. Llobet, J. Brezmes, P. Ivanov, X. Vilanova I. Gràcia, C. Cané and X. Correig, “Optimized temperature modulation of micro-hotplate gas sensors through pseudorandom binary sequences”, IEEE Sensor Journal, vol. 5, (6), pp. 1369-1378, 2005.

[14] A. Vergara, E. Llobet, J. Brezmes, P. Ivanov, X. Vilanova I. Gràcia, C. Cané and X. Correig, “Optimised Temperature Modulation of Metal Oxide Micro-Hotplates Gas Sensors through Multi-Level pseudo random sequences”, Sensors and Actuators B, vol. 111-112, pp. 271-280, 2005.

[15] A. Vergara, E. Llobet, E. Martinelli, C. Di Natale, A. D'Amico, X. Correig, "Feature extraction of metal oxide gas sensors using dynamic moments", Sensors and Actuators B, in press 2006.

[16] A. Vergara, E. Llobet, J. Brezmes, P. Ivanov, C. Cané, I. Gràcia, X. Vilanova, X. Correig, "Quantitative gas mixture analysis using temperature-modulated microhotplate gas sensors: Selection and validation of the optimal modulating frequencies",

[17] C. Schultealbert, T. Baur, A. Schütze T. Sauerwald, Facile Quantification and Identification Techniques for Reducing Gases over a Wide Concentration Range Using a MOS Sensor in Temperature-Cycled Operation, March 2018, Sensors 18(3):744

[18] M. Dominguez-Pumar; L. Kowalski; R. Calavia; E. Llobet. Smart control of chemical gas sensors for the reduction of their time response. Sensors and Actuators B-Chemical. 229, pp. 1 - 6. (Switzerland): 2016.

[19] M. Dominguez-Pumar; L. Kowalski; E. Llobet; R. Calavia. Active Control of the Surface Potential of Nanostructured, Layers. IEEE Sensors Journal. 16 - 8, pp. 2213 - 2214. (United States of America): 2016. Available

[20] L. Kowalski , J. Pons-Nin , E. Navarrete , E. Llobet and M. Domínguez-Pumar . Using a Second Order Sigma-Delta Control to Improve the Performance of Metal-Oxide Gas Sensors. Sensors (Basel). 2018 Feb 23;18(2). pii: E654. doi: 10.3390/s18020654.

[21] P. Camagni, G. Faglia, P. Galinetto, C. Perego, G. Samoggia, G. Sberveglieri, Photosensitivity activation of SnO2 thin film gas sensors at room temperature, Sensors and Actuators. B 31 (1996) 99 -103

[22] E. Comini, A. Cristalli, G. Faglia, G. Sberveglieri, Light enhanced gas sensing properties of indium oxide and tin dioxide sensors, Sensors and Actuators B 65 260-263

[23] E. Comini, G. Faglia, G. Sberveglieri, UV light activation of tin oxide thin films for NO2 sensing at low temperatures, Sensors and Actuators B 78 (2001) 73-77

[24] H.C. Lee, W.S. Hwang, Enhancing the sensitivity of oxygen sensors through the photocatalytic effect of SnO2/TiO2 film, Materials Transactions 46 (2005) 1942-1949

[25] M.G. Manera, A. Taurino, M. Catalano, R. Rella, A.P. Caricato, R. Buonsanti, P.D. Cozzoli, M. Martino, Enhancement of the optically activated NO2 gas sensing response of brookite TiO2 nanorods/nanoparticles thin films deposited by matrix-assisted pulsed-laser evaporation, Sensors and Actuators B 161 (2012) 869-879

[26] S.N. Zhang, T. Lei, D. Li, G.Z. Zhang, C.S. Xie, UV light activation of TiO2 for sensing formaldehyde: How to be sensitive, recovering fast, and humidity less sensitive, Sensors and Actuators B 202 (2014) 964-970

[27] Structural characteristics and UV-light enhanced gas sensitivity of La-doped ZnO nanoparticles Ge, C.Q.; Xie, C.S.; Hu, ML; Gui, YH; Bai, ZK; Zeng, DW, Materials Science and Engineering B-Solid State Materials for Advanced Technology 141 (2007) 43-48

[28] B.P.J. Costello, R.J. Ewen, N.M. Ratcliffe, M. Richards, Highly sensitive room temperature sensors based on the UV-LED activation of zinc oxide nanoparticles, Sensors and Actuators B 134 (2008) 945-952

[29] L. Peng, Q.D. Zhao, D.J. Wang, J.L. Zhai, P. Wang, S. Pang, T.F. Xie, Ultraviolet-assisted gas sensing: A potential formaldehyde detection approach at room temperature based on zinc oxide nanorods, Sensors and Actuators B 136 (2009) 80-85

[30] S.W. Fan, A.K. Srivastava, V.P. Dravid, UV-activated room-temperature gas sensing mechanism of polycrystalline ZnO, Applied Physics Letters 95 (2009) 142106

[31] L.A. Peng, J.L. Zhai, D.J. Wang, Y. Zhang, P. Wang, Q.D. Zhao, T.F. Xie, Size- and photoelectric characteristics-dependent formaldehyde sensitivity of ZnO irradiated with UV light Sensors and Actuators B 148 (2010) 66-73

[32] L. Luo, B.D. Sosnowchik, L.W. Lin, Local vapor transport synthesis of zinc oxide nanowires for ultraviolet-enhanced gas sensing, Nanotechnology 21 (2010) 495502

[33] M.P. Trawka, J.M. Smulko, L.Z. Hasse, C.G. Granqvist, R. Ionescu, E. Llobet, F.E. Annanouch, L.B. Kish, UV-Light-Induced Fluctuation Enhanced Sensing by WO3-Based Gas Sensors IEEE Sensors Journal 16 (2016) 5152-5159

[34] G.K. Mor, O.K. Varghese, M. Paulose, C.A. Grimes, A self-cleaning, room-temperature titania-nanotube hydrogen gas sensor, Sensor Letters 1 (2003) 42-46

[35] S. Trocino, P. Frontera, A. Donato, C. Busacca, L.A. Scarpino, P. Antonucci, G. Neri, Gas sensing properties under UV radiation of In2O3 nanostructures processed by electrospinning, Materials Chemistry and Physics 147 (2014) 35-41

[36] S. Roso Synthesis of single crystalline In2O3 octahedra for the selective detection of NO2 and H2 at trace levels

[37] O. Gonzalez, S. Roso, R. Calavia, X. Vilanova, E. Llobet, NO2 sensing properties of thermally or UV activated In2O3 nano-octahedra, Procedia Engineering 120 (2015) 773-776

[38] O. Gonzalez, S. Roso, X. Vilanova, E. Llobet, Enhanced detection of nitrogen dioxide via combined heating and pulsed UV operation of indium oxide nano-octahedra, Beilstein Journal of Nanotechnology 7 (2016) 1507-1518

[39] O. González, S.Roso, E. Llobet, X. Vilanova "Response of indium oxide nano-octahedra activated by switching UV light" oral presentation at the E-MRS 2016 Spring Meeting, Lille, France

[40] O. Gonzalez, T. Welearegay, E. Llobet, X. Vilanova, Pulsed UV light activated gas sensing in tungsten oxide nanowires, Procedia Engineering 168 (2016) 351-354

[41] O. Gonzalez, T. G. Welearegay, X. Vilanova and Eduard Llobet "Using the Transient Response of WO3 Nanoneedles under Pulsed UV Light in the Detection of NH3 and NO2" Sensors 2018, 18(5), 1346

[42] O. Gonzalez, C. Jaeschke, T. G. Welearegay, E. Llobet, "Combined pulsed UV and temperature activation of metal oxide nanomaterials in breath analysis applications", ISOCS/IEEE International Symposium on Olfaction and Electronic Nose (ISOEN) Montreal, Canada. 2017

ARTICLE

2. Synthesis of single crystalline In_2O_3 octahedra for the selective detection of NO_2 and H_2 at trace levels

S. Roso; C. Bittencourt; P. Umek; **O. González**; F. Güel; A. Urakawa and E. Llobet

Journal of Materials Chemistry C, Vol:4, pp 9418 – 9427**,** 2016

After conducting a literature search for previous works using UV irradiation in metal oxide gas sensors, we found several papers using UV activation of IN2O3. We then decided to start focusing in this material. Therefore, this paper reports a vapour phase transport method, which is run at high temperatures for synthesising single crystalline, nanostructured indium oxide (In2O3) in the form of octahedral. The resulting material was characterized by FE-SEM, HR-TEM, XRD, XPS and PL.

First of all we tested the material under standard conditions, namely employing a heating element within the transducer substrate of the sensor. In this way, the gas sensing properties against oxidizing and reducing species were investigated. A high response towards NO2 was obtained at a relatively low optimal operating temperature (i.e., 130 °C) and even some response at room temperature was obtained (at RT baseline recovery was very poor).

This article sets the starting point for testing the effect of UV light activation in order to improve the performance achieved.

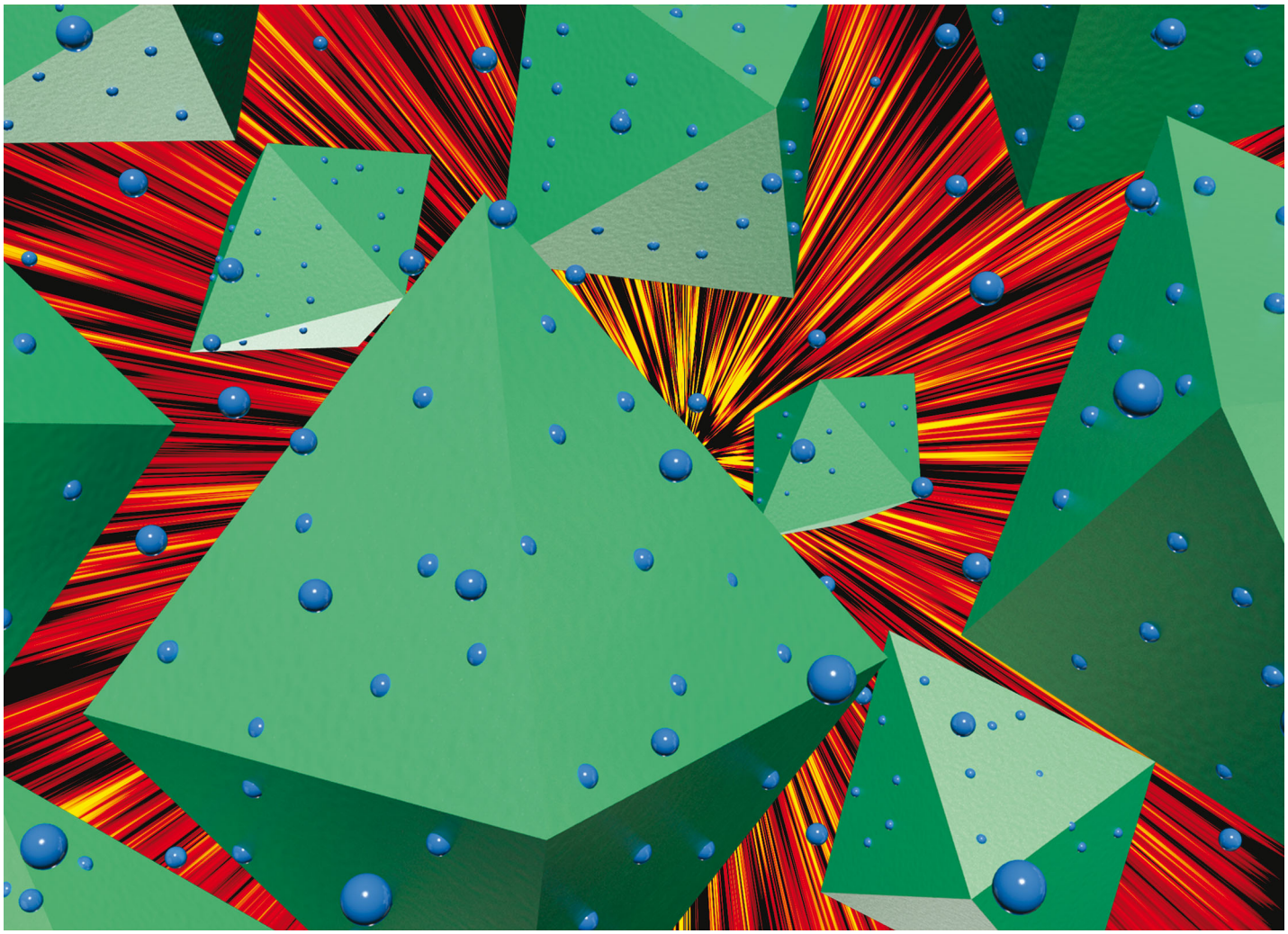

Showcasing research from School of Engineering, Research Center in Engineering of Materials and Micro/Nano Systems, Universitat Rovira i Virgili, Tarragona, Spain.

Synthesis of single crystalline In_2O_3 octahedra for the selective detection of NO_2 and H_2 at trace levels

A facile method for synthesizing pure or metal decorated, single crystalline, indium oxide octahedra is demonstrated. While pure In_2O_3 shows outstanding sensitivity to nitrogen dioxide in the presence of ambient moisture, metal-loaded In_2O_3 is highly sensitive to hydrogen.

As featured in:

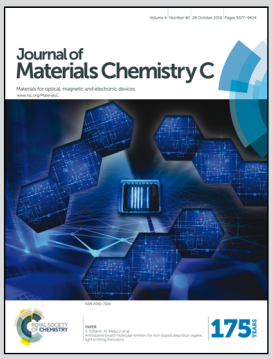

See Eduard Llobet *et al.*, *J. Mater. Chem. C*, 2016, **4**, 9418.

ROYAL SOCIETY OF CHEMISTRY

www.rsc.org/MaterialsC

Registered charity number: 207890

Journal of
Materials Chemistry C

PAPER

View Article Online
View Journal | View Issue

Cite this: J. Mater. Chem. C, 2016, 4, 9418

Synthesis of single crystalline In_2O_3 octahedra for the selective detection of NO_2 and H_2 at trace levels†

Sergio Roso,[ab] Carla Bittencourt,[c] Polona Umek,[d] Oriol González,[a] Frank Güell,[e] Atsushi Urakawa[b] and Eduard Llobet*[a]

Received 28th July 2016,
Accepted 9th September 2016

DOI: 10.1039/c6tc03218d

www.rsc.org/MaterialsC

Single crystalline indium oxide (In_2O_3) octahedra have been synthesized by means of a vapor phase transport method at high temperature. The resulting material has been characterized by FE-SEM, HR-TEM, XRD, XPS and PL. The gas sensing properties of this material against oxidizing and reducing gases have been examined and the conditions for selectively detecting such gases have been established. A high response towards NO_2 has been obtained at a relatively low optimal operating temperature (*i.e.*, 130 °C) and even at room temperature. The fact that the response of the nanomaterial is more than two orders of magnitude higher for NO_2 than for H_2, even in the presence of ambient moisture, makes it very promising for the selective detection of oxidizing species (at ppb levels) under real ambient conditions. The addition of noble metal nanoparticles (Pt and Pd) combined with an increase in the operating temperature (*i.e.*, 250 °C) significantly increases H_2 sensitivity and dramatically decreases the response to NO_2. However, in this case, the presence of humidity negatively affects the response to H_2. The sensing mechanisms are introduced and discussed.

Introduction

Semiconductor metal oxides have become fascinating materials due to their application in numerous fields such as gas sensing, heterogeneous catalysis and solar cells among many others. Considering their application in gas sensing the presence of oxygen vacancies on the oxide surface plays an important role in the sensing mechanism.[1] In the case of n-type semiconductors, in the presence of oxidizing gases, for instance NO_2, electrons are withdrawn from the conduction band, resulting in an increase in the resistivity of the metal oxide.[2] In contrast, when the metal oxide is in contact with a reducing species, such as H_2, the gas reacts with the oxygen adsorbed at the surface of the material, resulting in a decrease in its electrical resistivity.[3,4]

Nanostructured materials have attracted attention over the past few years, in an attempt to overcome some of the drawbacks found when sensing gases employing bulk materials. Nanomaterials show higher surface activity, superior responsiveness at lower operating temperatures (*i.e.* require lower power consumption) and superior long-term stability than their bulk counterparts. Among all metal oxide semiconductors, indium oxide (In_2O_3) is one of the most important n-type, wide direct band-gap (around 3.6 eV at room temperature) semiconductors due to its excellent electronic and optical properties. The concern for environmental protection, human health and green energy has led to an increasing number of publications for an efficient gas detection of different toxic and volatile gases using In_2O_3 nanostructure based sensors. Many morphologies have been reported, including nanowires,[5] nanofibers,[6] nanotubes,[7] nanoparticles, nanosheets, and nano-flower like structures[8] among many others. However, little has been reported about the sensing properties of other polyhedral morphologies such as cubes, hexahedra, octahedra and dodecahedra.[9] The advantage of using morphologies like octahedra is that they possess sharp edges and tips, which provides more active sites and smooth surfaces and unique and perfectly defined crystalline facets (*i.e.* (111)) exposed to the gas atmosphere.

Also, there is a lack of information regarding gas sensing properties under humidity conditions in previous In_2O_3 studies. A summary of the gas sensing properties of nanostructured In_2O_3 synthesized employing different methods is shown in Table 1. According to what has been reported on the detection of hydrogen and nitrogen dioxide with In_2O_3 films, there is no

[a] Mlnos-Emas, Universitat Rovira i Virgili, Av. Països Catalans 26, 43007 Tarragona, Spain. E-mail: eduard.llobet@urv.cat
[b] Institute of Chemica Research of Catalonia (ICIQ), The Barcelona Institute of Science and Technology, Av. Països Catalans 16, 43007 Tarragona, Spain
[c] Materia Nova, Université de Mons, Parc Initialis, Avenue N. Copernic, 1, B-7000 Mons, Belgium
[d] Department of Solid-State Physics, Jožef Stefan Institute, Jamova cesta 39, 1000 Ljubljana, Slovenia
[e] Department D'Enginyeries, Electrònica, Universitat de Barcelona, C/Martí Franqès 1, 08028 Barcelona, Catalunya, Spain

† Electronic supplementary information (ESI) available. See DOI: 10.1039/c6tc03218d

Table 1 Gas sensing properties of nanostructured In_2O_3

Synthesis method	Morphology	Target gas	Working temperature	Response	Ref.
Laser ablation	Nanowires	NO_2 (200 ppb)	Room temperature	-0.6^a	14
Thermal evaporation	Nanotowers	H_2 (2–1000 ppm)	240 °C	$85\%^b$	15
In situ oxidation	Nanoparticle	NO_2 (100 ppm)	300 °C	32^c	16
Sol–gel	Octahedra	NO_2 (100 ppm)	Room temperature	40^c	17
AA-CVD	Thin film	NO_2 (80 ppb)	400 °C	2^c	18
Hydrothermal	Flower-like	NO_2 (200 ppb)	140 °C	40^c	19
Ammonolysis and re-oxidation	Octahedra strings	HCHO (100 ppm)	420 °C	1.8^d	20
CVD	Nanoneedles	H_2 (350 ppm)	200 °C	0.25^e	21
Ionic layer deposition	Thin film	H_2 (1000 ppm)	450 °C	8.5^d	22
Hydrothermal	Nanocubes	H_2 (5 ppm)	150 °C	25^d	23
Vapor phase transport	Octahedra	NO_2 (1 ppm)@50% R.H.	130 °C	120^c	This work

[a] Response calculated as $S = R_a/R_g - 1$. [b] Response calculated as $S = [(R_o - R_g)/R_o] \times 100$. [c] Response calculated as $S = R_g/R_o$. [d] Response calculated as $S = R_o/R_g$. [e] Response calculated as $S = 1 - R_a/R_g$.

clear pattern on the optimum operating temperatures for the detection of these two gases.

Even though pure metal oxide sensors can be very responsive to some gases, they often show poor selectivity. To overcome this drawback, noble metal particles can be added to the surface of the metal oxide active layer, improving their sensitivity towards a given target gas. Noble metals, such as Au,[10] Pt[10] or Pd,[11] are usually added to metal oxide nanostructures through a variety of methods, among which RF sputtering is one of the most commonly used. Its effectiveness has been demonstrated when used for functionalizing metal oxide nanomaterials.[12,13]

Besides, In_2O_3 nanostructures show a strong photoluminescence (PL) emission in the visible range of the electromagnetic spectrum.[24] This broad emission located mainly at around 580 nm is thought to be originated from different kinds of defects present in the material. Among them, oxygen vacancies, oxygen interstitials, indium interstitials and oxygen antisite may be responsible for the broad emission observed by PL[25,26]. These defects play a key role in the detection mechanism of semiconductor metal oxides. Therefore, PL studies can help to better understand the sensing mechanisms of indium oxide towards oxidizing and reducing agents.

In this work, we have synthesized In_2O_3 octahedra *via* vapor phase transport at high temperatures. The aim of the study is to shed light, for the first time, on the effect of the octahedral morphology on the gas sensing properties of In_2O_3 nanomaterials. Furthermore, it will be shown that the addition of Pt or Pd nanoparticles to the pure In_2O_3 octahedra can help tuning the gas sensing properties for the detection of hydrogen. PL measurements have been performed on sensors under *operando* conditions in the presence of air and NO_2 diluted in air flows, in order to further confirm the sensing mechanism of In_2O_3 octahedra.

Experimental

In_2O_3 octahedra were synthesized on top of Si/SiO_2 substrates *via* a vapor-phase transport method using a horizontal chemical vapor deposition (CVD) furnace. Si/SiO_2 substrates were previously cleaned by sonication. The cleaning process follows three steps of 5 minutes each in acetone, ethanol and deionized water, and then dried in synthetic air. In a typical experimental procedure, 0.3 g of high purity In metal (99.99%) was placed on an alumina boat. Next to it, at a distance of around 1 cm the Si/SiO_2 wafer was placed. Then, the alumina boat with the precursor and the wafer were placed at the center of the horizontal furnace. The temperature was raised to 1000 °C at a rate of 15 °C min^{-1}, and kept constant for 120 min. The reaction took place in a dynamic Ar atmosphere (300 mL min^{-1}).

When the furnace was cooled down to room temperature, a pale green product was found on top of the Si/SiO_2 wafer. The crystalline phase and morphological structural features were studied by means of X-ray diffraction (XRD, Bruker-AXS D8-Discover diffractometer with parallel incident beam), a field emission scanning electron microscope (FESEM, Jeol 7600F), and high resolution transmission electron microscopy (TEM and HR-TEM, JEOL 2100). For TEM and HR-TEM analyses, a methanol dispersion of the sample was ultrasonicated for 20 minutes and a drop of it was deposited on a lacy carbon film supported by a nickel grid. For SEM analysis a product was scratched from the Si/SiO_2 substrate and placed on a carbon tape attached to an aluminum sample holder. Prior to the SEM investigation the sample was coated with a 3 nm thick carbon layer.

After that, the material was removed from the Si/SiO_2 substrate and mixed in a solution of 1,2-propanediol. The resultant ink was used to deposit the material by screen printing on top of an alumina substrate with interdigitated Pt electrodes. At the back side of such a substrate, a Pt heater was placed in order to perform gas tests at different temperatures. It is worth saying that in each CVD synthesis, a quantity of 5–8 mg of In_2O_3 octahedra is obtained, and this is enough for producing 1–2 sensors.

After the screen printing deposition of the nanomaterial, a 6 μm thick layer is obtained on top of the alumina substrate. A SEM micrograph (cross-sectional view) can be found in the ESI.†

In order to deposit Pt or Pd nanoparticles on In_2O_3 sensors, an RF sputtering system was used. For Pt, 30 W and 8 s were used for the deposition and, for Pd, 50 W and 8 s were used, both under 3.75 mTorr and at room temperature. This process was conducted as a second step after the screen-printing of pure In_2O_3. The sputtering process parameters had been optimized

previously for obtaining small and well-dispersed Pt or Pd nanoparticles, avoiding coalescence of the nanoparticles. It is not realistic to vary these parameters in view of altering Pd or Pt loading, as it is not the only variable that changes, particle size changes as well. It has been shown previously that sensing performance in Pd/SnO_2 samples improves with decreasing Pd particle size.[27] The amount of metal loading employed in the In_2O_3 sensors was guided by the results showing that reducing the amount of metal sputtered reduced the size of metal nanoparticles.

The chemical characterization of the active layers was performed using X-ray photoelectron spectroscopy (XPS); the XPS analysis was carried out using a Physical Electronics, VERSAPROBE PHI 5000 spectrometer equipped with monochromatic AlKα radiation with 0.7 eV energy resolution and a dual-beam charge-compensation system. All the XPS data were elaborated using Casa XPS v.2.3 software and binding energies were referenced with respect to the C 1s peak at 284.5 eV.

For obtaining the PL spectra, a Hd-Cd laser at 325 nm was used in order to overcome the band gap barrier of the In_2O_3 nanomaterial. The luminescence was dispersed using an Oriel Instruments 74 000 monochromator and detected using a Hamamatsu H8259-02 with a socket assembly E717-500 photomultiplier. All sources of noise were removed using a Stanford Research System SR830 DSP lock-in amplifier.[28] Sensors were hosted in a specially designed chamber fitted with a UV-quality quartz window, which allowed us to run PL measurements in the presence of either dry air or nitrogen dioxide diluted in air.

Results and discussion

In_2O_3 nanostructures were synthesized *via* a vapor-solid mechanism, as indicated by the absence of the metal catalyst on the substrate. After melting of In grains, In vapor reacts with residual oxygen present in the furnace, thus forming oxidized clusters. When the temperature further increases, the oxidized In clusters act as nucleation centers for the formation of In_2O_3 crystals. The formation of In_2O_3 nuclei will lead to the formation of In_2O_3 with the desired morphology depending on the reaction temperature.[29,30] At 700 °C, In_2O_3 triangular crystals are formed whereas at 800–1000 °C pyramids and octahedra can be obtained. The facets exposed correspond to the most energetically stable atomic planes in the lattice. Fig. 1 shows FESEM images of the In_2O_3 octahedra synthesized at 1000 °C. As shown, the final product consists of a high density of octahedral shaped structures (Fig. 1, upper panel). No other morphologies are observed, which indicates the uniformity of the process. A regular octahedron is composed of eight equilateral triangles, four of which meet at the same vertex. The side of each triangle is about 500 nm and all the faces are almost perfectly smooth and without any visible structural defects (Fig. 1, lower panel). Moreover, these structures possess sharp edges and vertexes.

Further characterization has been carried out using TEM and HRTEM. Fig. 2 shows TEM and HRTEM images of the In_2O_3 octahedra. As observed, the side length of the octahedron

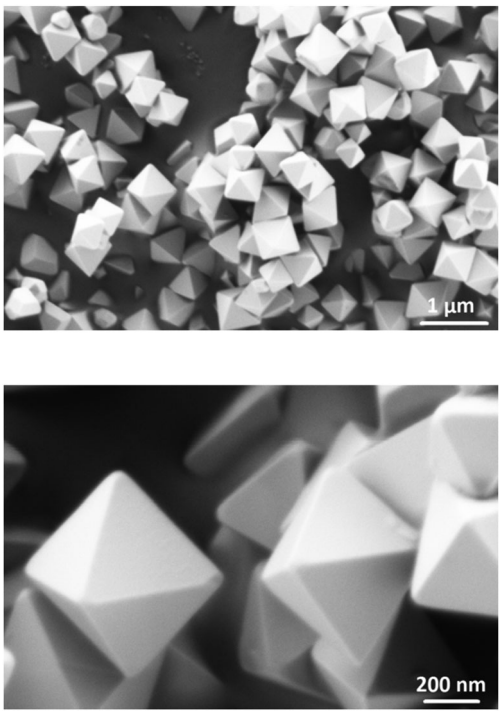

Fig. 1 Low and high magnification ESEM images of the In_2O_3 octahedra.

is about 500 nm, which is consistent with that observed in the FESEM images. The inset of Fig. 2 exhibits a HRTEM image of the edge of the ocahedron. It clearly exhibits the continuous lattice fringes of the structures, showing the crystalline nature of the In_2O_3 octahedra. The distance measured between two adjacent fringes is 0.29 nm, which corresponds to the {111} interplanar distance of the cubic phase of In_2O_3 according to ICDD card no. 01-071-2194.

EDS carried out in an area of several In_2O_3 octahedra confirms that there are no impurities present as no other peaks other than those of indium and oxygen could be found (Fig. S2, ESI†).

Next, characterization of the sputtering-deposited Pt and Pd nanoparticles on top of the In_2O_3 octahedra was carried out. HR-TEM images of the Pt and Pd nanoparticles are shown in Fig. 3 and 4 respectively. As shown, after the deposition of Pt or

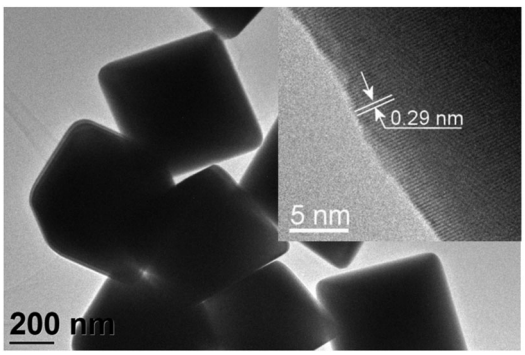

Fig. 2 TEM and HRTEM (inset) of the In_2O_3 octahedra.

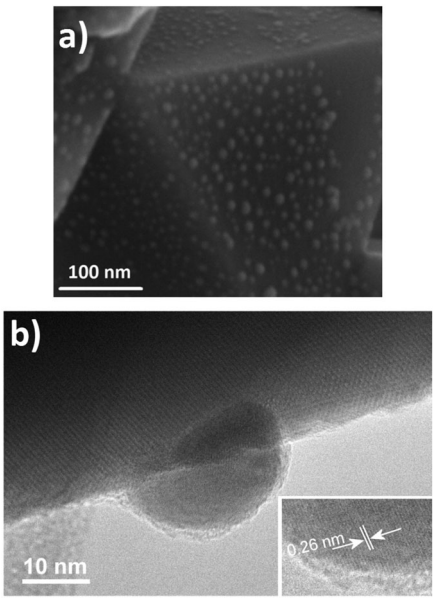

Fig. 3 (a) FESEM image of the Pt/In_2O_3 octahedra, and (b) HR-TEM image of a Pt nanoparticle attached to an In_2O_3 octahedron. The inset shows the interlayer distance of the Pt nanoparticle.

Pd nanoparticles, the octahedral morphology was preserved. Furthermore, Pt nanoparticles appear to be homogenously distributed on the faces of the octahedra. The size of such nanoparticles is about 10–20 nm, as shown in Fig. 3. Closer inspection reveals that the measured interlayer distance is 0.26 thus corresponding to the {111} interplanar spacing of PtO according to ICDD card no. 43-1100.

By analyzing the Pd decorated samples we can observe that the Pd nanoparticles are also homogeneously distributed along the faces of the In_2O_3 octahedra. In contrast to the nanoparticles sputtered with a Pt target, these nanoparticles appear to be smaller, as their size ranges between 8 and 10 nm. Such nanoparticles have an interplanar spacing of 0.259 and 0.263 nm. Such lattice parameters are close to the interplanar spacing of tetragonal PdO (d_{111} = 0.263 nm and d_{002} = 0.266 nm according to ICDD card no 01-085-0624). In addition, according to Kibis *et al.*[31] these values are characteristic of highly oxidized palladium nanoparticles where palladium is mainly in the +2 oxidation state.

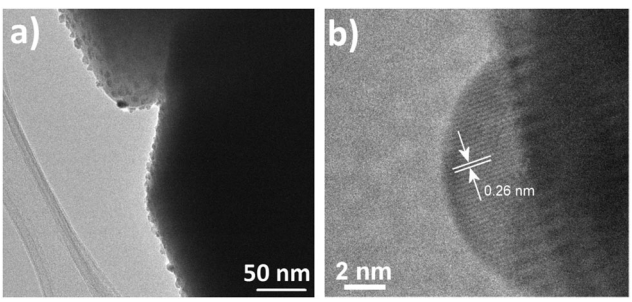

Fig. 4 (a) HR-TEM image of the Pd/In_2O_3 octahedra, and (b) HR-TEM image a single Pd nanoparticle attached to an In_2O_3 octahedron.

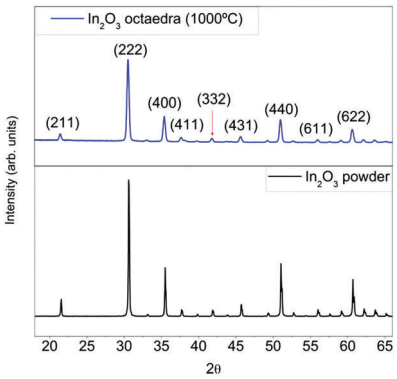

Fig. 5 XRD patterns of the pure In_2O_3 octahedra (top) and a commercial In_2O_3 powder (bottom).

The crystalline phase was confirmed by means of X-ray diffraction (XRD). As shown in Fig. 5, pure samples show the typical features of cubic In_2O_3. No peaks belonging to other materials or impurities could be found.

Additional XRD measurements for Pt and Pd-doped In_2O_3 samples were performed (Fig. S3, ESI†). These results confirm that metal decoration does not affect the crystallinity of In_2O_3 octahedra, which retain the cubic phase. Due to the low amount of metal loading, no peaks arising from Pt or Pd could be found. This is often the case for the typical amounts of metal loading used in gas sensing applications.[20,32]

With the aim to identify the chemical state of elements in the indium oxide and in the catalyst particles (Pt, Pd), XPS analysis was carried out on the nanostructures deposited on the sensor substrates. The In 3d core level spectra of both samples are shown in Fig. S5 of the ESI.† These are composed of two components, relative to the spin–orbit doublets ($3d_{5/2}$ and $3d_{3/2}$), respectively, at 444.2 eV and 451.8 eV indicating that In is mainly found in the +3 oxidation state, which almost corresponds to the stoichiometric state.[33] The O 1s XP spectra are comprised of two intense peaks centered at 529.8 eV and 531.8 eV (Fig. 6). The more intense peak has been ascribed to oxygen bonds in In–O–In, while the high binding energy peak at 531.2 eV is possibly partially related to oxygen vacancies in the bulk of metal oxides.[34]

By inspecting the Pt 4f XP spectrum we observe two doublets (Fig. 7), one with the $4f_{7/2}$ component at 71.2 eV and the other at 72.5 eV. The existence of these two doublets suggests the presence of a core–shell structure with the low-binding energy doublet assigned to photoelectrons emitted from Pt atoms in the core of the particles, while the high-energy component is assigned to an oxidized shell. Assignment to a particular platinum oxide is complex as several intermediate oxidation states between PtO and PtO_2 have been reported to have peak positions in the range between PtO at 71.3 eV and PtO_2 at 74.1 eV.[35]

Conversely, in Fig. 7(b) the Pd $3d_{5/2}$ component at 336.2 eV clearly indicates the formation of PdO while the Pd $3d_{5/2}$ component at 335.1 eV indicates the presence of Pd0.[36] Due to the small amount of Pt and Pd atoms deposited on the sample surface, the signal generated by photoelectrons emitted

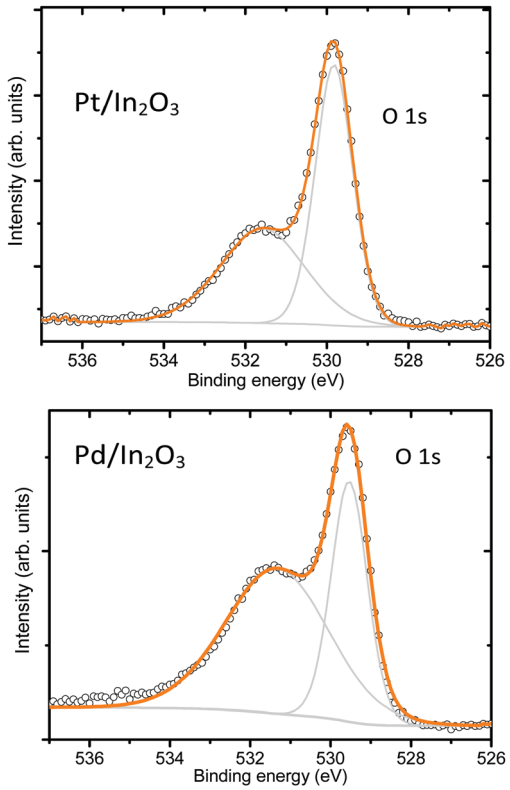

Fig. 6 O 1s core level XP spectra of Pt/In_2O_3 and Pd/In_2O_3.

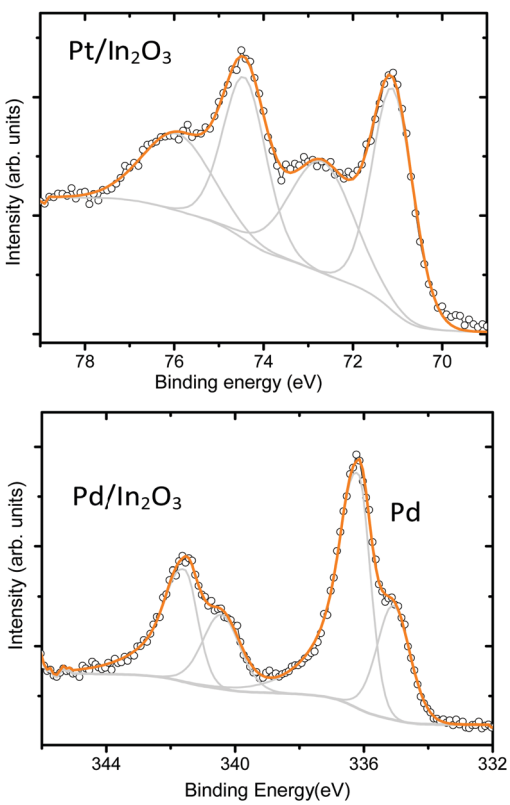

Fig. 7 XP spectrum of Pt (4f) and Pd (3d).

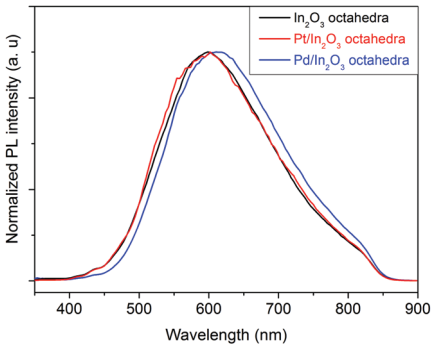

Fig. 8 PL spectra of the three sensors under dry air conditions.

from oxygen atoms bound to Pt appears in the background of the O 1s peak. If we compare the XPS results recorded on the metal decorated samples with the ones recorded on the pristine In_2O_3 samples (shown in Fig. S4 in the ESI†), we observe that the decoration with metal nanoparticles has no influence in the oxidation state of the In_2O_3 octahedra.

Furthermore, *in situ* PL experiments under air conditions have been performed on sensors employing pristine In_2O_3, Pt or Pd decorated In_2O_3 octahedra. PL spectra were obtained for sensors operated at 130 °C in a flow of dry air.

Fig. 8 shows the normalized photoluminescence spectra of different indium oxide sensors operated at 130 °C in dry air. As one can observe, for the pristine In_2O_3 and the Pt decorated In_2O_3 octahedra, there is a strong PL emission at 600 nm whereas for the Pd decorated In_2O_3 octahedra, the strong emission occurs at 610 nm. This indicates that similar types of defects are present in the three samples. Such an orange emission band is thought to have its origin in deep In interstitials present in the nanomaterial.[25]

Finally, the In_2O_3 octahedra samples were subjected to gas sensing tests using oxidizing (NO_2) and reducing (H_2) gases by means of DC resistance measurements performed at different operating temperatures (100–250 °C). All sensors were exposed to 15 minutes of a given concentration of a species, followed by a 30 minute cleaning phase in dry air. All sensors showed an increase or decrease in resistance under exposure to oxidizing or reducing gases, respectively. This implies that In_2O_3 behaves as an n-type semiconductor.

The typical response and recovery cycles of an In_2O_3 octahedra sensor toward increasing concentrations of NO_2 in dry air at 130 °C are presented in Fig. 9(a). It is well known that NO_2 is a very oxidizing gas and can be easily adsorbed on In_2O_3 structures, which leads to a decrease of the electron density of In_2O_3 and thus, a decrease in conductance.

The response and recovery time for all the concentrations is around 200 and 300 s, respectively, which is in the range of the response and recovery time of other studies of the In_2O_3 material.[37,38] Furthermore, the baseline resistance can be recovered after exposing the sensor to dry air, which shows that the sensor is completely reversible. Also, it is seen that the signal to noise ratio is excellent. Fig. 9(b) shows the dependence of the In_2O_3 octahedra sensor as a function of different

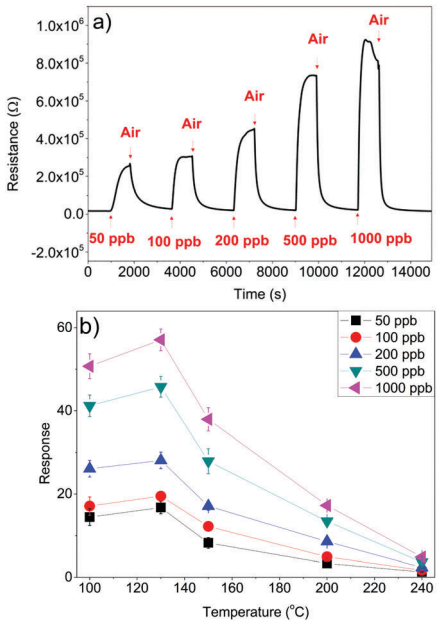

Fig. 9 (a) Response of the In_2O_3 octahedra sensor at 130 °C and (b) performance of the sensor as a function of temperature.

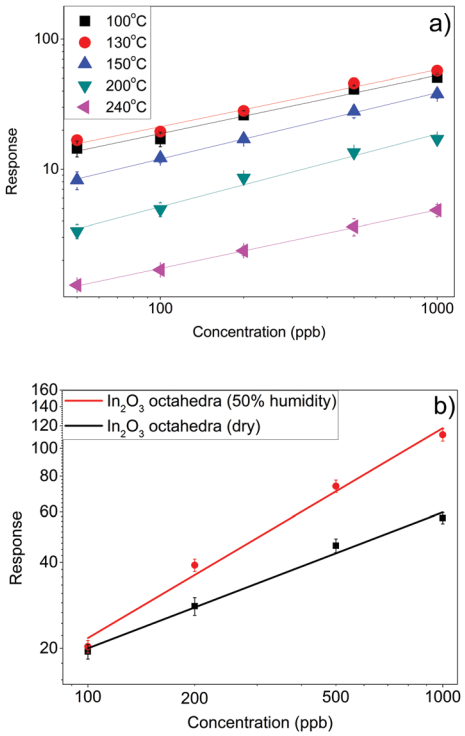

Fig. 10 (a) Response of the In_2O_3 octahedra sensor as a function of NO_2 concentration and (b) performance of the sensor at 130 °C under humid conditions (50% R.H. at 22 °C).

concentrations of NO_2 as a function of different operating temperatures.

As shown in Fig. 9(b), sensors work optimum when operated at a relatively low temperature of 130 °C. Comparing these results with those available in the literature for similar In_2O_3 structures, Mu *et al.*[17] reported a response that is 4 times lower with very slow response and recovery dynamics at room temperature for 100 ppb NO_2. Bloor *et al.*[18] reported a response that is 8 times lower at a much higher operating temperature (*i.e.* 400 °C). If we keep increasing the temperature, the performance sensors clearly worsen.

Moreover, gas sensing tests on low concentrations of NO_2 at room temperature have been performed. As shown in Fig. S6 of the ESI,† the sensor achieves a response of $R_{gas}/R_{air} = 2.46$ when exposed to 200 ppb of NO_2 in air. This shows that our nanomaterials have potential for detecting oxidizing species even when operated at room temperature.

It is important to note that our sensors are able to detect NO_2 in the range of ppb with an excellent signal to noise ratio, which means that it is possible to detect even lower concentrations of this gas (the theoretical limit of detection can be estimated at units of ppb). A correlation between the logarithm of the sensor response and the concentration was easily obtained and it is shown in Fig. 10(a). As observed, a linear fit can be obtained from the response as a function of the concentration of NO_2, with an r-square of nearly 0.99 in all the cases.

Furthermore gas sensing performance of an In_2O_3 octahedra sensor under humid conditions was examined by exposing it to NO_2(g) in a background of air at 50% relative humidity (at 22 °C) and the response was compared to that under dry conditions. The sensitivity towards NO_2 (the slope of the red curve in Fig. 10(b)) under humid conditions is significantly higher than that under dry conditions (the slope of the black curve in Fig. 10(b)).

Comparing the performance of the In_2O_3 octahedra sensors with that of sensors employing a commercially available In_2O_3 nanopowder (Sigma-Aldrich, 632317), it is observed that our nanomaterial shows a higher response under optimum working conditions, *i.e.* 130 °C, as shown in Fig. S7 of the ESI.†

Also, the performance of Pt and Pd-doped In_2O_3 octahedra sensors was examined under dry conditions. The responses obtained were extremely low compared to the response of pure In_2O_3 octahedra sensors under the optimum working conditions as presented in Table S2 of the ESI.†

Additionally, *in situ* PL experiments on the sensors under 100 ppm of NO_2 target gas have been performed at 130 °C.

Fig. S8 of the ESI† shows the PL spectra of different indium oxide sensors operated at 130 °C in the presence of 100 ppm of NO_2 in air. In this case, the strong PL emission is located at 600 nm for the three samples. This also suggests that the defects responsible for this emission are In interstitials.

As one can see, there is no significant difference between the normalized spectra under dry air shown in Fig. 8 and under NO_2 concentration. This implies that there is no change in the concentration of In interstitials on the nanomaterial upon interaction with nitrogen dioxide. Also, the change in the number of oxygen vacancies caused by the presence of NO_2 does not substantially modify the PL.

The sensing mechanism of semiconductor materials consists of two steps: the first one is the receptor function which involves the recognition of the species through gas–solid interaction, and the second one is the transduction function which

involves the change in the electrical resistance of the sensor.[13] At low operating temperatures (*i.e.*, lower than 130 °C), when In_2O_3 octahedra are exposed to NO_2(g), the gas becomes ionosorbed on the surface of the material due to its high electrophilic properties, resulting in an increase of the overall resistance of the sensor:

$$NO_{2(gas)} + e^- \rightarrow NO_{2(ads)}^-$$

The rapid decrease in the response of the sensor at temperatures higher than 130 °C can be explained be the decreasing number of active sites for the adsorption of NO_2 molecules. At higher temperatures, the amount of oxygen molecules adsorbed is greatly increased and as a consequence, the number of free active sites suitable for the adsorption of NO_2 molecules is reduced. Therefore, the response of the sensor is sharply decreased. The presence of Pt or Pd nanoparticles on the surface of In_2O_3 favors, *via* a chemical sensitization, the increase in the number of adsorbed oxygen species at the surface of the metal oxide.[13] This, once more, significantly reduces the number of active sites for the adsorption of NO_2 and explains the dramatically reduced NO_2 response observed for metal decorated samples.

Regarding the measurements under humid conditions shown in Fig. 9(b), at moderate operating temperatures (*i.e.* ≤200 °C), the interaction of ambient moisture with different metal oxide surfaces can be summarized as follows. The interaction with water vapor results in an increase of bridging hydroxyls and the formation of terminal hydroxyl groups.[39,40] Also, dissociative adsorption of water takes place on surface metal atoms (S_{lat}) giving rise to terminal OH groups. Assuming the dissociation of water molecules, hydroxyl surface groups are formed:

$$H_2O^{gas} + S_{lat} + O_{lat} \leftrightarrow (S_{lat}^+ - OH^-) + (O_{lat}H)^+ + e^-$$

In addition to the ionosorption of NO_2 on the surface of the metal oxide, the following interaction mechanism might be possible between NO_2 and the terminal hydroxyl groups:[41]

$$NO_2^{gas} + (S_{lat}^+ - OH^-) + (O_{lat}H)^+ + 2e^- \leftrightarrow (S_{lat} - NO_2^-) + H_2O^{gas} + O_{lat}^-$$

As a consequence, additional electrons are trapped *via* the conduction band of the metal oxide material, leading to an increase in NO_2 response under humid air conditions.

Furthermore, the gas sensing properties of the In_2O_3 octahedra against a reducing gas such as H_2 were investigated. The experiments were performed under the same conditions as those previously described for NO_2. Fig. 11(a) shows the response of a sensor to low concentrations of H_2 at 200 °C. The sensor resistance decreases with increasing H_2 concentration, which is in agreement with the behavior of an n-type semiconductor exposed to a reducing gas. As in the case of NO_2 sensing, the signal to noise ratio is excellent for H_2 sensing, and the sensor will be able to detect concentrations in the ppb range (the theoretical limit of detection for hydrogen is in the tens of ppb range).

In contrast to NO_2 sensing, the optimal operating temperature is higher for H_2 sensing. The best performance of the sensor is found at the highest examined temperature of 250 °C (Fig. 11(b)).

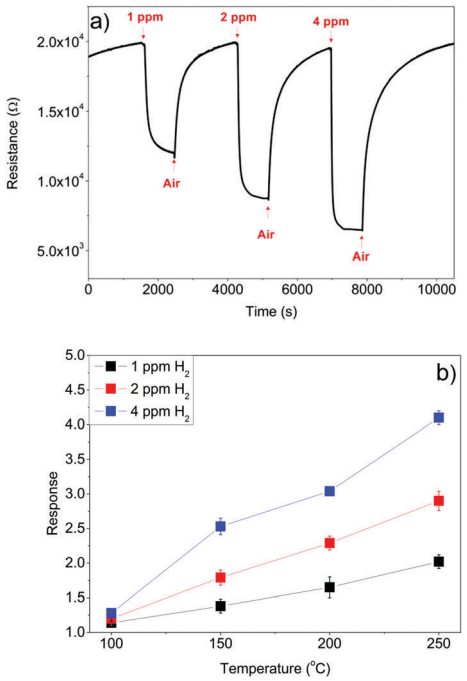

Fig. 11 (a) Response of the In_2O_3 octahedra sensor to different concentrations of H_2 at 200 °C, and (b) response of the sensor as a function of the temperature.

This suggests that we can make the sensor more selective to a target gas by properly choosing an operating temperature; low temperatures (*e.g.* 130 °C) will be optimal for NO_2 detection, while higher temperatures (*e.g.* 250 °C) are suited for H_2 detection. When operated at 130 °C and in a humid background, the sensor is very selective to selective oxidizing species because its response to 1 ppm NO_2 is more than two orders of magnitude higher than its response to 1 ppm H_2. When operated at 250 °C, the sensor becomes responsive to hydrogen. However, its response to nitrogen dioxide, although significantly decreases, remains of the same order of magnitude as that of hydrogen.

A possible approach to increase the sensitivity of In_2O_3 octahedra sensors to reducing gases like H_2 is to load In_2O_3 with different noble metal nanoparticles. In this work, Pt and Pd nanoparticles have been chosen because they are well-known sensitizers for hydrogen detection in metal oxides.[20,42]

The lack of complete baseline recovery in both cases (worsens if the operating temperature is lowered) implies that the dynamics of sensor recovery is lower for H_2 than for NO_2 (Fig. 12).

Fig. 13 shows the comparison between pure In_2O_3 octahedra and Pt/Pd-doped In_2O_3 octahedra for H_2 sensing. Both dopants improve the sensing characteristics of pure In_2O_3 octahedra. Particularly, it is easily observed that the best response in terms of H_2 sensing is achieved with the Pt-doped In_2O_3 octahedra with the optimum temperature of 200 °C, lower than that of pure In_2O_3 octahedra. Recalling that metal loading resulted in a very significant decrease in sensitivity to nitrogen dioxide (see ESI†), Pt loading, in contrast, facilitates the selective detection of H_2.

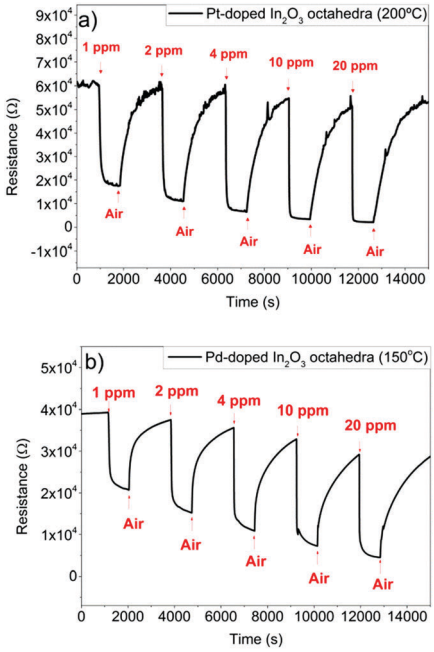

Fig. 12 (a) Response of the Pt-doped In_2O_3 octahedra sensor to different concentrations of H_2 at 200 °C, and (b) response of the Pd-doped In_2O_3 octahedra to different concentrations of H_2 at 150 °C.

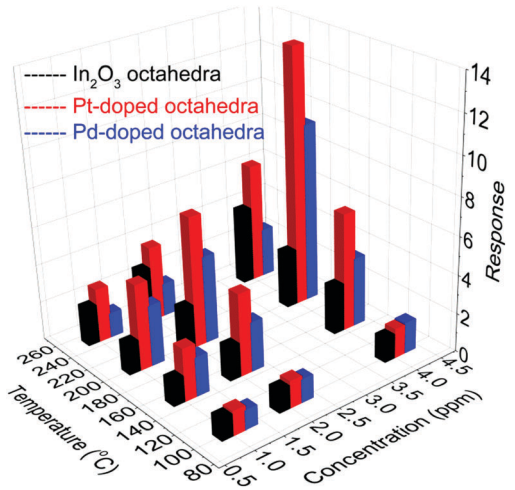

Fig. 13 Performance of the undoped and Pt/Pd-doped In_2O_3 octahedra sensors as a function of the operating temperature for H_2.

Moreover, the performance of Pt-doped In_2O_3 sensors operating in a humid background has been tested. The sensors operated at 200 °C were exposed to different concentrations of H_2 gas (1, 2, 4, 10 and 20 ppm) in a background of air at 50% relative humidity (at 22 °C) as shown in Fig. 14. The sensor under 50% humidity shows significantly lower sensitivity (0.44 ppm^{-1}) than the sensor under dry conditions (0.72 ppm^{-1}).

Also, the response to H_2 at 250 °C of Pt–In_2O_3 octahedra sensors is one order of magnitude higher than that of the same sensors to NO_2 gas, as can be deduced from Table S1 in the ESI.† In other words, sensors become selective to reducing species (*e.g.* H_2) by increasing the operating temperature

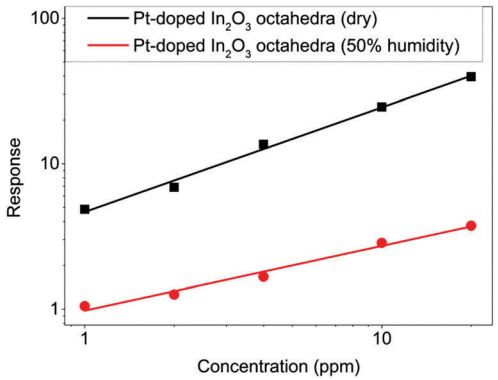

Fig. 14 Comparison between the responses of the Pt-doped sensor under dry and humid conditions at 200 °C.

and decorating the material with noble metal nanoparticles such as Pt.

It is generally accepted that reducing gases change surface conductivity due to a change in the oxidation state of the material. The fact that there is a sharp decrease in the response of the Pt-doped In_2O_3 sensor when exposed to H_2 gas with 50% of relative humidity can be explained as follows: at relatively low temperatures, vapors of both H_2 and H_2O interact in the same way with the surface of the material, creating new OH groups and consuming the bridging oxygen atoms. As a consequence, the combined interaction of hydrogen and water vapors with the surface becomes competitive.[39] Therefore, the response of the sensor is greatly decreased as shown in Fig. 14.

As previously stated, the sensing mechanism of n-type sensors is based on the variation of the electrical resistance of the sensing element, which depends basically on the gas atmosphere, the operating temperature and morphology of the sensing material among other factors. When the sensor is exposed to dry air, oxygen molecules adsorb on the surface of the material, capturing electrons of the conduction band. This creates a depletion layer derived from the adsorbed oxygen. As H_2 is introduced in the measurement cell, H_2 molecules react with the chemisorbed oxygen, releasing an electron back to the semiconductor, and thus, reducing the resistance of the sensor:[39]

$$H_2 + O^- \rightarrow H_2O + e^-$$

However, we have experimentally seen that modifying the bare oxide with noble metal nanoparticles greatly enhances the response towards reducing gases. In this case, the gas–solid interaction that involves the receptor function is the catalytic oxidation of the target gas over the grain surface. When H_2 molecules are in contact with the metal nanoparticles, they dissociate into H atoms that can spill-over to the semiconductor surface to react with the adsorbed oxygen. Therefore, the addition of the metal nanoparticle favors the reaction of the target gas with the semiconductor oxide *via* catalytic oxidation (chemical sensitization). In that way, the metal additive facilitates the interaction between the gas species and the semiconductor oxide. This type of interaction occurs mainly in the Pt-doped sensors.[13]

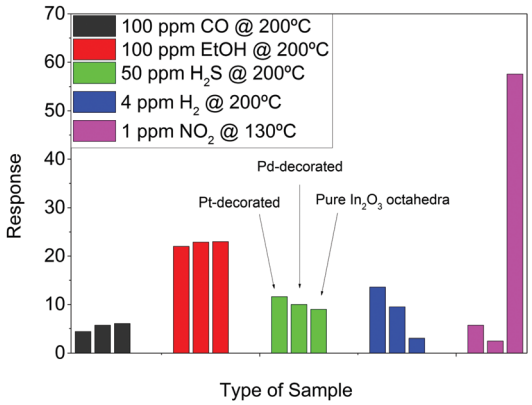

Fig. 15 Comparison between the responses of the Pt-doped, Pd-doped and pure In_2O_3 octahedra to several gases. Each colour represents a different gas. For each set of columns, the left one represents Pt-decorated In_2O_3 octahedra, the middle one represents Pd-decorated In_2O_3 octahedra and the right one represents pure In_2O_3 octahedra.

In a different mechanism, the metal additive in the oxidized state acts as a strong electron acceptor from the oxide creating a space charge layer. Then, the additive is reduced when it makes contact with the target gas; it relaxes the space charge layer by giving back the electrons to the semiconductor oxide. This type of interaction is named electronic sensitization and it occurs with noble metals like Pd. When Pd is exposed to dry air, it forms a stable metal oxide (PdO) that interacts with the In_2O_3 octahedra. When in contact with H_2, they are converted back to the metallic state (Pd) resulting in the disappearance of the electronic interaction with In_2O_3.[42] The results of the XPS analysis performed over the samples and shown in Fig. 7 confirm the presence of PtO and PdO on our sensors.

The reason why the response of the Pd-doped sensor is lower than the response of the Pt-doped one might be that the behaviour of the latter is a combination of the chemical sensitization and the electronic sensitization stated above.

In addition to the above-discussed chemical and electronic sensitization mechanisms, sensor response is also influenced by the amount of metal loading. However, the sputtering process was conducted in order to obtain nanoparticles with near to optimal sizes, according to previous studies.[27,42]

To further study the selectivity, all sensors were exposed to CO, EtOH, H_2S, H_2 and NO_2, as shown in Fig. 15.

In Fig. 15, one can see the response of the three types of materials exposed to several gases/vapors under their optimum working conditions. As observed, the best response is obtained for the pure In_2O_3 octahedra exposed to NO_2 at a relatively low temperature (130 °C). Furthermore, a good response to ethanol vapors is also observed. However, the sensing temperature is much higher than that for NO_2 and the concentration is two orders of magnitude higher.

If we focus only on the reducing species, we can see that at the same working temperature (200 °C), Pt-decorated sensors are able to detect 4 ppm of H_2 with a good response, if we take into account that hydrogen concentration is nearly two orders of magnitude lower than that of EtOH, CO and H_2S.

Conclusions

We have developed a facile method to synthesize high crystalline In_2O_3 octahedra at high temperatures, whose face size is around 500 nm. Furthermore, an easy way to decorate such nanostructures with noble metal nanoparticles has been shown. XPS measurements have shown that the metal nanoparticles have a core–shell structure in which the core of the particle corresponds to the metal and the shell corresponds to the oxidized metal.

Additionally, we can say that pure In_2O_3 octahedra are excellent for detecting NO_2 gas with outstanding sensitivity (0.43 ppb^{-1}) at low temperatures (130 °C), while the response to H_2 remains two orders of magnitude lower under the same conditions. In addition, the presence of humidity increases the sensitivity to NO_2 and, at the same time, reduces the response to H_2, which results in increased selectivity. This makes our sensor an excellent candidate to detect, in a selective way, oxidizing gases such as NO_2 at low operating temperatures, even showing potential for room temperature operation, with excellent sensitivity even in the presence of humidity.

Furthermore, increasing the operating temperature and loading the octahedra with Pt, result in the quenching of the response to NO_2 and in an increase in the response towards H_2. In this way, one can make the sensor more selective to reducing gases such as H_2. However, in this case the presence of ambient humidity negatively influences the response of the sensor.

As a consequence, our nanomaterial can be made selective to oxidizing or reducing gases by varying the operating temperature and by metal loading.

These significant differences revealed by this study suggest that engineering the morphology and the crystallinity of the material can be really useful and need further research, since it may become an effective strategy for enhancing the sensitivity and selectivity of In_2O_3 sensors.

Acknowledgements

This work has been funded in part by MINECO under grant no. TEC2015-71663-R. S. Roso and A. Urakawa would like to thank MINECO for support through Severo Ochoa Excellence Accreditation 2014-2018 (SEV-2013-0319). C. Bittencourt is a Research Associate of the National Funds for Scientific Research (FRS-FNRS, Belgium). S. Roso is also grateful for the URV-ICIQ fellowship. E. Llobet is supported by the Catalan Institute for Research and Advanced Studies *via* the ICREA Academia Award. S. Roso is also grateful to Dr Raúl Calavia for his help in conducting the experiments.

References

1 S. Pati, S. B. Majumder and P. Banerji, *J. Alloys Compd.*, 2012, **541**, 376–379.
2 D. Meng, N. M. Shaalan, T. Yamazaki and T. Kikuta, *Sens. Actuators, B*, 2012, **169**, 113–120.
3 M. I. Baraton, L. Merhari, H. Ferkel and J. F. Castagnet, *Mater. Sci. Eng., C*, 2002, **19**, 315–321.

4 D. Caruntu, K. Yao, Z. Zhang, T. Austin, W. Zhou and C. J. O'Connor, *J. Phys. Chem. C*, 2010, **114**, 4875–4886.
5 X. C. Wu, J. M. Hong, Z. J. Han and Y. R. Tao, *Chem. Phys. Lett.*, 2003, **373**, 28–32.
6 C. H. Liang, G. W. Meng, Y. Lei, F. Phillipp and L. D. Zhang, *Adv. Mater.*, 2001, **13**, 1330–1333.
7 X.-P. Shen, H.-J. Liu, X. Fan, Y. Jiang, J.-M. Hong and Z. Xu, *J. Cryst. Growth*, 2005, **276**, 471–477.
8 X. Xu, D. Wang, W. Wang, P. Sun, J. Ma, X. Liang, Y. Sun, Y. Ma and G. Lu, *Sens. Actuators, B*, 2012, **171–172**, 1066–1072.
9 M. Shi, F. Xu, K. Yu, Z. Zhu and J. Fang, *J. Phys. Chem. C*, 2007, **111**, 16267–16271.
10 K. Yao, D. Caruntu, S. Wozny, R. Huang, Y. H. Ikuhara, B. Cao, C. J. O'Connor and W. Zhou, *J. Mater. Chem.*, 2012, **22**, 7308–7313.
11 L. Liu, T. Zhang, S. Li, L. Wang and Y. Tian, *Mater. Lett.*, 2009, **63**, 1975–1977.
12 S. Vallejos, P. Umek, T. Stoycheva, F. Annanouch, E. Llobet, X. Correig, P. De Marco, C. Bittencourt and C. Blackman, *Adv. Funct. Mater.*, 2013, **23**, 1313–1322.
13 N. Yamazoe, G. Sakai and K. Shimanoe, *Catal. Surv. Asia*, 2003, **7**, 63–75.
14 D. Zhang, Z. Liu, C. Li, T. Tang, X. Liu, S. Han, B. Lei and C. Zhou, *Nano Lett.*, 2004, **4**, 1919–1924.
15 Z. Q. Zheng, L. F. Zhu and B. Wang, *Nanoscale Res. Lett.*, 2015, **10**, 293.
16 F. Li, J. Jian, R. Wu, J. Li and Y. Sun, *J. Alloys Compd.*, 2015, **645**, 178–183.
17 X. Mu, C. Chen, L. Han, B. Shao, Y. Wei, Q. Liu and P. Zhu, *J. Alloys Compd.*, 2015, **637**, 55–61.
18 L. G. Bloor, J. Manzi, R. Binions, I. P. Parkin, D. Pugh, A. Afonja, C. S. Blackman, S. Sathasivam and C. J. Carmalt, *Chem. Mater.*, 2012, **24**, 2864–2871.
19 X. Xu, X. Li, H. Zhang, C. Feng, C. Wang, F. Liu, Y. Sun, P. Sun and G. Lu, *RSC Adv.*, 2015, **5**, 30297–30302.
20 W. Yang, P. Wan, X. Zhou, J. Hu, Y. Guan and L. Feng, *Sens. Actuators, B*, 2014, **201**, 228–233.
21 A. Qurashi, E. M. El-Maghraby, T. Yamazaki and T. Kikuta, *Sens. Actuators, B*, 2010, **147**, 48–54.
22 A. Shanmugasundaram, B. Ramireddy, P. Basak, S. V. Manorama and S. Srinath, *J. Phys. Chem. C*, 2014, **118**, 6909–6921.
23 G. Korotcenkov, V. Brinzari, S. H. Han and B. K. Cho, *Mater. Chem. Phys.*, 2016, **175**, 188–199.
24 S.-T. Jean and Y.-C. Her, *Cryst. Growth Des.*, 2010, **10**, 2104–2110.
25 M. Kumar, V. N. Singh, F. Singh, K. V. Lakshmi, B. R. Mehta and J. P. Singh, *Appl. Phys. Lett.*, 2008, **92**, 171907.
26 K. Yadav, B. R. Mehta and J. P. Singh, *RSC Adv.*, 2015, **5**, 1581–1586.
27 N. Ma, K. Suematsu, M. Yuasa and K. Shimanoe, *ACS Appl. Mater. Interfaces*, 2015, **7**, 15618–15625.
28 S. Roso, F. Güell, P. R. Martínez-Alanis, A. Urakawa and E. Llobet, *Sens. Actuators, B*, 2016, **230**, 109–114.
29 A. Qurashi, E. M. El-Maghraby, T. Yamazaki and T. Kikuta, *J. Alloys Compd.*, 2009, **480**, L9–L12.
30 A. Gurlo, *Nanoscale*, 2011, **3**, 154–165.
31 L. S. Kibis, A. I. Stadnichenko, S. V. Koscheev, V. I. Zaikovskii and A. I. Boronin, *J. Phys. Chem. C*, 2012, **116**, 19342–19348.
32 F. E. Annanouch, Z. Haddi, S. Vallejos, P. Umek, P. Guttmann, C. Bittencourt and E. Llobet, *ACS Appl. Mater. Interfaces*, 2015, **7**, 6842–6851.
33 D. V. Shinde, D. Y. Ahn, V. V. Jadhav, D. Y. Lee, N. K. Shrestha, J. K. Lee, H. Y. Lee, R. S. Mane and S.-H. Han, *J. Mater. Chem. A*, 2014, **2**, 5490–5498.
34 J. Gan, X. Lu, J. Wu, S. Xie, T. Zhai, M. Yu, Z. Zhang, Y. Mao, S. C. I. Wang, Y. Shen and Y. Tong, *Sci. Rep.*, 2013, **3**, 1021.
35 J. J. Blackstock, D. R. Stewart and Z. Li, *Appl. Phys. A: Mater. Sci. Process.*, 2005, **80**, 1343–1353.
36 G. B. Hoflund, H. A. E. Hagelin, J. F. Weaver and G. N. Salaita, *Appl. Surf. Sci.*, 2003, **205**, 102–112.
37 W. Zheng, X. Lu, W. Wang, Z. Li, H. Zhang, Z. Wang, X. Xu, S. Li and C. Wang, *J. Colloid Interface Sci.*, 2009, **338**, 366–370.
38 A. Gurlo, M. Ivanovskaya, N. Bârsan, M. Schweizer-Berberich, U. Weimar, W. Göpel and A. Diéguez, *Sens. Actuators, B*, 1997, **44**, 327–333.
39 R. G. Pavelko, H. Daly, C. Hardacre, A. A. Vasiliev and E. Llobet, *Phys. Chem. Chem. Phys.*, 2010, **12**, 2639–2647.
40 P. A. Thiel and T. E. Madey, *Surf. Sci. Rep.*, 1987, **7**, 211–385.
41 A. Stănoiu, C. E. Simion and S. Somăcescu, *Sens. Actuators, B*, 2013, **186**, 687–694.
42 F. E. Annanouch, Z. Haddi, M. Ling, F. Di Maggio, S. Vallejos, T. Vilic, Y. Zhu, T. Shujah, P. Umek, C. Bittencourt, C. Blackman and E. Llobet, *ACS Appl. Mater. Interfaces*, 2016, **8**, 10413–10421.

ARTICLE

3. Enhanced detection of nitrogen dioxide via combined heating and pulsed UV operation of indium oxide nano-octahedra

O. Gonzalez, S. Roso, X. Vilanova, E. Llobet,

Beilstein Journal of Nanotechnology 7(1):1507-1518,

October 2016

This is our first journal paper reporting the pulsed-UV excitation of metal oxide gas sensors, which is the core of the present thesis. Here we developed the experimental setup that allowed us to control the temperature of the sensing layer and the UV source. Here, this approach was applied to the sensors that were developed and discussed in the previous article of this thesis.

In this paper, we report on the use of combined heating and pulsed UV light activation of indium oxide gas sensors for enhancing their performance in the detection of nitrogen dioxide in air. These results are compared to the standard, constant temperature operation of the sensor. Specifically, we applied either UV light excitation exclusively (i.e., sensor was kept at RT) or mild heating (e.g., 50 °C or 100 °C) together with pulsed UV light irradiation. The UV source consisted of a commercially available, 325 nm UV diode.

This resulted in an up to 80-fold enhancement in sensitivity to nitrogen dioxide. In addition, our approach enables saving power consumption and significantly reducing response time for a lower sensor activation temperature. These results are achieved by exploiting the dynamics of sensor response under pulsed UV light, which convey important information for the quantitative analysis of nitrogen dioxide.

BEILSTEIN JOURNAL OF NANOTECHNOLOGY

Enhanced detection of nitrogen dioxide via combined heating and pulsed UV operation of indium oxide nano-octahedra

Oriol Gonzalez[1], Sergio Roso[1,2], Xavier Vilanova[1] and Eduard Llobet[*1]

Full Research Paper

Open Access

Address:
[1]MINOS-EMaS, Universitat Rovira i Virgili, Avda. Països Catalans, 26, 43007, Tarragona, Spain and [2]ICIQ, Institute of Chemical Research of Catalonia, Avda. Països Catalans, 16, 43007, Tarragona, Spain

Email:
Eduard Llobet[*] - eduard.llobet@urv.cat

* Corresponding author

Keywords:
dynamic gas sensing; indium oxide; nitrogen dioxide; pulsed UV light; UV-activated metal oxide

Beilstein J. Nanotechnol. **2016,** *7,* 1507–1518.
doi:10.3762/bjnano.7.144

Received: 29 June 2016
Accepted: 05 October 2016
Published: 25 October 2016

This article is part of the Thematic Series "Functional materials for environmental sensors and energy systems".

Guest Editor: M. Penza

Abstract

We report on the use of combined heating and pulsed UV light activation of indium oxide gas sensors for enhancing their performance in the detection of nitrogen dioxide in air. Indium oxide nano-octahedra were synthesized at high temperature (900 °C) via vapour-phase transport and screen-printed onto alumina transducers that comprised interdigitated electrodes and a heating resistor. Compared to the standard, constant temperature operation of the sensor, mild heating (e.g., 100 °C) together with pulsed UV light irradiation employing a commercially available, 325 nm UV diode (square, 1 min period, 15 mA drive current signal), results in an up to 80-fold enhancement in sensitivity to nitrogen dioxide. Furthermore, this combined operation method allows for making savings in power consumption that range from 35% to over 80%. These results are achieved by exploiting the dynamics of sensor response under pulsed UV light, which convey important information for the quantitative analysis of nitrogen dioxide.

Introduction

Technological barriers related to sensor performance and power consumption are currently limiting the implementation of widely distributed, smart wireless sensor systems that can be deployed and then remain in operation with no further human intervention. Overcoming these barriers entails developing gas sensors featuring low cost, small size, enhanced sensitivity, selectivity, stability and low power consumption. The task of indoor and outdoor air pollution monitoring would certainly benefit from the implementation of grids of wireless sensing nodes [1]. In particular, radio frequency identification (RFID), has been identified as a widely extended technology in which the integration of one or more gas sensors in a tag, would turn the tag into a wireless sensor that could be easily read with an inexpensive reader via a radiofrequency link [2,3]. Nowadays, distributed wireless boxes to monitor air pollution already exist. These employ electrochemical gas sensors that are ultra-low power and very sensitive. However, such systems do not meet the requirements of personalized or indoor air pollution monitoring because of the high cost and size of the sensors.

In environmental pollution monitoring, the detection of nitrogen dioxide is of particular interest because this pollutant is known

to be a source of acid rain and fog, to catalyse the formation of ozone and to trigger diseases of the respiratory system in humans [4,5]. The combustion of transportation fuels is responsible for over 50% of the anthropogenic emissions of nitrogen oxides. Some metal oxide semiconductors have been found to be highly sensitive to nitrogen dioxide levels in air [6,7] and there are commercially available metal oxide NO_2 sensors [8]. In particular, many authors have reported nanostructured indium oxide as a promising material for the sensitive detection of nitrogen dioxide at trace levels in air [9-12]. However, the facts that metal oxides are known for their lack of selectivity and this, combined with their normally high operating temperatures, have prevented their integration as gas sensitive material in the tags of RFID sensing systems.

However, there have been reports of gas sensors using ultraviolet (UV) activated metal oxides [13-16]. These works employ UV light as an energy efficient alternative to heating for activating chemical reactions occurring at the surface of metal oxides during gas detection. This approach could significantly cut power consumption in metal oxides and, therefore, help re-considering the suitability of these materials for integrating wireless sensors. Integrating gas sensors with UV LEDs would certainly increase the cost of production (LED and packaging). However, these extra costs could be kept at a fraction of those incurred when producing a standard MOX sensor if UV-activated sensors were produced in big numbers. UV light has often been used exclusively for promoting desorption of surface species from the sensing layer, rather than to modify its sensing properties. It is only very recently that UV activation in addition to heating has been explored for improving sensitivity and selectivity of metal oxides [17].

In this paper the use of heating and pulsed UV irradiation is investigated in view of enhancing the sensitivity and lowering power consumption of a resistive, nitrogen dioxide sensor that employs semiconducting indium oxide nano-octahedra as gas-sensitive nanomaterial (a detailed description of the sensor fabrication procedure can be found in the Experimental section). The dynamics of sensor response towards different concentrations of nitrogen dioxide under pulsed UV light activation are presented and discussed. Dynamic response is employed to obtain new response features that correlate well with nitrogen dioxide concentration. The usefulness of the technique is assessed in terms of sensitivity enhancement and reduction in power consumption.

Results and Discussion

Morphology and crystalline phase analysis

SEM was performed to study the morphology of the indium oxide nanomaterial. Figure 1 shows a SEM micrograph of the as-grown material. The image shows that the nanomaterial consists of well-defined octahedral shaped structures. No other morphologies are observed, which indicates the uniformity of the process. Regular octahedra consist of eight equilateral triangles, four of which meet at the same vertex. The size of the octahedra range between 200 and 500 nm. All faces are almost perfectly smooth and without any visible structural defects.

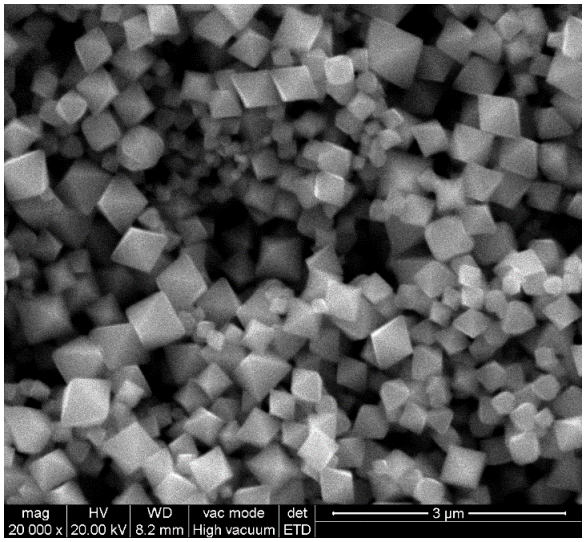

Figure 1: SEM micrograph of as-grown indium oxide nano-octahedra.

The crystalline phase was investigated by means of X-ray diffraction (XRD). As shown in Figure 2, the as-grown samples show the typical features of cubic In_2O_3. The XRD pattern for a commercially available, cubic phase indium oxide has been added for comparison. No peaks belonging to other materials or impurities were found.

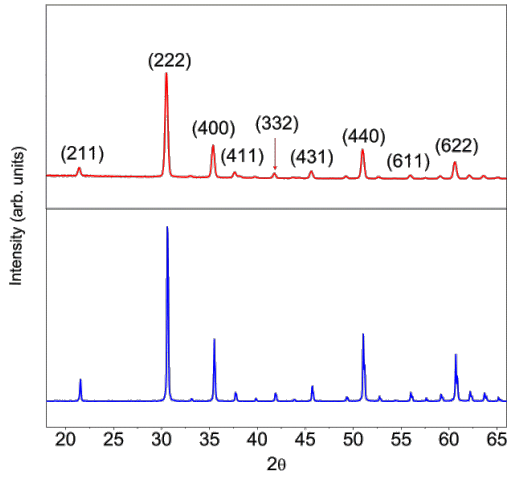

Figure 2: XRD patterns of the pure In_2O_3 octahedra (top) and a commercially available In_2O_3 powder (bottom). Adapted from [19].

Gas sensing analysis

Static sensor operation

At first, the response of the nanomaterial to nitrogen dioxide was measured when the sensor was operated at room temperature (22 °C) and in the absence of UV light. Under these conditions, the sensor response was weak and not reversible. Figure 3 shows the evolution of the resistance of the sensor for response and recovery cycles to successively increasing concentrations of nitrogen dioxide that ranged between 50 ppb and 1 ppm. The duration of gas exposure and cleaning cycles was set to 15 and 30 min, respectively. The sensor resistance monotonically increases with the nitrogen dioxide concentration and when the sensor is flushed with pure dry air during the cleaning phases, its baseline resistance is never regained. Nitrogen dioxide is an oxidizing species. When a nitrogen dioxide molecule gets adsorbed on the indium oxide, it traps electronic charge from the conduction band of the nanomaterial (which is an *n*-type semiconductor), which results in an increase in the resistance of the sensor. This ionosorption process is a thermally activated process and room temperature is rather low, which explains the weak intensity of response to nitrogen dioxide under these conditions. Furthermore, at such a low operating temperature, most of the ionosorbed nitrogen dioxide molecules remain attached to the surface on indium oxide during the cleaning phases with dry air, which results in irreversible changes in sensor resistance.

In the second step, the sensor was operated at temperatures well above room temperature by driving a constant current through its resistive heating element. Figure 4 shows response and recovery cycles during exposure to increasing concentrations of nitrogen dioxide when operated at 130 °C and without UV irradiation. Once more, the durations of gas exposure and cleaning cycles were set to 15 and 30 min, respectively. Different operating temperatures between 100 and 250 °C were investigated

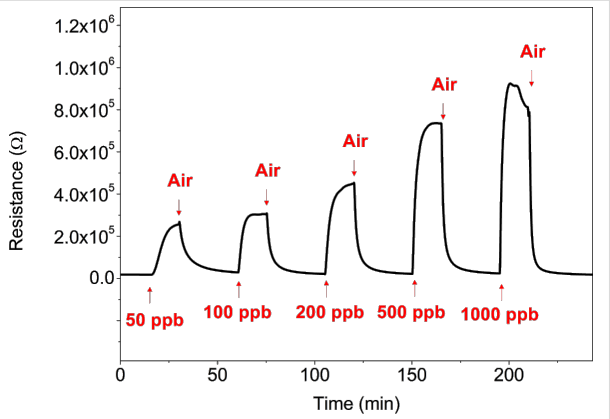

Figure 4: Successive response and recovery cycles during exposure to increasing concentrations of nitrogen dioxide of an indium oxide sensor operated at 130 °C. No UV irradiation was applied during these tests. Reproduced from [19].

and it was found that, when operated at 130 °C, the sensor showed the highest response to nitrogen dioxide. Furthermore, at this operating temperature, the sensing mechanism was fully reversible, since the sensor was able to regain its baseline resistance value during the cleaning phases. Sensor response, defined as the ratio between the sensor resistance in nitrogen dioxide and sensor resistance in dry air, ranged between 16.3 (50 ppb) and 60 (1 ppm). Response and recovery times, defined as the time needed to reach 90% of resistance change varied with nitrogen dioxide concentration between 4 and 8 min. Sensitivity to nitrogen dioxide, defined as the slope of the calibration curve in the range from 50 to 1000 ppb was 0.046 ± 0.004 ppb^{-1}.

Prior to employ UV activation for the detection of nitrogen dioxide, the effect of a sudden irradiation of the indium oxide nanomaterial with UV light was investigated. For this, the evolution of sensor resistance was monitored when a UV diode

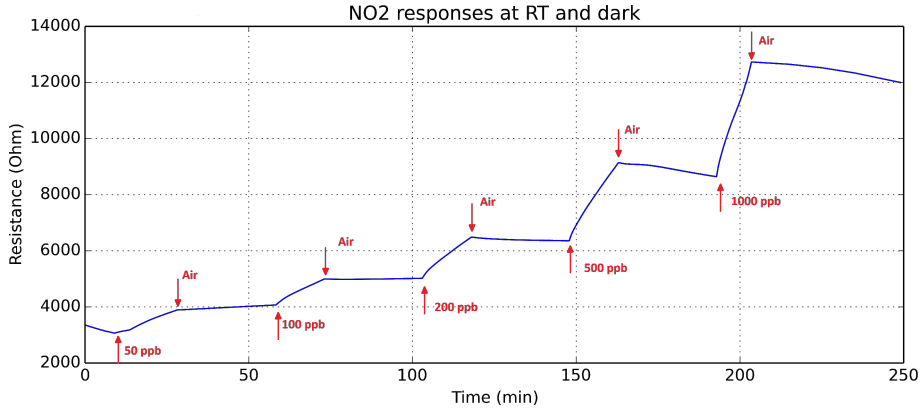

Figure 3: Successive response and recovery cycles during exposure to increasing concentrations of nitrogen dioxide of an indium oxide sensor operated at room temperature. No UV irradiation was applied during these tests. Reproduced from [19].

was switched on at $t = 0$. No current was driven through the heating element of the sensor during this test. The evolution of sensor resistance is shown in Figure 5. Upon exposure to UV light, there is a significant drop in sensor resistance. This resistance change tails off over many hours indicating that the sudden exposure to UV light results in the triggering of changes in the nanomaterial that have slow dynamics. The decrease in sensor resistance can be explained by different mechanisms.

- Electrons in the valence band of indium oxide absorb energy from the UV light to jump to the conduction band. The bandgap of cubic indium oxide is about 3 eV and the 325 nm UV diode employed (3.8 eV) should allow these transitions to occur. Such transitions decrease the resistance of an n-type semiconductor film.
- UV light has been reported to act as a cleaner of the surface of metal oxides by promoting the desorption of adsorbed surface species. When an indium oxide sensor is in the presence of oxidizing species (e.g., oxygen, nitrogen dioxide), UV irradiation will result in the lowering of the amount of oxygen and/or nitrogen dioxide adsorbates. Since indium oxide is an *n*-type semiconductor, the desorption of oxidizing species from its surface translates into an increase in the number of free charge carriers and, thus, in a decrease in the DC resistance of the gas sensor [18,19].
- Furthermore, the partial removal of oxygen adsorbates may trigger the diffusion of bulk oxygen towards the surface, especially when the UV irradiated metal oxide sensor is operated at temperatures well above room temperature [20].

These mechanisms are reversible and when the UV light diode is switched off, the sensor eventually returns to its original baseline resistance value. However, the third mechanism has rather slow dynamics and may be responsible for the long time needed (few hours) for stabilizing the DC resistance of a sensor operated at constant temperature, after a sudden change in UV irradiation.

The UV diode was switched on and the sensor was left for 8 h under a flow of pure dry air. Then, the response and recovery of the sensor to different concentrations of nitrogen dioxide was studied under constant UV irradiation, without driving current through the sensor heating element. Figure 6 shows these response and recovery transients.

Unlike when the sensor is operated at room temperature without UV irradiation, under constant UV light, the sensor tends to regain its baseline resistance. However, response intensity to nitrogen dioxide is smaller and response and recovery dynamics are slower than when the sensor is operated at 130 °C without UV irradiation. In fact, the recovery phase in every response/recovery cycle shown in Figure 6, which is set to 30 min, is not long enough for the baseline to be fully regained. This behaviour can be explained as follows. UV light helps desorbing ionosorbed species from the surface of indium oxide [18]. Therefore, during the cleaning phases in which the sensor is flushed with dry air, UV light helps desorbing nitrogen dioxide adsorbates, reducing the indium oxide and decreasing the resistance of the sensor. During the response phases, there is a competition between the ionosorption of new nitrogen dioxide molecules from the ambient onto the surface of indium oxide and the desorption of nitrogen dioxide adsorbates caused by UV irradiation. The equilibrium concentration of nitrogen dioxide adsorbates depends on the ambient concentration of nitrogen dioxide, which results in increasing sensor resistance values for increasing concentrations of this pollutant gas. Table 1 summarises and compares the detection of nitrogen dioxide under these two different operation modes (i.e., constant tem-

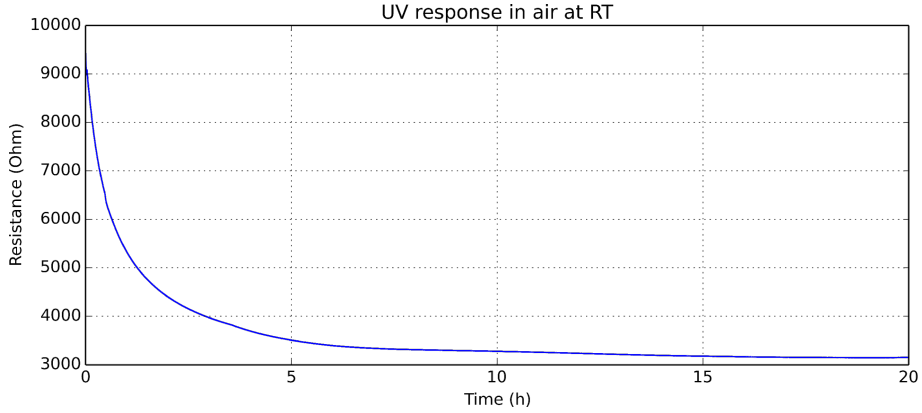

Figure 5: Resistance change of an indium oxide sensor suddenly exposed to UV light (the UV diode is switched on at time $t = 0$). The heating element of the sensor is not used in this test.

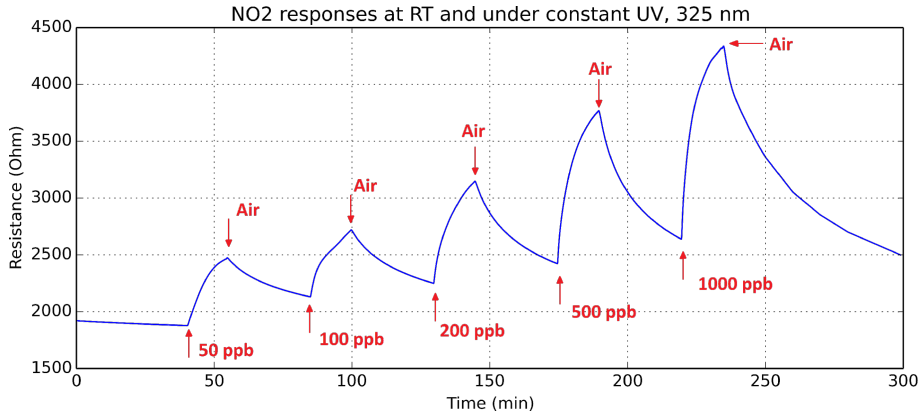

Figure 6: Response and recovery cycles of an indium oxide sensor exposed to different concentrations of nitrogen dioxide under constant UV light. The heating element of the sensor is not used in this test. The duration of exposure and recovery cycles was set to 15 and 30 min, respectively. Adapted from [19].

Table 1: Comparison of sensor response intensity, response and recovery times for an indium oxide sensor under two different operating conditions.

	response to NO_2, 500 ppb (R_{NO2}/R_{air})	response time (min)	recovery time (min)
sensor operated at 130 °C, UV diode off	47	4.5	5.3
sensor operated under constant UV light, heating element off	1.8	≈15	>30

perature and constant UV irradiation). From the results in this table, it can be derived that operating the sensor at 130 °C is more favourable than operating it under constant UV irradiation for detecting nitrogen dioxide.

Dynamic sensor operation

The effect of UV irradiation on sensor response was further studied under a dynamic operation mode. In that case, during response and recovery cycles, the UV diode was periodically switched on and off by employing a square driving current signal with a period set to 1 min, while the sensor was operated at a given constant temperature (room temperature, 50 °C or 100 °C). Both in the presence of nitrogen dioxide (detection phase) or in pure dry air (cleaning phase), the sensor resistance increases while the UV diode is switched off and decreases while the UV diode is switched on, which results in the overall sensor response presenting a ripple. This ripple appears because UV light reduces indium oxide, which tends to re-oxidise when UV light is switched on. This can be seen in Figure 7, in which a sensor is operated at room temperature under pulsed UV light.

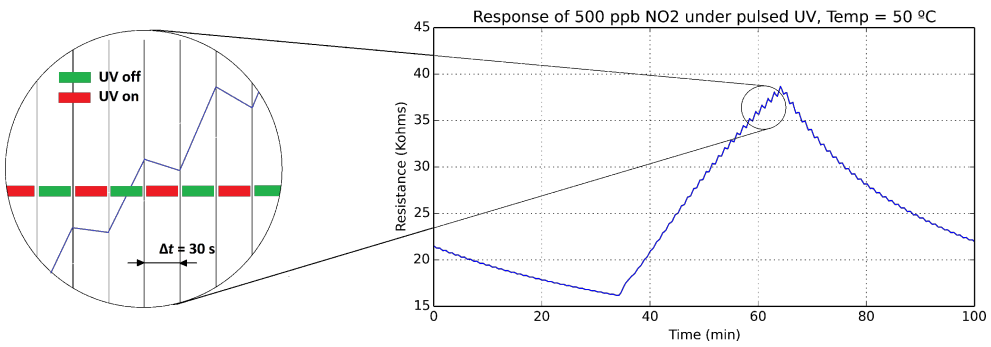

Figure 7: Successive recovery, response (nitrogen dioxide, 500 ppb) and recovery cycles of an indium oxide sensor under pulsed UV light. The heating element of the sensor is not used in this test. The inset shows an enlarged area of the evolution of sensor resistance in the presence of nitrogen dioxide. While the overall trend is for the resistance to increase due to the ionosorption of nitrogen dioxide molecules on the surface of indium oxide, locally, resistance decreases appear during the semi-period periods (30 s) in which the UV light is switched on.

The dynamics of UV pulsed operation have been studied by computing the evolution of reduction and oxidation rates. The instantaneous reduction rate is computed as the local derivative of the resistance response curve during a semi-period in which the UV diode is switched on. Similarly, the instantaneous oxidation rate is the local derivative of the response curve during a semi-period in which the diode is switched off. Figure 8 illustrates how these two rates are computed.

The oxidation and reduction rates were computed for an indium oxide sensor operated at room temperature, 50 °C and 100 °C, both during nitrogen dioxide detection and recovery events. Figures 9–11 show these results when 500 ppb of nitrogen dioxide were measured.

According to what is shown in Figures 9–11, it can be derived that increasing the operating temperature of the sensor results in an increase in the rates of oxidation and reduction. If we consider now the rate of reduction (in red in Figures 9–11), its value should be negative if the surface of the sensor is reduced

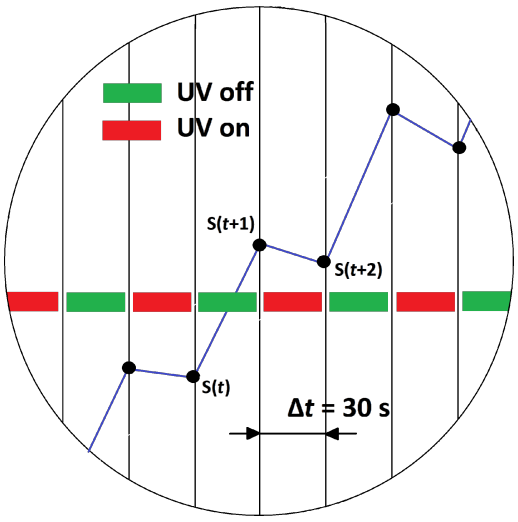

Figure 8: The instantaneous oxidation and reduction rates are defined as $R_{oxi} = [S(t + 1) - S(t)]/\Delta t$ and $R_{red} = [S(t + 2) - S(t + 1)]/\Delta t$, respectively. Where S is the curve of the evolution of sensor resistance and Δt is the semi-period in which the UV diode is kept switched on or off (Δt = 30 s).

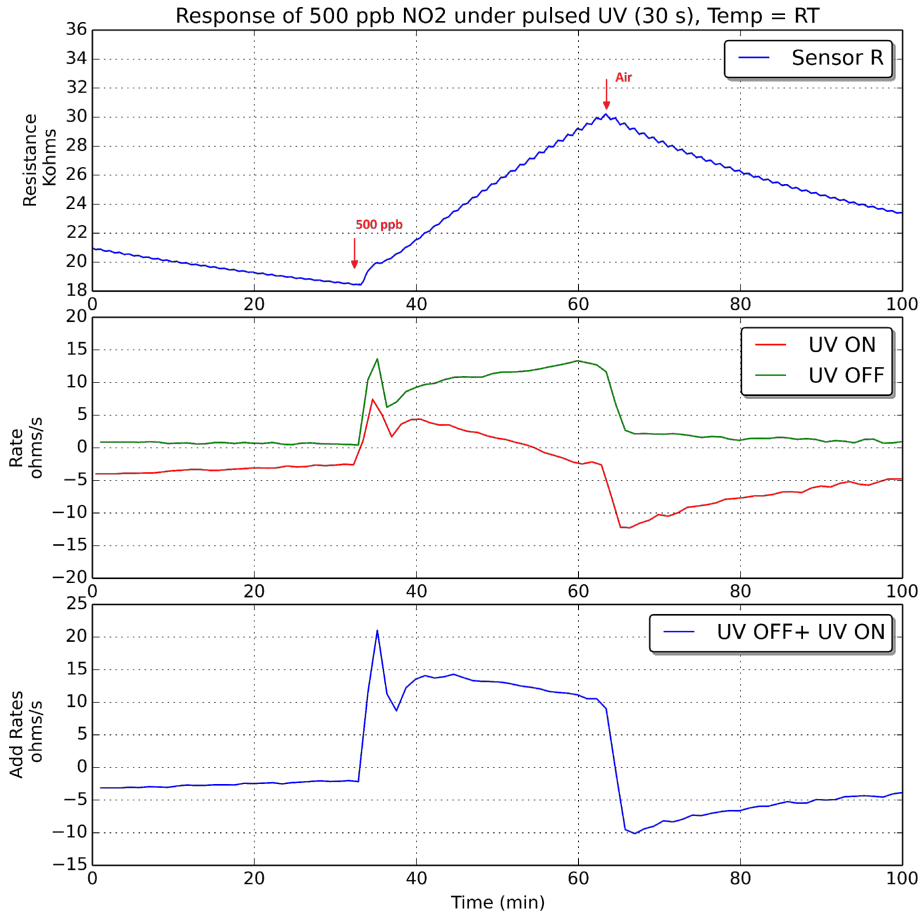

Figure 9: Indium oxide sensor response under pulsed UV irradiation. The sensor was operated at room temperature. Every panel shows the change in sensor resistance (top), the evolution of oxidation and reduction rates, which are plotted in green and red, respectively (middle), and the addition of these two rates (bottom) during the detection and recovery from an exposure to 500 ppb of nitrogen dioxide.

Beilstein J. Nanotechnol. **2016,** *7,* 1507–1518.

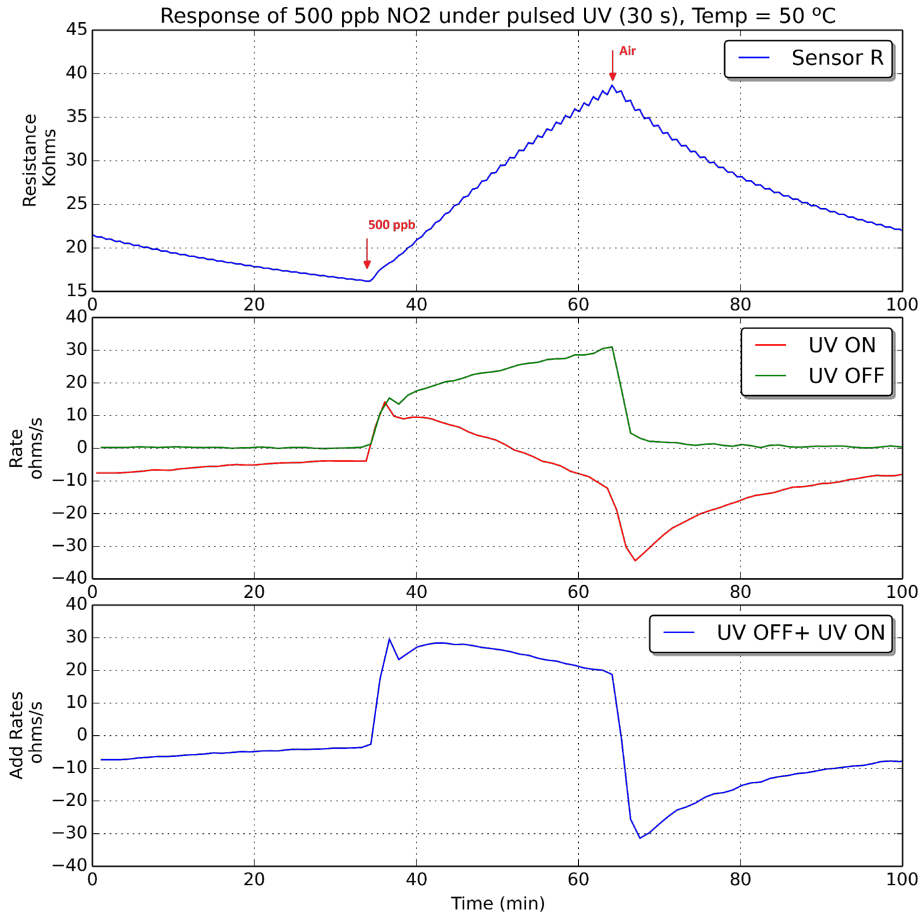

Figure 10: Indium oxide sensor response under pulsed UV irradiation. The sensor was operated at 50 °C. Every panel shows the change in sensor resistance (top), the evolution of oxidation and reduction rates, which are plotted in green and red, respectively (middle), and the addition of these two rates (bottom) during the detection and recovery from an exposure to 500 ppb of nitrogen dioxide.

during the semi-period in which the UV diode is on. However, this is not the case during the initial period after a sudden change from pure air to nitrogen dioxide diluted in air. During a time period after the injection of nitrogen dioxide, there is a fast increase in the number of nitrogen dioxide molecules ionosorbed on the surface of indium oxide, which becomes more oxidised, and this in spite of the surface cleaning effect of UV irradiation. Soon after this initial action, the rate of adsorption of new nitrogen dioxide molecules decreases and the rate of reduction becomes negative. In other words, after the initial action, during the semi-period in which the UV diode is on, the amount of ionosorbed nitrogen dioxide molecules diminishes and sensor resistance decreases. The duration of this initial action decreases if the operating temperature of the sensor increases.

At the beginning of a cleaning phase in which nitrogen dioxide is suddenly removed from the ambient of the sensor, the rate of reduction peaks at higher negative values. This is because there is a combined effect of cleaning the surface of indium oxide with UV light and flowing the sensor with pure dry air, which results in a faster rate of desorption of nitrogen dioxide adsorbates. After this initial action, as the surface becomes cleaner, the rate of reduction tails off.

If we consider now the rate of oxidation (in green in Figures 9–11), its value is positive and increases while nitrogen dioxide is present in the ambient of the sensor. When nitrogen dioxide is removed during a cleaning phase, the value of the oxidation rate decreases to zero. This is what it could be expected, because the rate of oxidation is computed when the UV diode is on. Finally, the curves appearing in the third sub-panel in Figures 9–11 show the addition of the rates of oxidation and reduction. It can be noted that these new curves are characterised by the presence of a maximum that appears at the initial stage of the transition between clean air and air in which nitrogen dioxide is diluted. Figure 12 shows the results of an experiment in which a sensor is exposed to successive response and recovery cycles to

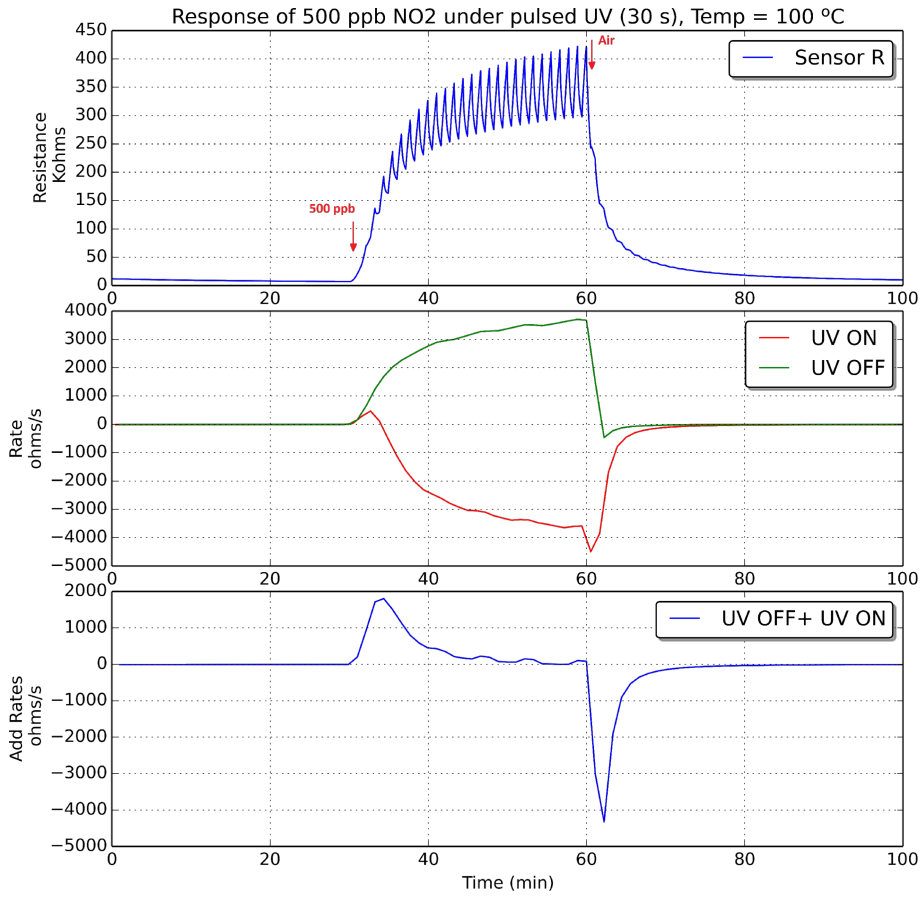

Figure 11: Indium oxide sensor response under pulsed UV irradiation. The sensor was operated at 100 °C. Every panel shows the change in sensor resistance (top), the evolution of oxidation and reduction rates, which are plotted in green and red, respectively (middle), and the addition of these two rates (bottom) during the detection and recovery from an exposure to 500 ppb of nitrogen dioxide.

increasing concentrations of nitrogen dioxide while being operated at 50 °C and under pulsed UV light (pulse duration is 30 s). The addition of the rates of oxidation and reduction shows an initial maximum, the height of which is clearly related to the concentration of nitrogen dioxide. This peak appears after each transition from pure air to air containing nitrogen dioxide.

Figure 13 shows the calibration curves obtained for the sensor response. The sensor response was measured as the intensity of the maximum of the addition curve (i.e., the sum of rates of reduction and oxidation) as a function of nitrogen dioxide concentration. These curves show that there is a quite linear behaviour of the response for the range of nitrogen dioxide concentrations measured and also that the sensitivity (i.e., slope of these calibration curves) increases with the operating temperature. In addition, to better assess the results obtained under pulsed UV light, the calibration curve of the sensor operated at 130 °C without UV activation is also shown in the left hand panel of Figure 13 (light green). For any of the values reported in Figure 13, the uncertainty (variance associated to the different sensors tested and replicated measurements performed) remains below 16%.

The sensitivity and response time to nitrogen dioxide of the indium oxide sensor under pulsed UV irradiation where computed. Sensitivity is generally defined as the change in response intensity for a given change in gas concentration. Given the fact that the calibration curves are linear, sensitivity is the slope of the calibration curves shown in Figure 13. Response time was defined as the time needed, after the injection of nitrogen dioxide, for the maximum to appear in the curve of the addition of reduction and oxidation rates (see Figure 12). These results are summarised in Table 2. In this table, the values for sensitivity and response time when the sensor is operated at 130 °C and without UV irradiation have also been included for better assessing the results obtained under pulsed UV light.

From the values reported in Table 2, it can be derived that the combined heating and pulsed UV activation of the indium oxide sensor is the best approach for enhancing the detection of

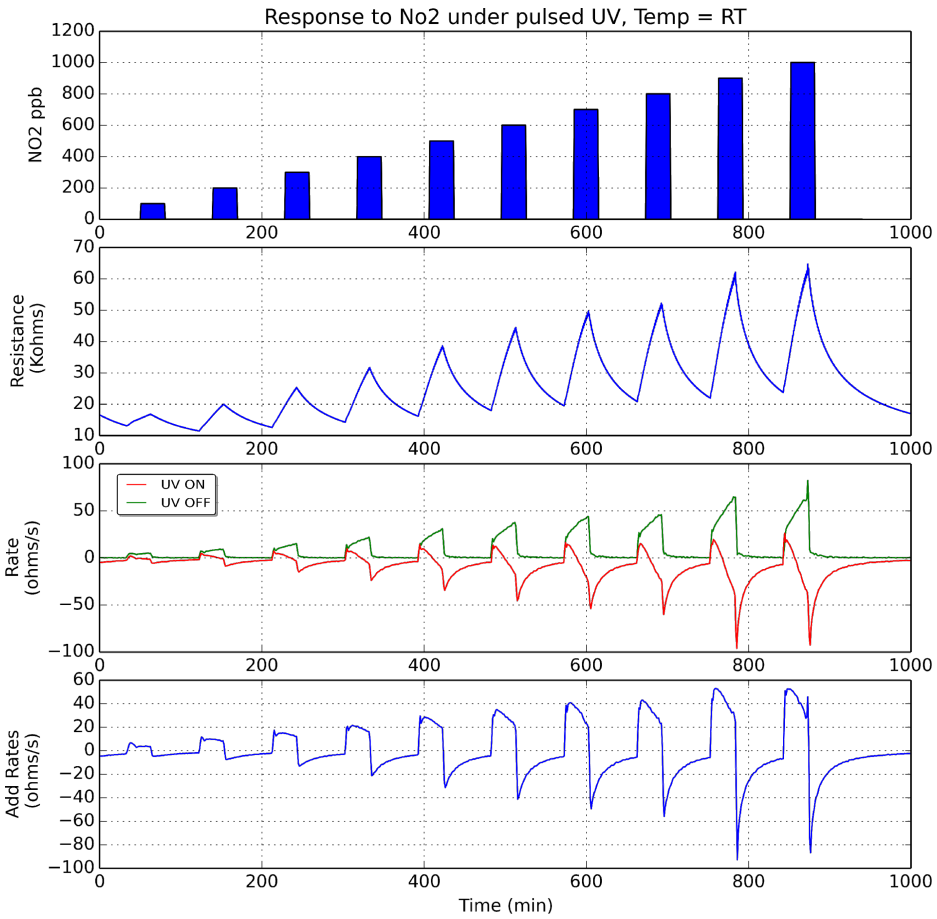

Figure 12: Analysis of the response of an indium oxide sensor operated at 50 °C under pulsing UV light. The upper sub-plot shows the pulses of increasing nitrogen dioxide concentrations (ranging from 100 to 1000 ppb) measured. The second sub-plot shows the dynamic response of the sensor (evolution of its resistance). The third sub-plot shows the evolution of the rates of reduction (in red) and oxidation (in green), which were computed as illustrated in Figure 8. The lower sub-plot shows the addition of the rates of reduction and oxidation.

nitrogen dioxide. When the sensor is operated at 50 °C under pulsed UV light, there is nearly a 40% increase in sensitivity to nitrogen dioxide and an over 80% reduction in power consumption (in comparison to the standard constant temperature operation of the sensor without UV activation). This is reached at the cost of increasing response time. However, if the sensor is operated at 100 °C under pulsed UV light, there is an 80-fold increase in sensitivity and there is still a 35% saving in power consumption. In this case, response time is similar to the one observed when the sensor is operated at a constant temperature of 130 °C without UV irradiation. The figures reported about power savings need to be considered with care, since our ceramic transducer has not been optimised for power consumption. However, most of commercially available metal oxide gas sensors still use ceramic substrates and their power consumption is in the range of few hundred milliwatts. Therefore, the UV pulsed operation would still help reducing overall power consumption.

Conclusion

The effects of heating and UV irradiation on the response toward nitrogen dioxide of screen-printed sensors employing vapour-phase transport synthesized indium oxide octahedra as active material have been studied. It was found that constant UV irradiation and no heating was unsuitable for reversibly detecting nitrogen dioxide with enough sensitivity. On the other hand, by combining mild heating (100 °C) with pulsed UV light irradiation of the sensor surface, resulted in a dramatic enhancement in sensitivity (up to an 80-fold increase) combined to the possibility of making significant savings in power consumption (at least 35% reduction) in comparison to the standard heated operation. This has been achieved by exploiting the dynamics of sensor response under pulsed UV light (i.e., the rates of oxidation and reduction of the indium oxide), which convey important information for the quantitative analysis of nitrogen dioxide. In the near future, further studies are envisaged to fully optimise the combined heating and UV pulsing operating mode

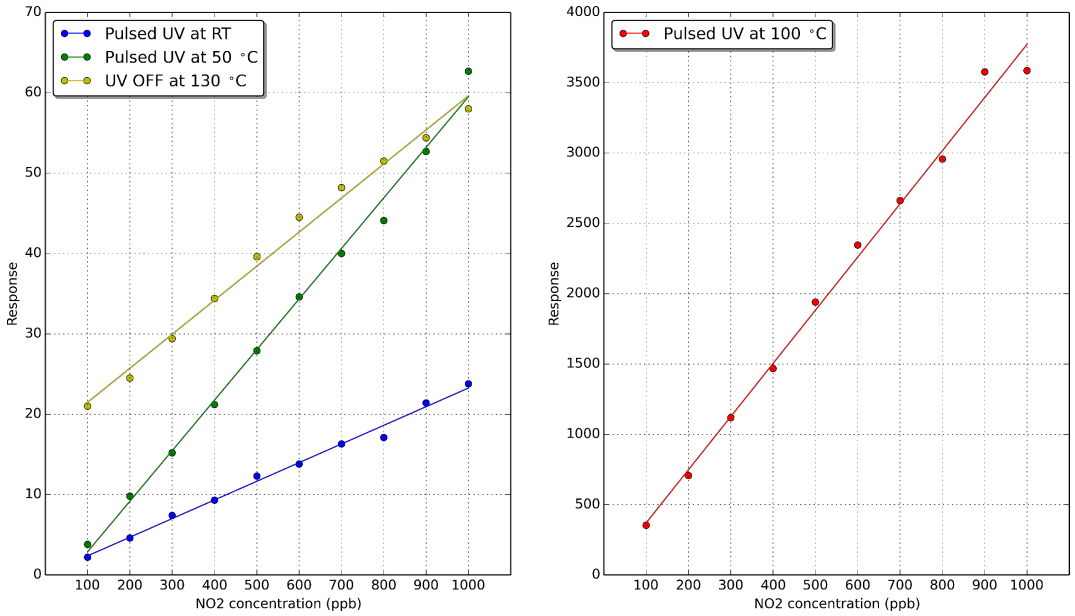

Figure 13: Calibration curves for the detection of nitrogen dioxide with an indium oxide sensor operated at three different temperatures under pulsed UV light. The calibration curve (light green) that appears in the left hand panel corresponds to the sensor operated at 130 °C and without UV activation. Response is either the ratio R_{NO2}/R_{air} when sensors are operated at 130 °C without UV activation or, the sum of oxidation and reduction rates (in Ω/s) when sensors are UV activated.

Table 2: Comparison of response time, sensitivity to nitrogen dioxide and power consumption for an indium oxide sensor under different operating conditions. Power consumption includes the power supplied to the heating element and/or the power supplied to the UV diode where relevant.

temperature	UV	response time (min)	sensitivity	power consumption
RT	pulsed	9.4	0.023[a]	41 mW
50 °C	pulsed	7.1	0.063[a]	151 mW
100 °C	pulsed	4.3	3.78[a]	560 mW
130 °C	off	4.5	0.046[b]	855 mW

[a]In Ω/s·ppb^{-1}; [b]in ppb^{-1}.

of metal oxide gas sensors and their integration in semi-passive, flexible polymeric RFID tags. The integration of gas sensors with UV LEDs would increase overall cost. However, this cost could be a fraction of those incurred when producing a standard MOX sensor, provided that UV-activated sensors were produced in big numbers. This could be the case if such sensors were to integrate widespread personal or indoor air monitors.

Experimental

The indium oxide nano-octahedra were grown onto silicon substrates via a vapour-phase transport method using a horizontal chemical vapour deposition (CVD) furnace. Substrates were cleaned before their insertion in the CVD reactor by three consecutive, five minutes long steps of sonication in acetone, ethanol and deionized water, respectively. Finally cleaned substrates were dried using a flow of pure dry air. In a typical synthesis, 0.3 g of high purity In metal powder (99.99% pure) purchased from Sigma Aldrich, was placed on an alumina boat. The distance between the alumina boat and the silicon substrate was 1 cm and these were placed at the centre of the furnace. Temperature was raised to 900 °C at a rate of 15 °C/min, and kept constant for 120 min. The indium oxide nano-octahedra were synthesized in a dynamic Ar atmosphere (300 mL/min) via a vapour–solid mechanism, since there was not need to pretreat the silicon substrate by depositing catalysts. Indium vapours were generated from the In powder, which reacted with residual oxygen present in the furnace, thus forming oxidized clusters. When the temperature further increases, the oxidized In clusters act as nucleation centres for the formation of Indium oxide crystals. It has been reported that at growth temperatures between 800 and 1000 °C pyramids and octahedra can be obtained [18]. The facets exposed correspond to the most energeti-

cally stable atomic planes in the lattice. The furnace was left to cool down to room temperature and a light green film was found to coat the silicon substrate. The crystalline phase and morphological structural features were studied by means of X-ray diffraction (XRD, Bruker-AXS D8-Discover diffractometer with parallel incident beam) and field emission scanning electron microscope (FESEM, Jeol 7600F).

For SEM analysis, samples were coated with a 3 nm thick carbon layer to avoid charging effects.

Sensors were produced by employing a screen-printing technique. The as-synthesized nano-octahedra were mechanically removed from the silicon substrate employing a razor blade and mixed in a solution of 1,2-propanediol to form a printable ink. This ink was screen-printed on top of commercially available (Ceram Tech GmbH, Germany), alumina transducer elements, which comprised a pair of Pt interdigitated electrodes (front side) and a Pt heating resistor (back side). Each electrode comprises 8 arms (300 µm in width) with an electrode gap of 300 µm. The electrodes cover an area of 2.5 × 2.5 mm^2. The heating element on the backside of the substrate had a resistance of 8 Ω at room temperature. Once printed, sensors were left for an hour to level and then were dried at 150 °C. Finally they were fired at 300 °C for 12 h. The active films were 6 µm thick, quite porous and with a surface roughness of about 2 µm [21]. The largest dimension of indium oxide octahedra is about 500 nm. Therefore, the UV light can reach the surface of a significant amount of the nanomaterial. In total three sensors were produced and tested.

A sensor test chamber was designed and constructed in Teflon. Its inner volume was 24 cm^3. The chamber contains sockets to which up to six sensors can be plugged in to be tested. The cover lid houses two UV LEDs so sensors can be operated in 'temperature mode' when a constant current is driven through their heating element while the UV diodes are off; in 'UV activation mode' when heaters are not used and the UV LEDs are on; and in 'mixed mode' when both heating elements and UV LEDs are used simultaneously. The LED to sensing film distance was set to 12 mm, which considering the radiation aperture of the LEDs used (120°), ensured achieving a homogeneous UV irradiation of the sensors. The UV LEDs employed were manufactured by SETI, Sensor Electronic Technology Inc., Columbia, SC, USA [22] (model UVTOP320TO39FW) and their maximal emitting optical power was 400 µW at 325 nm. The specifications of the UV LED indicate that to avoid saturation, the drive current should be kept below 30 mA at an ambient temperature under 55 °C. The drive current was pulsed (diode was on 50% of the time only) and limited to 15 mA. Furthermore, the LED was placed 2 cm away from the heated area of the sensor and kept inserted in a thermally insulating housing. Therefore, no saturation effect affected our experimental set-up. A picture of the sensor chamber and of a gas sensor is shown in Figure 14.

Figure 14: Sensor chamber used during the experiments, which can house up to six sensors (left). The chamber includes sockets for the UV diodes. Picture of an indium oxide gas sensor (right).

Gas mixing and delivery to the test chamber was performed by using a set of computer controlled mass-flow meters. A calibrated gas cylinder of nitrogen dioxide diluted in synthetic dry air and a zero-grade synthetic air gas cylinder were employed to deliver different, reproducible concentrations of nitrogen dioxide at constant flow of 100 sccm.

Acknowledgements

This work has been funded in part by MINECO under grant no. TEC2015-71663-R, by the European Commission via the European Regional Development Fund (ERDF) and by the European Science Foundation via the COST TD1105 Action 'EuNetAir'. E.L. is supported by the Catalan Institution for Research and Advanced Studies (ICREA) via the ICREA Academia Award.

References

1. Ammu, S.; Dua, V.; Agnihotra, S. R.; Surwade, S. P.; Phulgirkar, A.; Patel, S.; Manohar, S. K. *J. Am. Chem. Soc.* **2012,** *134,* 4553–4556. doi:10.1021/ja300420t
2. Thai, T. T.; Yang, L.; DeJean, G. R.; Tentzeris, M. M. *IEEE Microwave Mag.* **2011,** *12,* 84–95. doi:10.1109/MMM.2011.940594
3. Clément, P.; Ramos, A.; Lazaro, A.; Molina-Luna, L.; Bittencourt, C.; Girbau, G.; Llobet, E. *Sens. Actuators, B* **2015,** *208,* 444–449. doi:10.1016/j.snb.2014.11.059
4. Olivier, J. G. J.; Bouwman, A. F.; Van der Hoek, K. W.; Berdowski, J. J. M. *Environ. Pollut.* **1998,** *102,* 135–148. doi:10.1016/S0269-7491(98)80026-2
5. US Environmental Protection Agency. Nitrogen dioxide. https://www.epa.gov/no2-pollution (accessed June 28, 2016).

6. Hemberg, A.; Konstantinidis, S.; Viville, P.; Renaux, F.; Dauchot, J. P.; Llobet, E.; Snyders, R. *Sens. Actuators, B* **2012,** *171–172,* 18–24. doi:10.1016/j.snb.2012.03.037
7. Afzal, A.; Cioffi, N.; Sabbatini, L.; Torsi, L. *Sens. Actuators, B* **2012,** *171–172,* 25–42. doi:10.1016/j.snb.2012.05.026
8. MICS-6814, Gas Sensors, SGX Sensortech Limited (formerly e2v). https://sgx.cdistore.com/ProductDetail/MICS6814-SGX-Sensortech-Limited/464975/ (accessed Sept 16, 2016).
9. Zhang, D.; Liu, Z.; Li, C.; Tang, T.; Liu, X.; Han, S.; Lei, B.; Zhou, C. *Nano Lett.* **2004,** *4,* 1919–1924. doi:10.1021/nl0489283
10. Mu, X.; Chen, C.; Han, L.; Shao, B.; Wei, Y.; Liu, Q.; Zhu, P. *J. Alloys Compd.* **2015,** *637,* 55–61. doi:10.1016/j.jallcom.2015.03.002
11. Bloor, L. G.; Manzi, J.; Binions, R.; Parkin, I. P.; Pugh, D.; Afonja, A.; Blackman, C. S.; Sathasivam, S.; Carmalt, C. J. *Chem. Mater.* **2012,** *24,* 2864–2871. doi:10.1021/cm300596c
12. Xu, X.; Li, X.; Zhang, H.; Feng, C.; Wang, C.; Liu, F.; Sun, Y.; Sun, P.; Lu, G. *RSC Adv.* **2015,** *5,* 30297–30302. doi:10.1039/C4RA16632A
13. Gui, Y.; Li, S.; Xu, J.; Li, C. *Microelectron. J.* **2008,** *39,* 1120–1125. doi:10.1016/j.mejo.2008.01.052
14. Deng, L.; Ding, X.; Zeng, D.; Tian, S.; Li, H.; Xie, C. *Sens. Actuators, B* **2012,** *163,* 260–266. doi:10.1016/j.snb.2012.01.049
15. Geng, Q.; He, Z.; Chen, X.; Dai, W.; Wang, X. *Sens. Actuators, B* **2013,** *188,* 293–297. doi:10.1016/j.snb.2013.07.001
16. Chen, M.-H.; Lu, C.-S.; Wu, R.-J. *J. Taiwan Inst. Chem. Eng.* **2014,** *45,* 1043–1048. doi:10.1016/j.jtice.2013.08.020
17. Trawka, M. P.; Smulko, J. M.; Hasse, L. Z.; Granqvist, C.-G.; Ionescu, R.; Llobet, E.; Annanouch, F. E.; Kish, L. B. *IEEE Sens. J.* **2016,** *16,* 5152–5159. doi:10.1109/JSEN.2016.2567065
18. Zhang, D.; Li, C.; Han, S.; Liu, X.; Tang, T.; Jin, W.; Zhou, C. *Appl. Phys. A* **2003,** *77,* 163–166. doi:10.1007/s00339-003-2099-3
19. Gonzalez, O.; Roso, S.; Calavia, R.; Vilanova, X.; Llobet, E. *Procedia Eng.* **2015,** *120,* 773–776. doi:10.1016/j.proeng.2015.08.817
20. Wagner, T.; Kohl, C.-D.; Malagù, C.; Donato, N.; Latino, M.; Neri, G.; Tiemann, M. *Sens. Actuators, B* **2013,** *187,* 488–494. doi:10.1016/j.snb.2013.02.025
21. Roso, S.; Umek, P.; Bittencourt, C.; Gonzalez, O.; Güell, F.; Urakawa, A. *J. Mater. Chem. C* **2016,** *4,* 9418–9427. doi:10.1039/C6TC03218D
22. SETI Inc.. UV diodes datasheets. http://www.s-et.com/spec-sheets/320nm.pdf (accessed Sept 16, 2016).

License and Terms

ARTICLE

4. Using the Transient Response of WO_3 Nanoneedles under Pulsed UV Light in the Detection of NH_3 and NO_2

O. Gonzalez, T. G. Welearegay, X. Vilanova and Eduard Llobet

Sensors 2018, 18(5), 1346
DOI :10.3390/s18051346

After exploring the performance of UV-light excited In_2O_3 in the detection of nitrogen dioxide, our objectives were to check whether the methodology could be extended to other metal oxides and target gases. Therefore, we decided to use forests of randomly oriented WO_3 nanoneedles as gas sensitive films and, we tested them under pulsed UV light in the presence of either oxidising or reducing gases. Additionally, we studied the effect of ambient humidity in the detection of different NO2 concentrations. We selected WO3 nanoneedles because it is a well-known material, which is routinely synthesised by our research group. In general such films present high baseline resistance and require rather high operating temperatures for detecting some gases. By using our UV excitation method, we were able to dramatically decrease the baseline resistance of sensors and also the temperature needed for gas detection.

In this paper, we noticed an unexpected behaviour of sensor resistance under the exposure to NH3. Given the low operating temperatures employed under UV excitation, sensor resistance increases in the presence of ammonia and one would expect a decrease of resistance for a reducing gas. This abnormal behaviour had already been reported by different authors in the literature. In our paper, we show that the UV excitation technique is useful for detecting both oxidizing (NO_2) and reducing (NH_3) gases, even in the presence of different levels of ambient humidity. Room temperature operated sensors under pulsed UV light show good response towards ammonia and nitrogen dioxide at low power consumption levels. Increasing their operating temperature to 50 °C or 100 °C has the effect of further increasing sensitivity.

sensors

MDPI

Article

Using the Transient Response of WO_3 Nanoneedles under Pulsed UV Light in the Detection of NH_3 and NO_2

Oriol Gonzalez, Tesfalem G. Welearegay, Xavier Vilanova * and Eduard Llobet

MINOS-EMaS, Universitat Rovira i Virgili, Avda. Països Catalans, 26, 43007 Tarragona, Spain; oriol.gonzalez@urv.cat (O.G.); tesfalemgeremariam.welearegay@urv.cat (T.G.W.); eduard.llobet@urv.cat (E.L.)

* Correspondence: xavier.vilanova@urv.cat; Tel.: +34-977-558-502

Received: 3 April 2018; Accepted: 24 April 2018; Published: 26 April 2018

Abstract: Here we report on the use of pulsed UV light for activating the gas sensing response of metal oxides. Under pulsed UV light, the resistance of metal oxides presents a ripple due to light-induced transient adsorption and desorption phenomena. This methodology has been applied to tungsten oxide nanoneedle gas sensors operated either at room temperature or under mild heating (50 °C or 100 °C). It has been found that by analyzing the rate of resistance change caused by pulsed UV light, a fast determination of gas concentration is achieved (ten-fold improvement in response time). The technique is useful for detecting both oxidizing (NO_2) and reducing (NH_3) gases, even in the presence of different levels of ambient humidity. Room temperature operated sensors under pulsed UV light show good response towards ammonia and nitrogen dioxide at low power consumption levels. Increasing their operating temperature to 50 °C or 100 °C has the effect of further increasing sensitivity.

Keywords: UV light; WO_3 nanoneedles; NH_3; NO_2; gas sensor; dynamic operation

1. Introduction

Metal oxide gas sensors have been attracting important research efforts because of their low cost and good sensitivity. Current research is addressing different drawbacks associated to metal oxides, such as the high temperature required to activate their response to gases, their lack of selectivity and, very particularly, their cross-sensitivity to humidity. Extracting information from the transient response of metal oxide gas sensors has achieved good results in the improvement of selectivity. Response transients can be obtained by producing step-changes in gas concentration [1–6], or by modulating/pulsing the sensor operating temperature [7–12]. Often, low-temperature operated metal oxide sensors suffer from slow response and recovery dynamics, which is not desirable in the continuous monitoring of ambient gases. Here, we explore a new way to create a transient in sensor response by pulsing a source of UV light to enable gas detection. In this case, the information extracted from the transient response is not used to improve selectivity, but to estimate gas concentration in a faster way, despite sensors being operated at low temperatures (compared to the standard operating temperatures of non-illuminated sensors) or even at room temperature. Moreover, the prospects of this procedure for reducing the influence of ambient moisture in sensor response are also investigated. Using UV light to activate the reactions taking place on the surface of metal oxide gas sensors has been considered by different research groups. For example, Sbeveglieri and co-workers explored, in the late 1990s, the UV activation of both SnO_2 and In_2O_3 sensors operated at room temperature [13–15]. According to their research, excitation by means of UV light can affect, in different ways, charge carrier transport across the grain boundaries appearing in polycrystalline metal oxides. Namely,

increasing the density of free carriers by photo generation, decreasing the intergrain barrier height, affecting the intergrain states charge and increasing the probability of tunneling through intergrain barriers, since the depletion layer width of adjacent grains is decreased. Moreover, light can change the occupancy of defects by both electrons and holes, thus affecting the absorption capacity of the metal oxide surface. On the other hand, illumination can also cause structural defects in the oxide lattice. In this case, these defects disappear when UV light is turned off, but with a long recovery period, that is usually temperature dependent. More recently, many other researchers have used UV light to activate gas detection at room temperature employing metal oxides such as TiO_2 [16–18] or ZnO [19–24]. Trawka and co-workers [25] used a combination of heating and UV radiation to stimulate the interactions between WO_3 and the surrounding gases, analyzing the effect of such interactions on the noise generated.

In other cases, UV light is used exclusively to clean the metal oxide surface, avoiding poisoning [26]. In fact, Trocino and co-workers [27] found that using UV light exclusively during the recovery period of room temperature operated In_2O_3 gas sensors, was more efficient than continuous UV illumination for measuring NO_2. UV promotes desorption of NO_2 and helps in regaining the sensor baseline. Recently, we introduced the use of pulsed UV light combined with thermal activation for measuring NO_2 using In_2O_3 gas sensors [28,29]. Some preliminary results about the use of this technique in the measurement of NO_2 employing WO_3 sensors were presented in [30]. In this paper, we have explored further the approach of using pulsed UV to promote the response of WO_3 nanoneedle gas sensors, either operated at room temperature or under mild heating ($\leq$100 °C), in the presence of ammonia or nitrogen dioxide. The performance of this method in terms of response time, sensitivity, resilience to ambient moisture and power consumption is studied and compared against standard operation under constant heating.

2. Materials and Methods

The active layer of WO_3 nano-needles was directly grown on ceramic alumina substrates using an aerosol assisted CVD. 50 mg of tungsten hexacarbonyl ($W(CO)_6$) dissolved in a mixture of 15 mL of acetone and 5 mL of methanol were used as precursor. The substrates had printed Pt electrodes on one side and a Pt heater on the other side, allowing the sensor to be operated over room temperature. A piezoelectric ultrasonic atomizer generated an aerosol that was transported to the CVD reactor, where the substrates were located, by means of a flux of N_2. The CVD reactor temperature was set to 500 °C. The growth process took about 15 min to complete. This resulted in the growth of randomly oriented, tungsten oxide nanoneedles of about 19 microns in length and 140 nm in diameter, fully coating the electrode area of the alumina substrate. The morphology and composition of the active nanomaterial was studied and confirmed by scanning electron microscopy (SEM) and energy-dispersive X-ray spectroscopy (EDX). These results are summarized in the Supplementary Materials. Then, a 2-h annealing at 600 °C in air was conducted to stabilize the gas sensitive films. Further details on the growth, morphology and composition of pure tungsten oxide nanoneedles can be found elsewhere [31].

Calibrated gas cylinders of nitrogen dioxide and ammonia balanced in synthetic dry air (1 ppm and 20 ppm respectively) were used in combination with a synthetic air gas cylinder to set the desired concentrations (dilutions) by means an arrangement of mass flow controllers. In these cases, the residual relative humidity in the measurement rig (at a room temperature of 25 °C) was found to be near 3%. In some cases, diluted samples were also humidified. For this purpose, once more using mass flow controllers, part of the dry air employed for sample dilution was passed through a bubbler to saturate it with humidity. This humidity-saturated flux was mixed with the sample cylinder, which enabled the desired concentrations of target gases under different humidity backgrounds to be obtained.

A Teflon chamber with an inner volume of 24 cm^3 was used for characterizing the sensors. The chamber contains sockets allowing the connection of up to six sensors simultaneously. The chamber cover lid houses two UV LEDs, leaving a 12 mm spacing between the sensors and the LEDs. Since the

radiation aperture of the LEDs is 120°, this distance assures a homogenous irradiation of the active layers. The LEDs employed were the model UVTOP320TO39FW from Sensor Electronic Technology Inc., Columbia, SC, USA (SETI) [32], with a maximum emitting optical power of 400 µW at 325 nm. In order to generate a transient in the sensor resistance when exposed, either to the gas to be measured or air, the UV diode was periodically switched ON and OFF, with a period set to 1 minute. This period was chosen in order to obtain a good signal to noise ratio, especially when the sensor resistance was high.

UV pulses result in the occurrence of a ripple in sensor resistance. This is reflected in Figure 1. This ripple is considered a transient signal in sensor response and the rate of resistance change both when the UV is ON or OFF have been found to give useful information for determining gas concentration [29]. Especially the fact that the rate of resistance changes when the light is OFF will be explored here, since it can be assumed to be closely dependent on the adsorption and reaction processes taking place on the gas-sensitive surface. Evaluating the rate in the period when the light is ON leads to similar information, but the signal is noisier.

This rate is computed as the local derivative of the resistance response curve, that is, the derivative when the UV diode is switched OFF is calculated according to the following expression:

$$Rate(n) = \frac{R(n) - R(n-1)}{\Delta t} \quad (1)$$

where $R(n)$ and $R(n-1)$ correspond to the final and initial value of sensor resistance for a period in which UV light remains switched off and Δt is the duration of this period.

Although this methodology can be applied to sensors operated at room temperature, it will be applied as well to sensors under mild heating ($\leq$100 °C). This is because metal oxides show, in general, higher response and faster response kinetics (e.g., higher resistance change rates) when heated than when operated at room temperature.

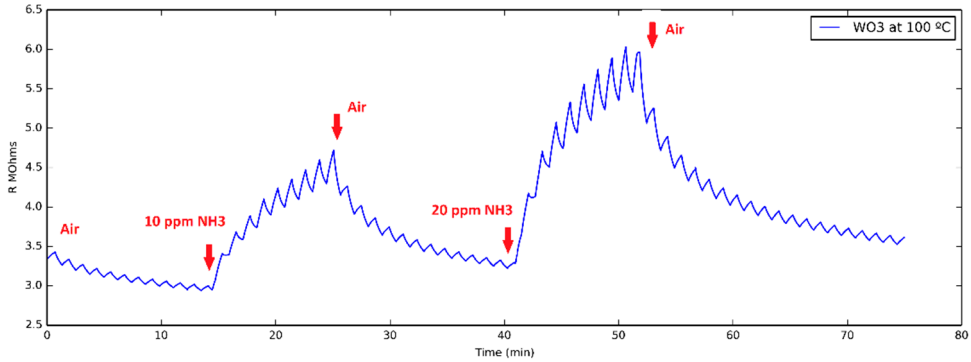

Figure 1. Typical evolution of the resistance of a WO_3 nanoneedle sensor operated at 100 °C to two successive 10 and 20 ppm pulses of ammonia. The ripple in the resistance value is generated by a pulsed UV light (30 s ON and 30 s OFF) applied during the whole measurement process.

3. Results

3.1. Ammonia Detection

In order to check the usefulness of this new methodology in the measurement of ammonia vapors, five different ammonia concentrations (i.e., 1, 2, 4 ppm, 10 and 20 ppm), were generated and delivered to the sensor test chamber (see Figure 2a). The response of the sensors operated under different conditions was recorded. As can be seen in Figure 2b, when a sensor was operated at room temperature without UV excitation, the changes in sensor resistance are rather small for the lower ammonia concentrations tested and slow, so baseline resistance is never regained. Moreover, as it is shown in Figure 2b, sensor resistance increases during ammonia exposure, instead of decreasing

as one would expect for an n-type semiconductor sensor exposed to a reducing species. Figure 2c confirms that when the sensor is operated at 200 °C, its behavior corresponds to the expected one, i.e., sensor resistance decreases when exposed to ammonia. Additionally, when heated, sensor response is faster, allowing the sensor to reach a steady state when exposed to ammonia and to recover its baseline when exposed to air. Nevertheless, the power consumption to reach 200 °C is rather large: 1.2 W.

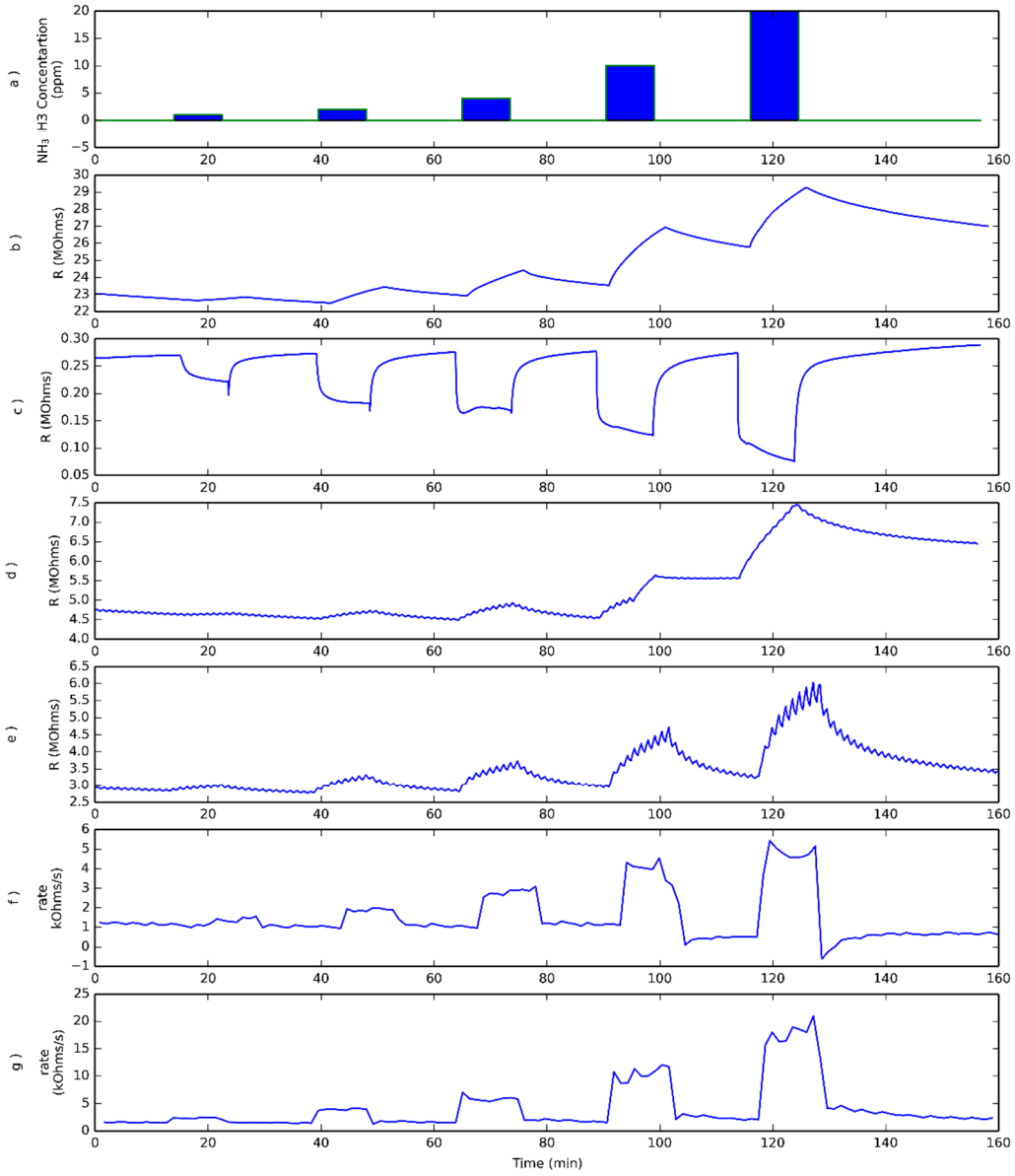

Figure 2. Increasing NH_3 concentration pulses have been tested (**a**). Typical evolution of the resistance recorded in the dark for a sensor operated at room temperature exposed to ammonia pulses (**b**) equivalent to panel (**b**), but when the sensor is operated at 200 °C (**c**). Panels (**d**,**e**) show the responses to ammonia pulses described in the upper panel when the sensor is under pulsed UV light while being operated at room temperature or 100 °C, respectively. Lower panels (**f**,**g**) show the rates of resistance change when the pulsed UV light is OFF, as described in Equation (1), for a sensor operated at room temperature and at 100 °C, respectively.

Subplots d and e in Figure 2 correspond to the response towards ammonia of a sensor operated under pulsed UV light at room temperature and heated to 100 °C, respectively. In those cases, power consumptions are 41 mW and 560 mW respectively. These figures, comprising the power to operate the

LED and to heat the sensor, are significantly lower than the 1.2 W required in the previous case. In both cases, the response ripple caused by pulsed UV light is clearly superimposed to the resistance change caused by the exposure of the sensor to ammonia or dry air. From the comparison of subplots b and d in Figure 2, it is clear that the trends in resistance change due to ammonia exposure are quite similar in both cases and the sensor does not reach the steady state, nor recovers the baseline, being the main difference the ripple superimposed in plot d. Another aspect that can be observed is that the sensor electrical resistance under pulsed UV light is substantially lower than the one corresponding to the sensor just operated at RT. When the sensor operating temperature is raised to 100 °C, the resistance change due to gas exposure is faster than in the previous case, but not as fast as the response recorded when the sensor is operated at 200 °C, as one can expect, since increasing the operating temperature in MOX sensors results in a reduction in response time

Finally, subplots f and g in Figure 2 show the rate of resistance change for sensors under pulsed UV light. The rates shown in subplots f and g were computed during the semi-periods in which the UV light was switched OFF and the sensor was operated either at room temperature or at 100 °C, respectively. It is clear from Figure 2 that the rate of resistance change shows a sudden increase when the sensor is exposed to ammonia, and that a quite stable plateau is attained, the value of which is related to ammonia concentration. When ammonia is removed from the ambient, this rate shows a sharp decrease as well. When the operating temperature is increased from RT to 100 °C, the value of the rate stabilizes at higher values, indicating that the adsorption-reaction process is faster. In order to compare the transient of the sensor resistance and the one corresponding to the evaluated rate, Figure 3 shows the resistance transient and the corresponding calculated rate both normalized. As shown in this figure, the rate shows a sharp change immediately after the sensor is exposed to the gas.

Figure 4 shows the calibration curves taking as response the rate of resistance change, evaluated when the sensor is operated under pulsed UV light at RT and at 100 °C. The error bars correspond to the maximum and minimum values obtained in the set of experiments. Even though the slope of the calibration curve (i.e., ammonia sensitivity) is higher when the sensor is operated at 100 °C, there is enough signal to reliably detect ammonia even when the sensor is operated at RT, with the consequent reduction in power consumption.

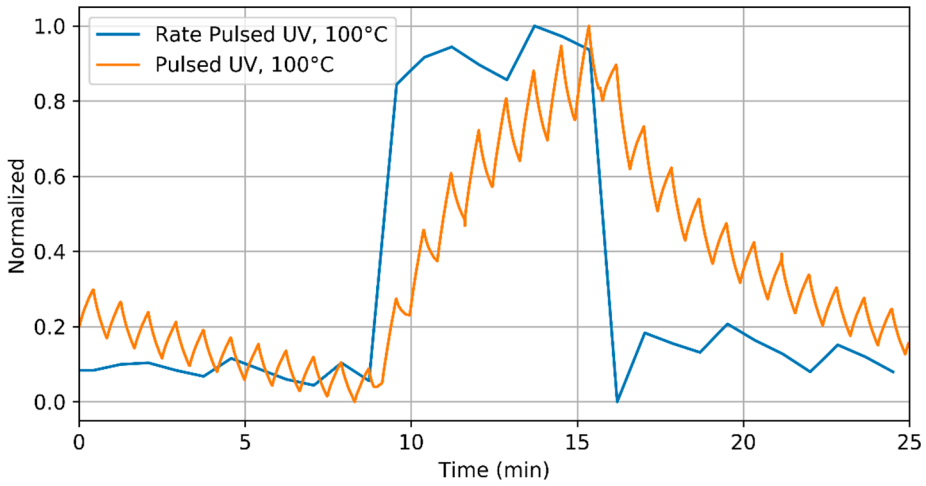

Figure 3. Detail of the sensor response to NH_3, 5 ppm, when operated at 100 °C under pulsed UV light and the corresponding evaluated rate. Both appear normalized for clarity.

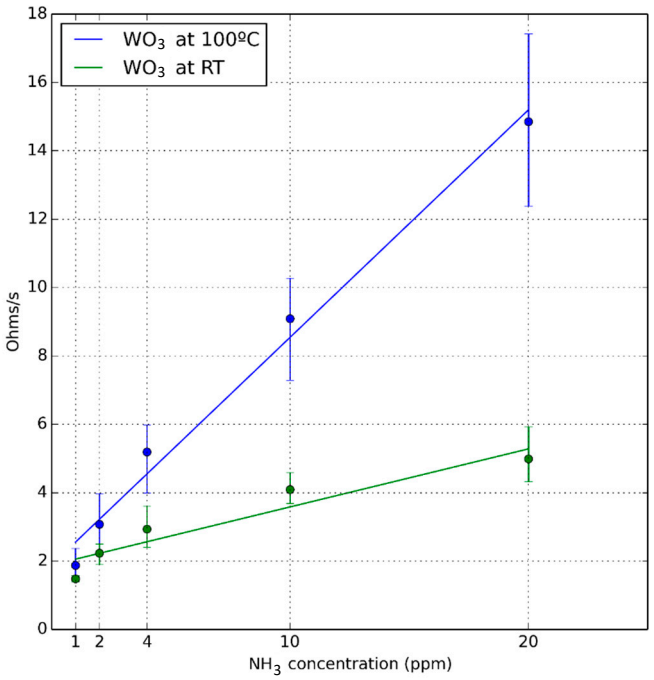

Figure 4. Calibration curves for the sensor operated at room temperature and at 100 °C. The response is the rate of resistance change as defined in Equation (1).

3.2. Nitrogen Dioxide Detection

In the case of nitrogen dioxide, 10 different concentrations were tested (100 to 1000 ppb measured at 100 ppb intervals), as can be seen in Figure 5a. In Figure 5b, the sensor working at room temperature without UV excitation shows a very slow response to nitrogen dioxide as can be also observed in the case of ammonia (Figure 2b). Figure 5c,d, show the changes in sensor resistance due to the combined effect of the exposure to nitrogen dioxide and pulsed UV light when the sensor was operated at RT and at 100 °C, respectively. Similar to what was observed for ammonia, sensor resistance does not reach steady state values during gas exposures nor is the baseline resistance regained during the cleaning phases. The resistance change rate, evaluated according to Equation (1), is depicted in Figure 5d,f, for a sensor operated at RT and 100 °C, respectively. When the sensor is operated at room temperature, once more, this response parameter shows a sharp increase upon exposure to nitrogen dioxide and reaches a plateau, which is clearly correlated to gas concentration. Furthermore, the rate returns to its baseline value during the cleaning phases. Nevertheless, when the sensor is operated at 100 °C the rate does not reach a completely stable value. It shows a sudden increase and then a drifting behavior with time.

Figure 6 shows details of the normalized transient response (both electrical resistance and resistance change rate) to 400 ppb of NO_2 when the sensor is operated at room temperature under pulsed UV light. As shown in this figure, the rate immediately reaches a stable value related to the gas concentration (this is similar to what was observed in Figure 3).

Figure 7 shows calibration curves for NO_2 at different operating temperatures. Similar to the case of ammonia, heating the sensors has the effect of increasing the slope of their calibration curves (i.e., nitrogen dioxide sensitivity increases). However, the response and signal to noise ratio is good enough for reliably detecting nitrogen dioxide when sensors under pulsed UV light are operated at room temperature.

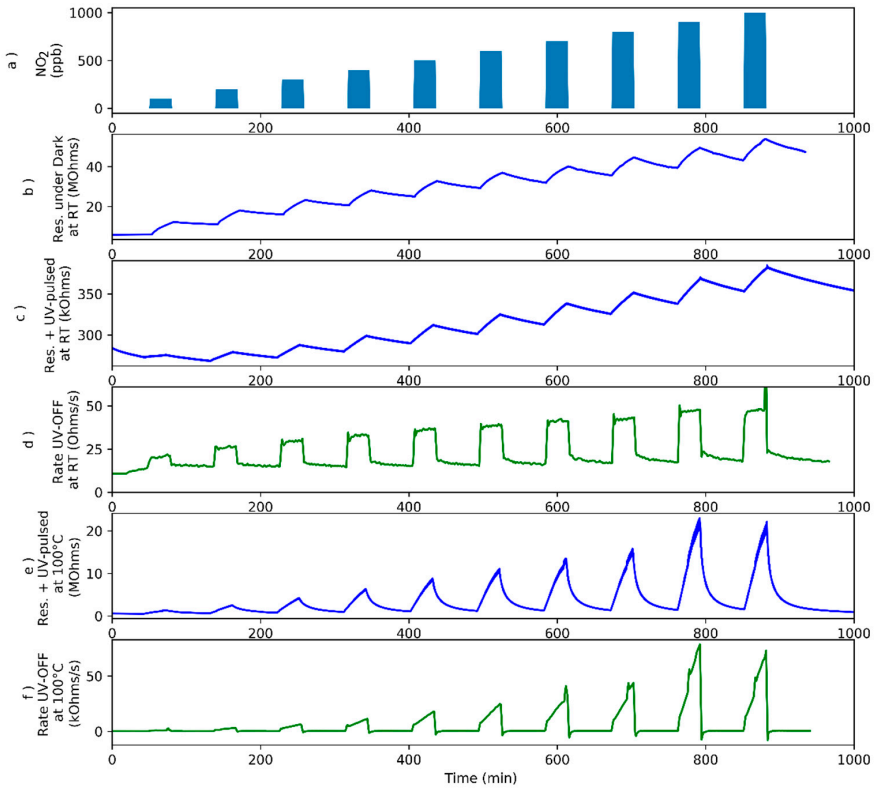

Figure 5. The sensor has been tested for several NO_2 concentrations (**a**). Evolution of sensor resistance under dark conditions in response to successively increasing NO_2 concentration pulses while the sensor is operated at room temperature (**b**). Evolution of sensor resistance under pulsed UV light in response to successively increasing NO_2 concentration pulses while the sensor is operated at room temperature (**c**). Rate of resistance change evaluated when UV light is OFF as defined in Equation (1) while the sensor is operated at room temperature (**d**). Evolution of sensor resistance under pulsed UV light in response to successively increasing NO_2 concentration pulses while the sensor is operated at 100 °C (**e**). Rate of resistance change evaluated when UV light is OFF as defined in Equation (1) while the sensor is operated at 100 °C (**f**).

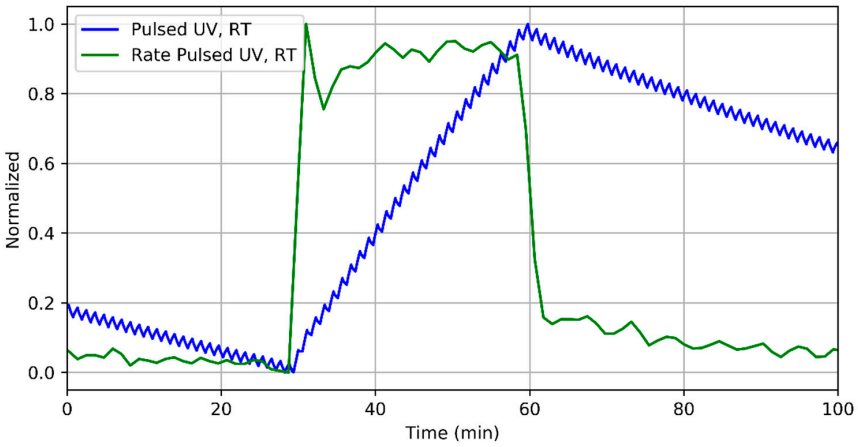

Figure 6. Detail of the sensor response to 400 ppb of NO_2 when operated at room temperature under pulsed UV light and the corresponding evaluated rate. Both curves are normalized for clarity.

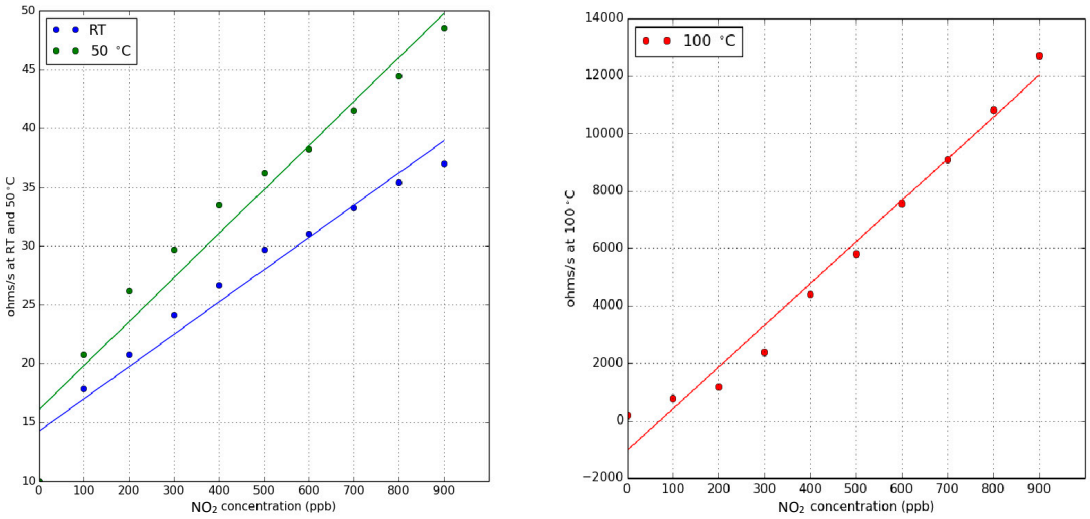

Figure 7. Calibration curves for nitrogen dioxide when the sensor is operated at room temperature, at 50 °C (**left panel**) and at 100 °C (**right panel**). The response is the rate of resistance change as defined in Equation (1). For any of the values reported in this figure, the uncertainty (variance associated to the diferent sensors tested and replicated measurements performed) remains below 15%. Reproduced from [30] © http://creativecommons.org/licenses/by-nc-nd/4.0/.

3.3. Humidity Effect

Additional measurements were performed at different humidity levels (dry air, 25% and 50% R.H.), considering three different NO_2 concentrations (200, 400 and 600 ppb), as depicted in Figure 8a,b. In this case, an operating temperature of 50 °C was set, just to ensure that all measurements were performed at the same temperature and to avoid the occurrence of water condensation, since the water vapor generation system slightly increases the temperature of the gas flow input to the sensor chamber. As can be seen in Figure 8c, the sensor resistance reaches neither the steady state nor the baseline, as in the previous measurements in dry air. A small peak appears systematically when the system passes from dry air to 25% RH. This peak does not appear during the transition from 25% to 50% RH levels, which led us to associate this peak to a response when the sensor changes from dry to humid operation. Checking Figure 6d, where the resistance change rate is depicted, the three gas concentrations can be easily identified in spite of the different ambient humidity levels. An additional peak appears when passing from dry air to 25% RH, which is related to the previously described peak that appears in sensor resistance. Checking the calibration curves obtained for the three relative humidity levels (see Figure 9), it is possible to notice that, in fact, humidity has the effect of slightly increasing the sensitivity towards nitrogen dioxide. Therefore, the system is not immune to humidity, but the effect is quite low (sensitivity increases by about 10% when RH changes from 25% to 50%).

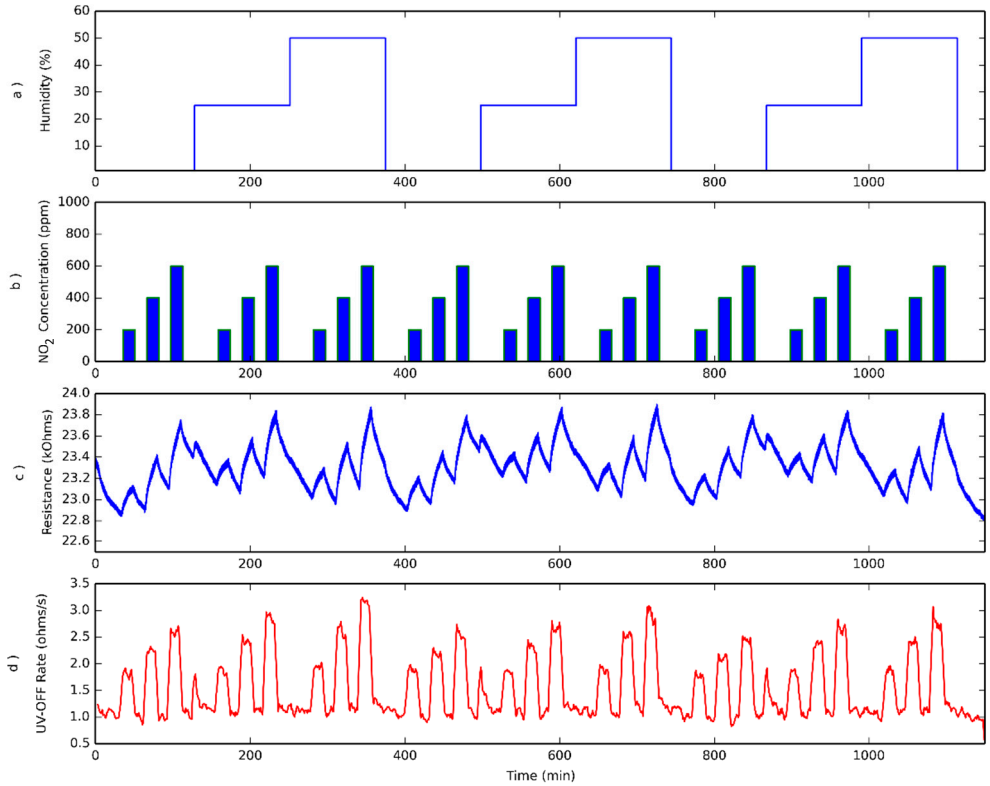

Figure 8. Effect of varying moisture levels on sensor response. The sensor has been characterized at three different humidity levels while operating at 50 °C (**a**), and at three different NO_2 concentrations (**b**). Evolution of sensor resistance under pulsed UV light for the different humidity levels and NO_2 concentrations shown in upper panels (**c**). Rate of resistance change evaluated when UV light is OFF, as defined in Equation (1), while the sensor is operated at 50 °C (**d**).

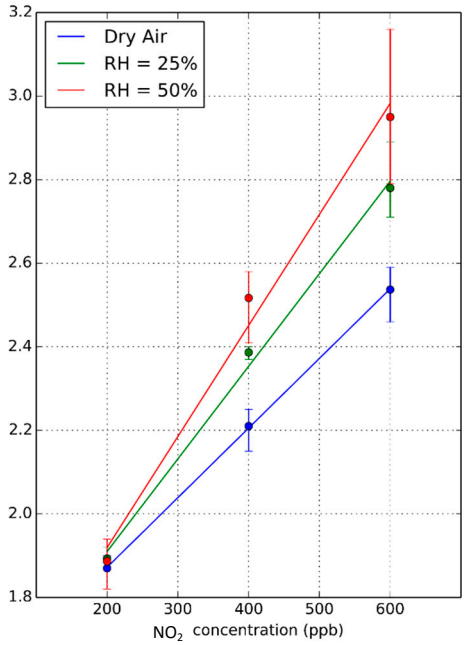

Figure 9. Calibration curves obtained from the rate of resistance change when pulsed UV light is OFF for three different humidity levels and for a sensor operated at 50 °C. Error bars correspond to the maximum and minimum values for the set of measurements gathered.

4. Discussion

According to the results reported by A. Giberti and co-workers [33], when WO_3 is under UV light, the electrical resistance decreases due to a trapped surface charge lowering caused by two different phenomena. In the first case, when an electron-hole pair is generated near the surface, the electric field transfers the hole to the surface, recombining with an electron trapped there in O_2^- form, causing as a result an O_2 molecule to desorb. In the second case, the process consists of the photon being absorbed by an O_2 molecule on the surface, allowing its desorption. Therefore, a new equilibrium between oxygen adsorption/desorption must be reached. In fact, photogenerated electrons can induce the adsorption of O_2 molecules to form new O_2^- ions, which are weakly bound to the WO_3 [22]. On the other hand, when the light is switched off, the sensor surface recovers the initial equilibrium with the surrounding atmosphere, which is a very slow process.

We assume that while the UV diode is switched ON, UV light results in photo-generated charge carriers but also helps desorbing, at least partially, previously adsorbed species from the surface of the active layer. The combined effect of, at least, the two phenomena is probably the reason that causes the rate of electrical change in this period to be noisier. On the other hand, when the UV diode is switched OFF, the cleaned sensor surface may react with the species present in the surrounding atmosphere. During this period, the dynamics of this transient response are limited by the kinetics of adsorption, surface diffusion and chemical reaction, which are heavily affected by operating temperature [7].

Regarding the results obtained when the sensor is exposed to ammonia, it has been shown that when the sensor is operated below 200 °C, sensor resistance behaves in an opposite way to the one that would be expected for an n-type metal oxide in the presence of a reducing species. The electrical resistance of the sensor increases when exposed to ammonia rather than decreasing. This behavior can be observed whether the sensor is exposed to pulsed UV-light or not. This abnormal behavior for WO_3 sensors when measuring ammonia at low operating temperatures (i.e., below 150 °C) has also been reported by other authors [34,35]. WO_3 has also been reported to change from n-type to p-type behavior when operated at low temperatures and exposed to ethanol [36]. This change in behavior can be associated with the competition of two different mechanisms: the target gas can react both with the adsorbed oxygen ions and with the protons from adsorbed water molecules. The reaction with the adsorbed oxygen ions can modify the intrinsic conductivity of the metal oxide by changing the electron concentration, while the reaction with the water molecules adsorbed on the surface can modify the conduction of the surface water layer, which also contributes to the total conductivity. Nevertheless, this abnormal behavior is still the subject of debate and beyond the scope of this paper. In any case, according to the results exposed in the previous section, it is clear that, to be able to determine the gas concentration in a short period of time using the classical approach (i.e., based on the electrical resistance change), higher temperatures (and consequently higher power consumption) are required. Nevertheless, using the UV pulsed mode and evaluating the rate of change of the sensor resistance when the UV light is OFF, allows determining the gas concentration without reaching the steady state. It is important to point out that the time needed for the rate of resistance change to reach a plateau is very short. Since the value of this plateau can be evaluated well in advance, the sensor resistance reaches a steady state value; this enables for a fast determination of both ammonia and NO_2 concentrations, even when the sensor is operated at low temperature, including RT. Therefore, this approach allows the determination of gas concentration for both chemical species in a shorter time, while keeping a reduced power consumption. Moreover, the effect of humidity in the measurements which is known to be of great importance for sensors based on pure WO_3 [37,38], has a reduced impact when using pulsed UV light, probably due to the neutralization of hydroxyl groups by photogenerated holes while UV light is ON [39].

5. Conclusions

The electrical resistance transient of WO_3 nanoneedle gas sensors under pulsed UV light has been analyzed. Pulsed UV light not only generates free charge carriers via valence to conduction band

transitions, but also alters adsorption, desorption and reaction phenomena occurring at the gas-solid interface in metal oxide gas sensors. As a result, a modulation of the concentration of free charge carriers in the semiconductor is achieved. The rate of change in sensor resistance gives information about the concentration of the gas present in the environment. Using this approach, metal oxide nanoneedle sensors can be operated at significantly lower temperatures, even at room temperature, reducing the required power: For example, from 1.2 W in a sensor heated at 200 °C down to 41 mW in a room-temperature operated, pulsed UV light excited sensor. In addition, gas concentration can be estimated much faster than when the standard change in electrical resistance is used (i.e., when sensor is operated well above room temperature and, upon a change in gas concentration, it is necessary to wait until a static regime is achieved). Moreover, this approach has also been shown to be less affected by changes in ambient moisture. The methodology has been shown to be useful both for oxidizing (NO_2) and reducing (NH_3) gases.

Supplementary Materials: The following are available online at http://www.mdpi.com/1424-8220/18/5/1346/s1. Figure S1: Sensor substrate used, Figure S2: SEM image of the WO_3 nanoneedles conforming the active layer of the sensor, Figure S3: Typical EDX spectrum of a sensing layer, Figure S4: XRD spectrum for the WO_3 nanoneedles, Figure S5: Raman spectrum for WO_3 nanoneedles.

Author Contributions: T.G.W. prepared and characterized (SEM and EDX) the sensors under the supervision of E.L. Sensor measurements were performed by O.G. under the supervision of X.V. All authors have participated in the discussion of results and the writing of the paper.

Funding: This research was funded by MINECO and European Regional Development Fund (ERDF) grant number TEC2015-71663-R, by European Science Foundation grant COST TD1105 Action 'EuNetAir' and by Catalan Institution for Research and Advanced Studies (ICREA).

Acknowledgments: This work has been funded in part by MINECO under grant no. TEC2015-71663-R, by the European Commission via the European Regional Development Fund (ERDF) and by the European Science Foundation via the COST TD1105 Action 'EuNetAir'. E.L. is supported by the Catalan Institution for Research and Advanced Studies (ICREA) via the ICREA Academia Award.

Conflicts of Interest: The authors declare no conflict of interest. The founding sponsors had no role in the design of the study; in the collection, analyses, or interpretation of data; in the writing of the manuscript, and in the decision to publish the results.

References

1. Llobet, E.; Vilanova, X.; Brezmes, J.; Alcubilla, R.; Calderer, J.; Sueiras, J.E.; Correig, X. Conductance-transient analysis of thick-flint tin oxide gas sensors under successive gas-injection steps. *Meas. Sci. Technol.* **1997**, *8*, 1133–1138. [CrossRef]
2. Llobet, E.; Brezmes, J.; Vilanova, X.; Sueiras, J.E.; Correig, X. Qualitative and quantitative analysis of volatile organic compounds using transient and steady-state responses of a thick-film tin oxide gas sensor array. *Sens. Actuators B* **1997**, *41*, 13–21. [CrossRef]
3. Llobet, E.; Vilanova, X.; Brezmes, J.; Sueiras, J.E.; Alcubilla, R.; Correig, X. Steady-state and transient behavior of thick-film tin oxide sensors in the presence of gas mixtures. *J. Electrochem. Soc.* **1998**, *145*, 1772–1779. [CrossRef]
4. Llobet, E.; Vilanova, X.; Brezmes, J.; Sueiras, J.E.; Correig, X. Transient response of thick-film tin oxide gas-sensors to multicomponent gas mixtures. *Sens. Actuators B Chem.* **1998**, *47*, 104–112. [CrossRef]
5. Gutierrez-Osuna, R.; Nagle, H.T.; Schiffman, S.S. Transient response analysis of an electronic nose using multi-exponential models. *Sens. Actuators B Chem.* **1999**, *61*, 170–182. [CrossRef]
6. Ngo, K.A.; Lauque, P.; Aguir, K. Identification of toxic gases using steady-state and transient responses of gas sensor array. *Sens. Mater.* **2006**, *18*, 251–260.
7. Clifford, P.K.; Tuma, D.T. Characteristics of semiconductor gas sensors 2. Transient-response to temperature-change. *Sens. Actuators* **1983**, *3*, 255–281. [CrossRef]
8. Kato, Y.; Yoshikawa, K.; Kitora, M. Temperature-dependent dynamic response enables the qualification and quantification of gases by a single sensor. *Sens. Actuators B Chem.* **1997**, *40*, 33–37. [CrossRef]

9. Kohler, H.; Rober, J.; Link, N.; Bouzid, I. New applications of tin oxide gas sensors: I. Molecular identification by cyclic variation of the working temperature and numerical analysis of the signals. *Sens. Actuators B Chem.* **1999**, *61*, 163–169. [CrossRef]
10. Gutierrez-Osuna, R.; Gutierrez-Galvez, A.; Powar, N. Transient response analysis for temperature-modulated chemoresistors. *Sens. Actuators B Chem.* **2003**, *93*, 57–66. [CrossRef]
11. Yamada, Y.; Ogita, M. Transient response of resistive-type NO_2 sensor on temperature change. *Sens. Actuators B Chem.* **2003**, *93*, 546–551. [CrossRef]
12. Parret, F.; Menini, P.; Martinez, A.; Soulantica, K.; Maisonnat, A.; Chaudret, B. Improvement of micromachined SnO_2 gas sensors selectivity by optimised dynamic temperature operating mode. *Sens. Actuators B Chem.* **2006**, *118*, 276–282. [CrossRef]
13. Camagni, P.; Faglia, G.; Galinetto, P.; Perego, C.; Samoggia, G.; Sberveglieri, G. Photosensitivity activation of SnO_2 thin film gas sensors at room temperature. *Sens. Actuators B Chem.* **1996**, *31*, 99–103. [CrossRef]
14. Comini, E.; Cristalli, A.; Faglia, G.; Sberveglieri, G. Light enhanced gas sensing properties of indium oxide and tin dioxide sensors. *Sens. Actuators B Chem.* **2000**, *65*, 260–263. [CrossRef]
15. Comini, E.; Faglia, G.; Sberveglieri, G. UV light activation of tin oxide thin films for NO_2 sensing at low temperatures. *Sens. Actuators B Chem.* **2001**, *78*, 73–77. [CrossRef]
16. Lee, H.C.; Hwang, W.S. Enhancing the sensitivity of oxygen sensors through the photocatalytic effect of SnO_2/TiO_2 film. *Mater. Trans.* **2005**, *46*, 1942–1949. [CrossRef]
17. Manera, M.G.; Taurino, A.; Catalano, M.; Rella, R.; Caricato, A.P.; Buonsanti, R.; Cozzoli, P.D.; Martino, M. Enhancement of the optically activated NO_2 gas sensing response of brookite TiO_2 nanorods/nanoparticles thin films deposited by matrix-assisted pulsed-laser evaporation. *Sens. Actuators B Chem.* **2012**, *161*, 869–879. [CrossRef]
18. Zhang, S.N.; Lei, T.; Li, D.; Zhang, G.Z.; Xie, C.S. UV light activation of TiO_2 for sensing formaldehyde: How to be sensitive, recovering fast, and humidity less sensitive. *Sens. Actuators B Chem.* **2014**, *202*, 964–970. [CrossRef]
19. Ge, C.Q.; Xie, C.S.; Hu, M.L.; Gui, Y.H.; Bai, Z.K.; Zeng, D.W. Structural characteristics and UV-light enhanced gas sensitivity of La-doped ZnO nanoparticles. *Mater. Sci. Eng. B Solid State Mater. Adv. Technol.* **2007**, *141*, 43–48. [CrossRef]
20. Costello, B.P.J.; Ewen, R.J.; Ratcliffe, N.M.; Richards, M. Highly sensitive room temperature sensors based on the UV-LED activation of zinc oxide nanoparticles. *Sens. Actuators B Chem.* **2008**, *134*, 945–952. [CrossRef]
21. Peng, L.; Zhao, Q.D.; Wang, D.J.; Zhai, J.L.; Wang, P.; Pang, S.; Xie, T.F. Ultraviolet-assisted gas sensing: A potential formaldehyde detection approach at room temperature based on zinc oxide nanorods. *Sens. Actuators B Chem.* **2009**, *136*, 80–85. [CrossRef]
22. Fan, S.W.; Srivastava, A.K.; Dravid, V.P. UV-activated room-temperature gas sensing mechanism of polycrystalline ZnO. *Appl. Phys. Lett.* **2009**, *95*, 142106. [CrossRef]
23. Peng, L.A.; Zhai, J.L.; Wang, D.J.; Zhang, Y.; Wang, P.; Zhao, Q.D.; Xie, T.F. Size- and photoelectric characteristics-dependent formaldehyde sensitivity of ZnO irradiated with UV light. *Sens. Actuators B Chem.* **2010**, *148*, 66–73. [CrossRef]
24. Luo, L.; Sosnowchik, B.D.; Lin, L.W. Local vapor transport synthesis of zinc oxide nanowires for ultraviolet-enhanced gas sensing. *Nanotechnology* **2010**, *21*, 495502. [CrossRef] [PubMed]
25. Trawka, M.P.; Smulko, J.M.; Hasse, L.Z.; Granqvist, C.G.; Ionescu, R.; Llobet, E.; Annanouch, F.E.; Kish, L.B. UV-Light-Induced Fluctuation Enhanced Sensing by WO_3-Based Gas Sensors. *IEEE Sens. J.* **2016**, *16*, 5152–5159. [CrossRef]
26. Mor, G.K.; Varghese, O.K.; Paulose, M.; Grimes, C.A. A self-cleaning, room-temperature titania-nanotube hydrogen gas sensor. *Sens. Lett.* **2003**, *1*, 42–46. [CrossRef]
27. Trocino, S.; Frontera, P.; Donato, A.; Busacca, C.; Scarpino, L.A.; Antonucci, P.; Neri, G. Gas sensing properties under UV radiation of In_2O_3 nanostructures processed by electrospinning. *Mater. Chem. Phys.* **2014**, *147*, 35–41. [CrossRef]
28. Gonzalez, O.; Roso, S.; Calavia, R.; Vilanova, X.; Llobet, E. NO_2 sensing properties of thermally or UV activated In_2O_3 nano-octahedra. *Procedia Eng.* **2015**, *120*, 773–776. [CrossRef]
29. Gonzalez, O.; Roso, S.; Vilanova, X.; Llobet, E. Enhanced detection of nitrogen dioxide via combined heating and pulsed UV operation of indium oxide nano-octahedra. *Beilstein J. Nanotechnol.* **2016**, *7*, 1507–1518. [CrossRef] [PubMed]

30. Gonzalez, O.; Welearegay, T.; Llobet, E.; Vilanova, X. Pulsed UV light activated gas sensing in tungsten oxide nanowires. *Procedia Eng.* **2016**, *168*, 351–354. [CrossRef]
31. Vallejos, S.; Umek, P.; Stoycheva, T.; Annanouch, F.; Llobet, E.; Correig, X.; de Marco, P.; Bittencourt, C.; Blackman, C. Single-Step Deposition of Au- and Pt-Nanoparticle-Functionalized Tungsten Oxide Nanoneedles Synthesized Via Aerosol-Assisted CVD, and Used for Fabrication of Selective Gas Microsensor Arrays. *Adv. Funct. Mater.* **2013**, *10*, 1313–1322. [CrossRef]
32. SETI Inc. UV Diodes Datasheets. 2017. Available online: http://web.sensor-ic.com:8000/zlxiazai/s-et/320nm.pdf (accessed on 22 November 2017).
33. Giberti, A.; Malagù, C.; Guidi, V. WO_3 sensing properties enhanced by UV illumination: An evidence of surface effect. *Sens. Actuators B Chem.* **2012**, *165*, 59–61. [CrossRef]
34. Dao, D.V.; Shibuya, K.; Bui, T.T.; Sugiyama, S. Micromachined NH3 gas sensor with ppb-level sensitivity based on WO_3 nanoparticles Thinfilm. *Procedia Eng.* **2011**, *25*, 1149. [CrossRef]
35. Nguyen, D.D.; Dang, D.V.; Nguyen, D.C. Hydrothermal synthesis and NH_3 gas sensing property of WO_3 nanorods at low temperature. *Adv. Nat. Sci. Nanosci. Nanotechnol.* **2015**, *6*, 035006. [CrossRef]
36. Li, H.; Xie, W.; Ye, T.; Liu, B.; Xiao, S.; Wang, C.; Wang, Y.; Li, Q.; Wang, T. Temperature-Dependent Abnormal and Tunable p-n Response of Tungsten Oxide–Tin Oxide Based Gas Sensors. *ACS Appl. Mater. Interfaces* **2015**, *7*, 24887–24894. [CrossRef] [PubMed]
37. Annanouch, F.E.; Haddi, Z.; Vallejos, S.; Umek, P.; Guttmann, P.; Bittencourt, C.; Llobet, E. Aerosol-Assisted CVD-Grown WO_3 Nanoneedles Decorated with Copper Oxide Nanoparticles for the Selective and Humidity-Resilient Detection of H_2S. *ACS Appl. Mater. Interfaces* **2015**, *7*, 6842–6851. [CrossRef] [PubMed]
38. Annanouch, F.E.; Haddi, Z.; Ling, M.; di Maggio, F.; Vallejos, S.; Vilic, T.; Zhu, Y.; Shujah, T.; Umek, P.; Bittencourt, C.; et al. Aerosol-Assisted CVD-Grown PdO Nanoparticle-Decorated Tungsten Oxide Nanoneedles Extremely Sensitive and Selective to Hydrogen. *ACS Appl. Mater. Interfaces* **2016**, *8*, 10413–10421. [CrossRef] [PubMed]
39. Liu, L.; Li, X.; Dutta, P.K.; Wang, J. Room temperature impedance spectroscopy-based sensing of formaldehyde with porous TiO_2 under UV illumination. *Sens. Actuators B Chem.* **2013**, *185*, 1–9. [CrossRef]

CONFERENCE PAPER

5 Combined pulsed UV and temperature activation of metal oxide nanomaterials in breath analysis applications

O. Gonzalez, C. Jaeschke, T. G. Welearegay, E. Llobet

ISOCS/IEEE International Symposium on Olfaction and Electronic Nose (ISOEN)
Montreal, Canada. 2017

This is not a journal paper, it is a conference paper. We have decided to have it included here because it contains important results. This paper combines the materials described in the previous articles (IN_2O_3 and WO_3) in a long experiment (24 h) switching between reducing gases (ethanol and acetone) under 4 different sensor operation modes. These modes comprise: Heating + pulsed UV light; RT + pulsed UV light; RT only and heating only. This is helpful for easily observing the effect of temperature and the effect of UV light excitation on sensor response. For example, at RT there is no response at all, but using UV, a huge response towards acetone is achieved.

So this last experiment of the thesis opens new fundamental questions about the actual sensing mechanisms under UV activation. Also the observed behaviour here, matches the unexpected response for another reducing gas (NH_3) that we reported in the previous article. These aspects are worth studying in future works.

COMBINED PULSED UV AND TEMPERATURE ACTIVATION OF METAL OXIDE NANOMATERIALS IN BREATH ANALYSIS APPLICATIONS

O. Gonzalez [1], C. Jaeschke[2] ,T. Wewearegay[1] , S. Roso[1,3], X. Vilanova[1] and E. Llobet[1]

[1]MINOS-EMaS, Universitat Rovira i Virgili, Avda. Països Catalans, 26, 43007, Tarragona, Spain.
[2]JLM Innovation, Tübingen, Germany
[3]ICIQ, Institute of Chemical Research of Catalonia, Avda. Països Catalans, 16, 43007, Tarragona, Spain.

ABSTRACT

The aim of this work is to develop a system for breath analysis, introducing a new methodology for improving the discrimination between ethanol and acetone at high humidity levels. Ethanol and acetone are present in exhaled breath and have been identified as biomarkers of different diseases especially in patients suffering from colorectal cancer [1]. The system comprises a 6-element sensor array employing In_2O_3 and WO_3 nanomaterials, which are operated under pulsed-UV and at two different temperatures. Two response variables are obtained for each sensor: the rate of electrical resistance change when UV is on and the same when UV is off. Those rates are input to a non-supervised method: PCA. The results obtained strongly suggest that this setup could be useful for detecting these biomarkers in breath analysis applications.

Index Terms— Pulsed-UV, breath analysis

INTRODUCTION

Nowadays lot of efforts are focused in developing non-invasive systems to diagnose diseases by analyzing exhaled breath. But there are challenging problems in such an approach as the high levels of humidity and the low concentrations of biomarkers for the different diseases.
The capacity of UV light to clean and desorb the species previously adsorbed on the surface of metal oxides has been reported [2]. It is also known that temperature modulation of metal oxide gas sensors is useful for extracting additional information and ameliorating their selectivity. In previous works, we have modulated UV light (325 nm) in order to study the transients of oxidation (when UV is OFF for 60 s) and transients of reduction or cleaning (UV ON for 60 s) in tungsten oxide nano-needle films in the presence of nitrogen dioxide [3]. When combined, the pulsed UV operation results in response patterns that appear to depend on the species present in the sensor environment. This is illustrated in Figure 1. In the present work we use Pulsed-UV to discriminate between acetone and ethanol in a high humidity background.

EXPERIMENTAL

Pure or metal doped tungsten oxide (WO_3) nano-needles were directly grown on ceramic substrates at 500 ºC via a hot wall aerosol assisted CVD method employing tungsten hexacarbonyl ($W(CO)_6$, 50 mg) dissolved in acetone (15 ml) and methanol (5 ml) as precursor. A piezoelectric ultrasonic atomizer was used to generate an aerosol of the solute, while N_2 was used as carrier gas [3]. The ceramic substrates have printed Pt electrodes on one side and a Pt heater on the other side. Indium oxide nano-octahedra were synthesized at high temperature (900ºC) via vapor-phase transport and screen-printed onto same alumina transducers. [2]. The sensor array is listed in Table 1

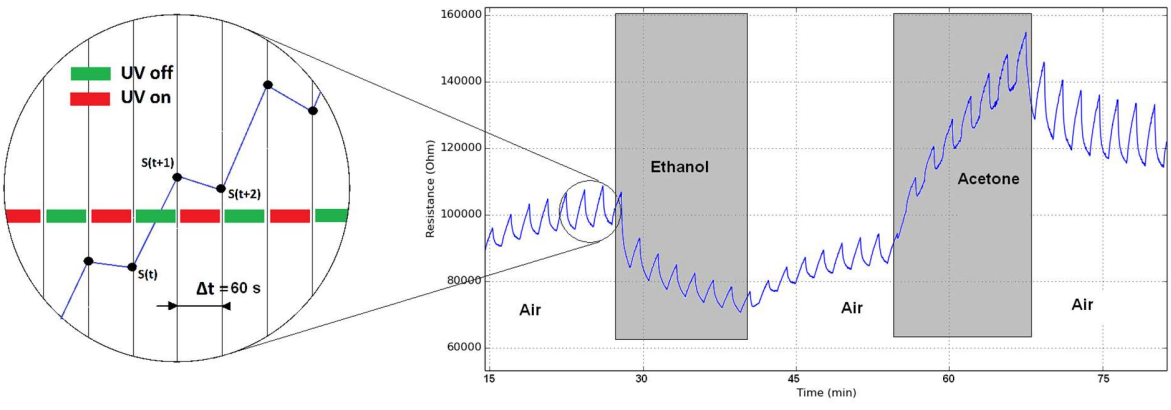

Figure 1: Ripple of the resistance in sensor WO3 + Fe (sensor id 5) produced by UV effect at 40 ºC

id	Material	R0
1	WO3 NW	26 kΩ
2	WO3 NW + Ni NP	100 kΩ
3	WO3 NW + Pt & Au NP	218 kΩ
4	WO3 NW + Pd NP	787 kΩ
5	WO3 NW + Fe NP	1.42 MΩ
6	In2O3 Octahedra	842 Ω

Table 1: Sensor array, Ro is the baseline resistance at 40 ºC

A sensor test chamber with inner volume of 24 cm^3 was designed and constructed in Teflon. The chamber contains sockets to which up to six sensors can be plugged in to be tested. The cover lid houses two UV LEDs model UVTOP320TO39FW, manufactured by SETI, (Sensor Electronic Technology Inc., Columbia, SC, USA) with a maximal emitting optical power of 400 µW at 355 nm. Therefore, sensors can heated when a constant current is driven through their heating element and simultaneously can be activated by UV light. For the sample gas generation we have developed a breath simulator. This system consists of 4 proportional valves controlling the flow of synthetic dry air as well as the flow rates from 3 different head-spaces: A first one only with water to obtain 100% RH, a second one with ethanol in water (10 ppm) at 100 % RH and a third one with acetone in water (15 ppm) at 100% RH.. The 3 headspaces and the sensors chamber are placed in a temperature controlled chamber at 40 ºC to simulate the temperature of exhaled gas. The concentrations in the headspace have been fixed in a previous work [4]. Figure 2 shows the system set-up.

Using this mixing system, we have programed a pattern of vapors in a balance of humidified air (70 % RH) to be delivered to the sensors. These samples simulate what would be obtained from breath samples. The pattern consists of 3.5 ppm of ethanol during 15 min, followed by 15 min with 7 ppm of ethanol, another 15 min with 5 ppm of acetone 15 min with 10 ppm of acetone, and between each concentration sensors are flown for 15 min with synthetic air at 70% RH.

Figure 2: Breath simulator set-up

This measurement pattern has been repeated 3 times for each one of the 4 different operating modes applied to the sensors M1 (sensors operated at 150 ºC and using Pulsed-UV), M2 (sensors at a room temperature of 40 ºC and using Pulsed-UV), M3 (sensors at a room temperature of 40 ºC in the dark) and M4 (sensors heated at 150ºC in the dark). The upper part of Figure 3 illustrates the total sequence used in the charactarisation. The sensing devices are MOXstick from JLM innovation.

RESULTS AND DISCUSION

The lower part of Figure 3 shows the temporal evolution of the electrical resistance of the indium oxide sensor under the different operating modes described above. It is easy to see that each operating mode produces a different response pattern of the sensor under gas exposure. It is clear that under the M3 operation mode there is no response to the species tested. This lack of response is observed for all the sensors tested under M3 operating conditions. So, M3 measurements were not used in the subsequent analysis. Furthermore, sensors 2 and 3 were not significantly responsive to ethanol or acetone under any of the operating regimes tested. Therefore, the sensor array was pruned and only sensors 1, 4 5 and 6 were employed. In operation

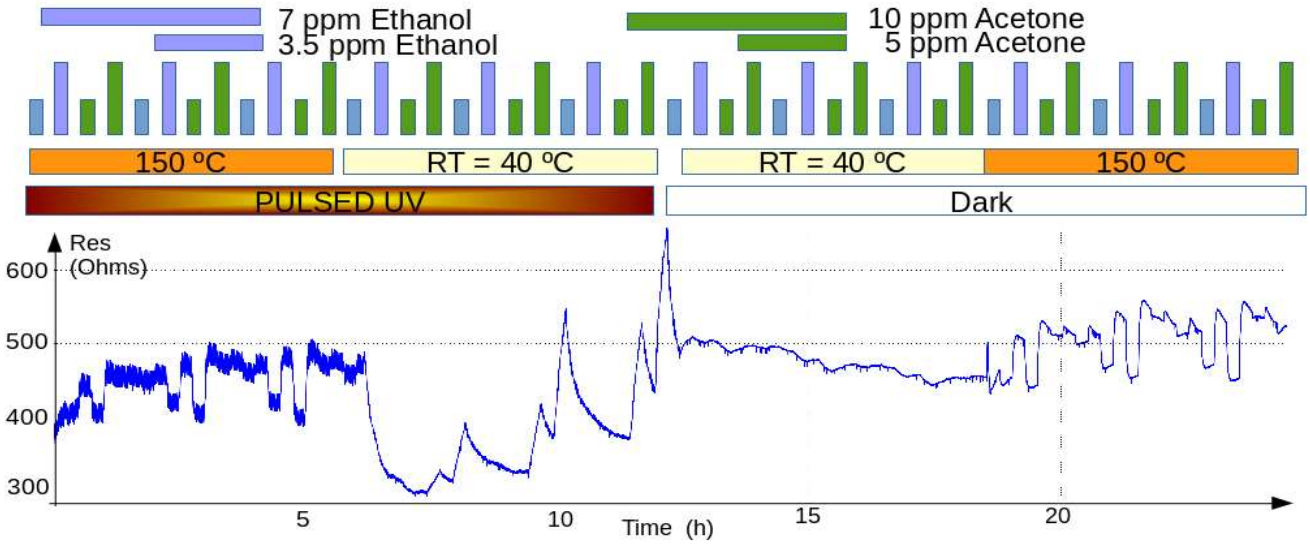

Figure 3: In2O3 octahedra (sensor id 6) response under different modes and gas concentrations.

modes M1 and M4, when the sensor temperature is kept at 150 ºC, the behavior of the electrical resistance is similar for both modes with the only difference being the ripple caused by switching on/off the LED under M1. A higher response is observed when the sensor is exposed to ethanol. The responses obtained under the M4 operating mode are not used in the subsequent analysis. Finally, for mode M2 we can observe (in figure 3) that the sensor only shows a response under acetone. When sensors 1, 5 and 6 (all based on WO3) are operated under the M2 mode, we obtained a similar response as the one shown in figure 1. When operated under M2 mode, the resistance of sensors in ethanol decreased and increased in acetone, which differs from what is observed under the M1 mode when the presence of ethanol or acetone, resulted in a decrease in sensor resistance (this decrease was significantly higher for ethanol). According to the results discussed, a PCA analysis was performed, which employed only the responses for operating modes M1 and M2 (modes under pulsed UV light).

The data set is composed by rates defined in [2] (UV_ON and UV_OFF). So we have the data organized in 16 variables (4 sensors x 2 temperatures x 2 UV-rates) that is synchronized with gas concentrations. This means that switching the UV source at a 2 min period and considering that each vapor concentration is held constant during 15 min, 7 to 8 points are acquired for a given species and concentration. Then the sensors are flowed with humid air before a new vapor concentration is measured. This can be observed in figure 4. To avoid uncertainties caused at the specific transitions between cleaning and gas exposures, the first and the last measurements point for each period have been discarded. In figure 2 we can also observe that the sensors are not fully stabilized at the beginning of such transitions, which supports our decision for removing these measurements from the database. With those considerations, we have obtained the PCA analysis that is plotted in figure 5.

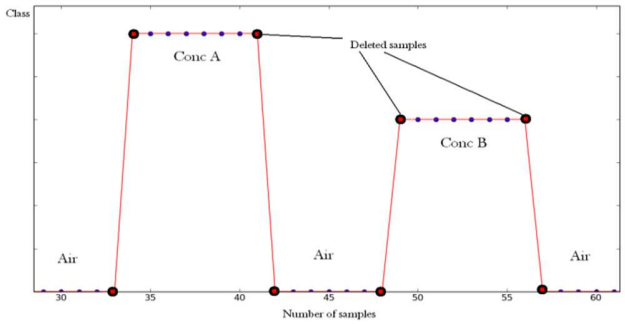

Figure 4: Data cleaning: Initial and final measurements within any given vapor exposure are discarded.

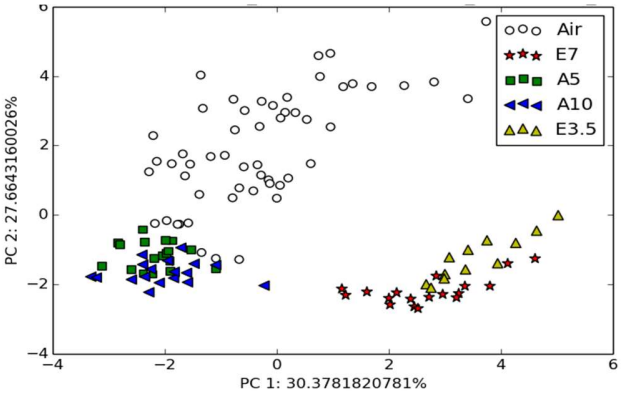

Figure 5: PCA result, for discriminate compounds.

The data set contains 72 points of Air (white), 12 of Ethanol 3.5 ppm (3.5E in yellow), 18 points of 7 ppm Ethanol (7E in red), 18 points of 5 ppm Acetone (5A in green) and 18 points of 10 ppm Acetone (10A in blue).

CONCLUSIONS

The effects of heating and UV irradiation in the response toward ethanol and acetone in an array of WO_3 nano-needles and screen-printed sensors employing vapor-phase transport synthesized indium oxide octahedra as active material have been studied under 70% RH. It was found that at almost RT (40 ºC), pulsed-UV irradiation and no heating was unsuitable for discriminating between those compounds. On the other hand, combining mild heating with pulsed UV light irradiation of the sensor surface, resulted in a dramatic enhancement in sensitivity and selectivity, combined to the possibility of making significant savings in power consumption. This has been achieved by exploiting the dynamics of sensor response under pulsed UV light (i.e., the rates of oxidation and reduction of the indium oxide). In the near future, further studies are envisaged to fully optimize the combined heating and UV pulsing operating mode of metal oxide gas sensors for lowering the detection limit of our system and meeting the specifications of a breathalyzer.

REFERENCES

[1] H. Amal, M. Leja et al. *Breath testing as potential colorectal cancer screening tool*, International Journal of Cancer 138, 229–236 (2016); doi: 10.1002/ijc.29701

[2] *O.Gonzalez, S.Roso, X.Vilanova and E.Llobet, Enhanced detection of nitrogen dioxide via combined heating and pulsed UV operation of indium oxide nano-octahedra, Beilstein J. Nanotechnol. 2016, 7, 1507–1518. 2016*

[3] O. *Gonzalez, T. Welearegay, E. Llobet, X. Vilanova. Pulsed UV Light Activated Gas Sensing in Tungsten Oxide Nanowires Procedia Engineering* Pages 351-354 *2016*

[4] A. Tripler. An introduction to headspace sampling in gas chromatography fundamentals and theory. PerkinElmer, Inc. 1014 (3-12)

6. Conclusions

In the present thesis we have developed a novel way to activate metal oxide gas sensitive layers, combining pulsed-UV light and low temperature heating. Before this thesis, there was no literature available on the implementation of this methodology. The approach developed in this thesis results in a dramatic enhancement in sensitivity, in significant savings in power consumption, significantly reduced response times and more reliable quantification. This has been achieved by exploiting the dynamics of sensor response under pulsed UV light.

The usefulness of this new approach has been proved employing two different sensing layers: In_2O_3 and WO_3 for detecting oxidising gases (nitrogen dioxide) and reducing gases (ethanol, acetone and ammonia). Results show, that a reduction in the operating temperature of the gas sensors (even RT operation) is achieved. This means savings in power consumption, and improved sensitivity when pulsed UV light excitation is combined to mild heating (up to 100ºC). This reduction in working temperature, would enable using these materials in a wide spectrum of application substrates, including flexible polymeric substrates such as Kapton or polyimide.

In addition, we have proved that a dramatic reduction in sensor response time (at lower operating temperatures) is achieved. This is due to the analysis of response transients employing the rate of resistance change that reaches a steady state value well before sensor resistance reaches the steady state. Furthermore, the recovery time for these transients is even faster than when only temperature excitation is employed.

It was noticed that this technique is useful for, not only increasing sensitivity, but also for improving the selectivity. For instance, when measuring ethanol and acetone at low operating temperature, both reducing gases show opposite behaviour, that is, in the case of acetone, the sensor behaves as a p-type semiconductor, while it behaves as a n-type semiconductor for ethanol.

We have also noticed that UV excitation has a stabilising effect on the baseline resistance, enlarging the lifetime of the sensor. Nevertheless, longer experiments and intensive use of the methodology are needed in order to better assess this characteristic.

7. Future work

After presenting this thesis, several questions remain open. Possibly, the most important one is to better understand what happens to the sensing layer under pulsed UV irradiation, which allows us to measure gases at RT. In other words, what the sensing mechanism is. Additionally, it is still necessary to study further if this methodology remains reproducible and stable over long periods of time, which would be indicative that pulsed UV does not degrade metal oxide layers. Finally, it seems worth studying if it is possible to improve performance by optimizing pulsed UV excitation, the extraction and processing of response features and building a dedicated device.

To investigate the sensing mechanism, we propose to focus on basic research by first targeting at a pure metal oxide material type, where we will be sure that the repeatability and stability of the different batches of sensors will not add complexity to our experiments. One possible method could be to observe the effect of Pulsed UV under vacuum or N_2 at different concentrations of oxygen, and the relationship with temperature. As it is not clear that the transients caused by the pulsed UV are only related to the oxidation and reducing mechanisms on the surface, experiments with different gases could also be performed, to come up with a model or possible chemical reaction explaining, for example, the unexpected response under acetone or ammonia that we saw in the experiments of the current thesis.

An additional investigation that could be performed in parallel, would consist of building a set-up that would allow for measuring with several sensors at the same time, while using different UV sources (excitation wavelengths), but the key to this new set up would be a fast sampling rate and a high frequency on the pulsed UV. This new set up would allow us to improve the signal quality and enable the analysis of the transients and the long-term stability.

Once the best sensing layer is selected and the test system is stable, it is important to focus on different UV wavelengths, and even visible light, in order to decrease the price of the UV source and also become totally selective due to the combination of the sensing layer, optimal temperature, and specific wavelength to optimize the detection and quantification of a selected target gas.